UNIVERSITEIT VAN PRETORIA
UNIVERSITY OF PRETORIA
YUNIBESITHI YA PRETORIA

Intermolecular bonding in water clusters from the molecular-wide and electron density-based (MOWED) perspective: a theoretical study

by

Stéfan Zaaiman

Supervisor: Prof. Ignacy Cukrowski
Co-Supervisor: Dr. Jurgens de Lange

Submitted in fulfilment of the requirements for the degree

Master of Science (Chemistry)

In the Faculty of Natural & Agricultural Sciences

University of Pretoria

Pretoria, South Africa

December 2023

Declaration

I, Stéfan Zaaiman, declare that the dissertation, which I hereby submit for the degree Master of

Science (Chemistry) at the University of Pretoria, is my own work and has not previously been

submitted by me for a degree at this or any other tertiary institution.

SIGNATURE: _____

DATE: 14 December 2023

Abstract

Cooperativity is a strange phenomenon in water clusters, characterized by a non-linear decrease in the average electronic energy of a water molecule or hydrogen bond with an increase in cluster size. The main aim of this theoretical study was to determine the effect cooperativity has on a water cluster and how it manifests, using novel theoretical tools and methodologies. Specifically, the MOlecular Wide Electron Density (MOWED) approach was used in this study to explore water clusters.

Modelled water clusters (which included 2D cyclic and various 3D conformers) displayed the expected non-linear decrease in electronic energy. A novel equation was developed and fitted to the clusters in order to predict maximum cooperativity effects and their relative rates of changes. The equation was then adapted to be able to accommodate any property for the applicable water clusters. The equation predicted a maximum stability for cyclic water clusters of –8.316 kcal/mol per water molecule. This is the limit in stability relative to the dimer that a cyclic water cluster can reach due to cooperativity.

The relationship between electron delocalization and cooperative stabilization was also explored extensively. It was found that intermolecular electron delocalization increases non-linearly with increasing cluster size and can be used to explain the origins of cooperativity. Intermolecular delocalization and interaction energies were also further decomposed into atomic and fragment contributions, and notably the 3-atom oxygen fragments contributed the most to the stability of the water clusters. Visualization of electron delocalization revealed 'highways' that electrons travel through within the water clusters, and 1D cross-section of an H-bond showed that a substantial amount of delocalized electron density is contributed by atoms other than the three present. The investigation of electron delocalization reveals that cooperativity is truly a molecular-

wide event that is driven primarily by O-atoms and directed by H-atoms. The mechanistic limits to the number of electrons that can be delocalized were also investigated and found to be primarily O-localized density.

Various cooperativity–induced effects – effects that result from cooperativity – were investigated. The atomic charge for oxygen showed a contribution from delocalized electrons resulting in the increased negative charge for the oxygen atom. The total interaction energy decreased while the exchange-correlation increased and had a positive sign. However, the total classic electrostatic interactions decreased and had a larger magnitude than total interaction energy. The increase and positive sign for exchange-correlation resulted from intramolecular interactions. Overall, the total intermolecular interaction energy and both its components contributed to the stability of the water cluster. The topological properties showed a stability increase at the critical point and increased covalency with the incremental increase of water molecules. Geometrical descriptors resulted in the same conclusions as found above.

Finally, similar cooperativity effects were revealed in a series of 3D hexamer clusters, where the number of water molecules remain constant but the number and nature of H-bonds increases. The same mechanism of intermolecular electron delocalization along 'highways' connecting neighbouring O-atoms were revealed to be the primary driver of cooperative stabilization. Unlike the cyclic structures, the primary source of delocalized electrons was shown to be intramolecular delocalization (such as O–H covalent bonds).

Keywords: Cooperativity, Water Cluster, FALDI, FAMSEC, Electron Delocalization, Electronic Energy.

Outputs of this work

Article titled **Molecular-wide and electron density (MOWED)-based definition and quantification of cooperativity in cyclic water clusters** submitted to *Physical Chemistry Chemical Physics* journal.

Table of Contents   Page

Chapter 3 Molecular-wide and electron density (MOWED)-based definition and quantification of cooperativity in cyclic water clusters

List of Figures

Chapter 1 Introduction

Chapter 3 Molecular-wide and electron density (MOWED)-based definition and quantification of cooperativity in cyclic water clusters

Chapter 4 Cooperativity Induced Effects

Chapter 5 3D hexamer water clusters

Appendix I

Appendix II

List of Tables

Chapter 3 Molecular-wide and electron density (MOWED)-based definition and quantification of cooperativity in cyclic water clusters

Chapter 4 Cooperativity Induced Effects

Chapter 5 3D hexamer water clusters

Appendix I

Appendix II

List of Abbreviations

AIL	Atomic Interaction Line
AIM	Atoms in Molecule
atom-ED	Atomic Electron Density
AU	Atomic Unit
aug	Augmented
B3LYP	Becke, 3-parameter, Lee-Yang-Parr
BBC1	Buijse and Baerends Correction 1
BCP	Bond Critical Point
BP	Bond Path
cc	Correlation consistent
CCSD	Coupled Cluster Singles and Doubles
DAFH	Domain Averaged Fermi Hole
DB	Density Bridge
DFT	Density Functional Theory
DI	Delocalization Index
ED	Electron Density
ESI	Electronic Supplementary Information
FALDI	Fragment, Atomic, Localized, Delocalized and Interatomic
FAMSEC	Fragment Attributed Molecular System Energy Change
FIR	Far Infrared
GD3	Grimmes Dispersion 3
GTO	Gaussian Type Orbitals
HF	Hartree Fock
IQA	Interacting Quantum Atoms
IUPAC	International Union of Pure and Applied Chemistry
LDO	Localized Delocalized Overlap
LI	Localization Index
LO	Localized Overlap
loc-FAMSEC	Local–Fragment Attributed Molecular System Energy Change
MCTBP	Monte Carlo Temperature Basin Paving
mol-FAMSEC	Molecular–Fragment Attributed Molecular System Energy Change
MOT	Molecular Orbital Theory
MOWED	Molecular Wide Electron Density
MP2	Møller-Plesset Perturbation Theory
NDF	Natural Density Function
NEDA	Natural Energy Decomposition Theory
PES	Potential Energy Surface
pVQ(T)Z	polarized Valence Quadruple (Triple) Zeta
QCT	Quantum Chemical Topology
QM	Quantum Mechanical

QTAIM	Quantum Theory of Atoms In Molecules
REP-FAMSEC	Reaction Profile–Fragment Attributed Molecular Energy Change
SCF	Self-Consistent Field
STO	Slater Type Orbitals
TIP4P	Transferable Intermolecular Potential with 4-Points
TPT2	Thermodynamic Perturbation Theory Second Order
VBT	Valence Bond Theory
VRT	Vibrational-Rotating Tunnelling

Chapter 1

Introduction

1

Water clusters

Water is arguably the most important substance on Earth. It displays remarkable properties that are well-documented in any general chemistry textbook, ranging from incredible solvation characteristics, unique physical properties and wide-ranging chemical reactivity. The unique properties of water can, however, only be understood at a fundamental level by investigating the smallest units of this substance: clusters of water molecules.

Water clusters are made up of water molecules arranged in either a 2D (cyclic clusters or linear chains) or a 3D fashion. Water clusters have been extensively researched by Xantheas,[1–6] who investigated the cyclic water trimer in 1993 using *ab initio* calculations.[6] Xantheas optimised the cyclic water trimer with MP2 level of theory, which is the first reported fully energy-optimised water trimer. Xantheas extended the optimised water cluster sizes to $(H_2O)_n$, $n = 1 - 6$. Also in 1993, Xantheas and Aprà[4] optimized the dimer to tetramer-sized cyclic water clusters with MP2 level of theory and augmented correlation-consistent quadruple zeta basis set (aug-cc-pVQZ), as well as optimizing the entire range of cyclic water clusters with Hartree-Fock level of theory. The extended set of water clusters closely matched the experimental evidence. Rakshit *et al.*[7] published an article in which they expanded the list of water clusters optimized by Xantheas to $(H_2O)_n$, $n = 3 - 25$. Rakshit *et al.* found the relative minima with a Monte Carlo Temperature Basin Paving (MCTBP) global optimization procedure. They then reoptimized the specific chosen structures using MP2/aug-cc-pVTZ level of theory to obtain the true minima structure. The experimental proof of the water clusters was found by Liu *et al.*[8–10] and the water dimer by Dyke *et al.*[11]

The smallest water cluster used in this study is the dimer, which has two water molecules bonded with an intermolecular H-bond. The two water molecules are oriented in such a way as to minimize the energy. They are positioned to form a proton donor and a proton acceptor pair

2

(donor-acceptor). The dimer geometry serves as the 'model' for all other H-bonds between two water molecules within the cyclic water cluster formation.

One reason why authors investigate water clusters is because liquid water consists of a spectrum of these water clusters.[12] Molecular systems that contain only water molecules other than the cyclic type are considered, such as the 3D orientations,[13] or where the environment around a water molecule is changed to see its interactions.[14–16] The water hexamer 3D orientations are a topic of interest in the literature.[17–19] The $(H_2O)_n$, $n = 6$ hexamer water clusters are the first set of water molecules where the lowest energy conformer is no longer a cyclic structure (2D).[17,19] The number of stable 3D conformers for a certain number of water molecules increases exponentially as the number of water molecules in the water cluster increases, which can be observed from the potential energy surface (PES).

In order to obtain the absolute minimum, the electronic energy must be considered, as this is the total energy of a water cluster. The electronic energy of a water cluster is used by our research group as the main energetic property to explain all other observed phenomena. The level of theory and choice of basis set has a very great bearing on the accuracy of the energy values obtained for a certain water molecule size. The level of theory describes the way in which the Schrödinger equation is solved, and the basis set defines the shape and number of atomic orbitals used to describe each atom in the molecular system. In this study the B3LYP hybrid functional is used to energy-optimize the water clusters. B3LYP is a good balance between accuracy and the computational resource requirement.[20]

The chemical bond

The starting point from which to define a chemical bond is to use a theoretical description, such as that obtained from the Quantum Theory of Atoms In Molecules (QTAIM).[23] The accumulation of electronic charge density is indicative of an atomic interaction line (AIL)

between two nuclei. Bader[23] described electronic charge density as the glue in chemistry. The density is maximally accumulated along the interaction line. Bader also explicitly stated that a bond path is not a 'bond': only when two nuclei are linked together are the corresponding atoms bonded. Two models have been proposed which are used primarily in the literature, namely valence bond theory (VBT)[24] and molecular orbital theory (MOT).[25]

The bonds within these water molecules define to a large extent the energy of the system–interaction energy component of electronic energy. Therefore, when looking at an atom it can be seen that its nucleus consists of protons and neutrons surrounded by electrons. The strength of the force keeping the electrons near the nucleus decreases as the distance from the nucleus increases (ionization potential), making it possible for valence electrons to be donated or shared with other nuclei without causing an instability. The valence electrons are the first electrons to become delocalized to another atom nucleus. Lower orbital electrons become delocalized or shared in chemical bonds as well.[21,22] Numerous chemical bonds have been quantified in recent years, but the main ones are ionic and covalent within solutions. Metal bonds are not important for this type of study. Ionic bonds are characterized by a difference in electrostatics, leading to the movement of an electron to another nucleus. Covalent bonds are characterized by the sharing of electrons through electron clouds, or as in conventional chemistry, the overlap of valence orbitals. The water clusters under investigation in this study have covalent bonds as well as intermolecular interactions between water molecules. The intermolecular interaction takes place over a distance larger than the distance of a covalent bond.

H-bond

The H-bond was first proposed by G.N. Lewis in 1920.[26] The H-bond plays a significant role in systems such as crystal engineering,[27] biochemistry,[28] and supramolecular chemistry,[29] to name a few examples. The H-bond is defined as X–H⋯Y–Z by IUPAC.[30] The 4-atom definition defines

X as a more electronegative atom than H, and Y, Z as two arbitrary atoms. The X–H covalent bond (polarized bond) is the hydrogen bond donor, meaning that it donates electron density to Y or to a Y–Z covalent bond. According to IUPAC, there are electrostatic forces present within an H-bond that bring about charge transfer between the donor and the acceptor, causing a partial covalent bond between H and Y. Dispersion forces are also present within an H-bond. The intermolecular H⋯Y bond increases in strength as the electronegativity increases for the X atom. The X–H⋯Y 3-atom H-bond is strongest when the dihedral angle is 180º and when the intermolecular bond length is the shortest. The covalent H-bond is defined as simply H–Z, where Z is an arbitrary atom and the atomic interaction line (AIL) connects the two atoms by sharing electron density. The focus of this work is primarily on the nature of the intermolecular H-bond.

There are two schools of thought when it comes to H-bonds: the one defines the H-bond as an electrostatic interaction,[31,32] as shown by the Buckingham-Fowler model,[33] and the other defines it as a covalency or delocalization of electrons forming the bond,[34,35] which is shown and explained in this work.

Cooperativity

The H-bond has a strong relationship with the concept of cooperativity. The H-bond is a popular choice to investigate cooperativity.[3,9,10,13,15,37-39,41-45,48,50,51-55] The above-mentioned characteristics and properties found within an H-bond are all investigated when the phenomenon known as cooperativity is investigated. To assist the reader to comprehend the way in which the literature is structured, with a primary focus on cooperativity within water clusters, the methods used are first introduced and then the types of water clusters investigated by the authors are discussed. Once all the methods have been explained, the results obtained by these authors are presented, maintaining the same order. An illustration is given of water clusters that differ in

conformation from that of cyclic and 3D geometry as used in this work. The reader is advised to consult the specific paper for the exhaustive representation and explanation of each water cluster.

The first mention of cooperativity is by Frank and Wen[36] who introduced the term in 1957. When examining a water dimer that consists of water molecules *a* and *b*, it can be seen that the hydrogen bond formed is an acid-base reaction. When the H-bond is formed, molecule *a* becomes more acidic and molecule *b* becomes more basic compared to a free water molecule. The bond formed between *a* and *b* becomes stronger when water molecules *a* and *b* form H-bonds with water molecules *c* and *d* respectively. Consequently, the formation of hydrogen bonds in liquid water is predominantly a cooperative effect. Furthermore, when one H-bond forms a lot, more will form, similar to when one breaks many others will also break. The stepwise formation is shown below in Figure 1.
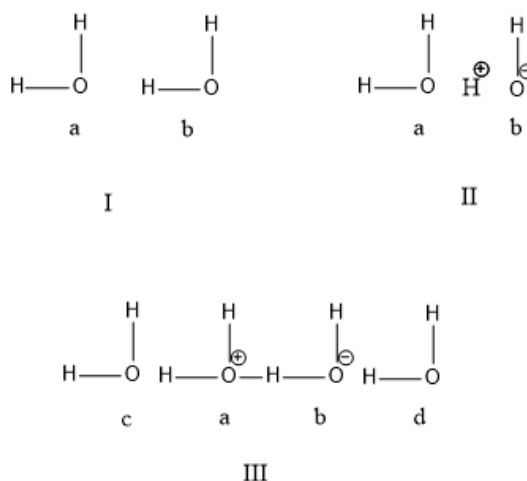
Figure 1 The stepwise formation of water clusters according to Frank and Wen.[36] Figure reproduced from Frank and Wen.

The most common explanation of cooperativity is that when the bond strength is enhanced by the addition of distant (non-local) bonds, the molecular energy is lower (higher stability). This is usually observed when a water molecule is added in water clusters. The way in which this enhancing effect is defined varies according to the author: some authors use the H-bond strength, or a non-additive increase of the H-bond energy, or the bond length. Cooperativity is often

6

simply mentioned by an author who does not explicitly define it. The problem is that a formal definition for cooperativity does not exist – it is only a generalized idea, which may lead some authors to use it in the wrong context.

Hankins *et al.*[37] were the first to observe cooperativity with a self-consistent field (SCF) computational study. They explored three different linear trimer configurations and computed the non-additive three-body potential between neighbouring water molecules for each configuration. The three-body potential is the first non-additive term. It is calculated as the difference between the energy of the three-atom molecule and the sum of the energy for each atom and the potential energy between two atoms, of which there are three combinations when three atoms are present. The three trimers configurations of linear water clusters investigated by the author are shown in Figure 2.
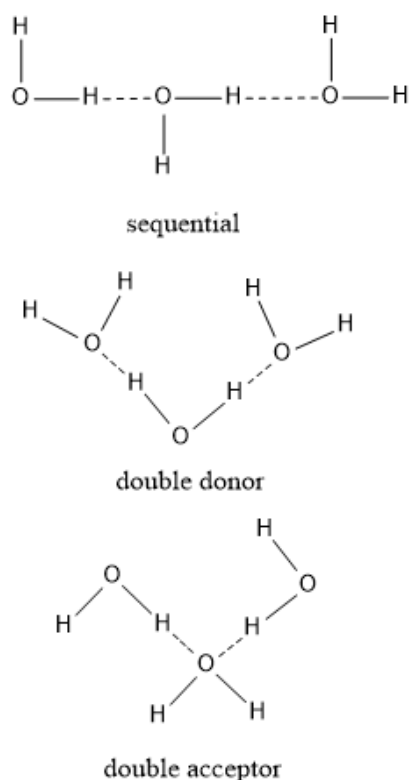
Figure 2 The three configurations of trimer linear water clusters investigated by Hankins *et al.*,[37] which include sequential, double donor and double acceptor water clusters. Reproduced from Hankins *et al.*

Xantheas[3] considered trimer to hexamer water clusters $((H_2O)_n, n = 3 - 6)$ with an H-bond network orientated in an acceptor-donor fashion. The arrangement of neighbouring water molecules significantly affects the cooperative effects. Moreover, Xantheas[3] investigated cooperativity by decomposing the interaction energy of an n-bodies system (ΔE_n). He followed the same method as Hankins et al.[37] Ohno et al.[38] developed an equation linking the H-bond patterns to their respective OH wave numbers. The equation quantifies the number of water molecules bonded to a specified dimer. The H-bond donors to a central dimer are summed, and the H-bond acceptors from the central dimer are subtracted. This yields a magnitude number with which comparisons are made. The fully coordinated water structure is shown in Figure 3. This structure is the fully coordinated form of the dimer water cluster.
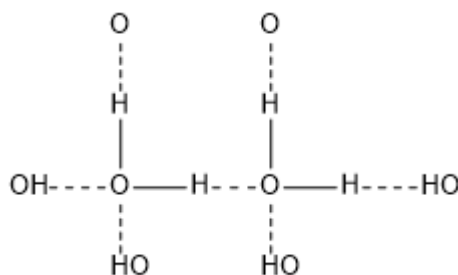
Figure 3 The fully coordinated water structure. Reproduced from Ohno et al.[38]

Although all the above-mentioned authors provide a definition of cooperativity, their methods of finding cooperativity within water clusters vary quite considerably. Numerous articles cite the equation developed by Ohno et al.[38] The equation proposed by Ohno et al. works in some cases but not in others, as pointed out by Bakó.[13]

Ahirwar et al.[39] considered water clusters ranging from $(H_2O)_n$, $n = 3 - 8$. As an energy value for H-bond cooperativity, the difference between the energy of a single H-bond in the water cluster and the energy of an H-bond in the water dimer was computed. Glendening[7] used natural energy decomposition analysis (NEDA) to explore the origin of cooperative effects in the dimer, trimer and tetramer water clusters. To calculate cooperativity, ~~he expanded~~ the total interaction

energy (ΔE_n) is expanded as a sum of many-body interactions in the same manner as Hankins *et al.*[37] used. The NEDA enables one to obtain a possible origin of cooperativity. Liu *et al.*[9] used far-infrared (FIR) laser vibration-rotation tunnelling (VRT) spectroscopy to first determine the existence of the trimer, tetramer and pentamer cyclic water clusters. They considered the O···O separation distance from experimental data as well as computed data to determine whether cooperative effects are present within experimentally determined structures. Neela *et al.*[15] looked at the complexation energy, which is the difference between the total energy of the water clusters and the energy of the number of water monomers present in the water cluster. They considered different water cluster arrangements to study the different forms of H-bonding observed. The arrangements of the water clusters were linear assembly, helical arrangement and caged structures obtained from the Cambridge Cluster Database.[40] They then calculated the complexation energy per H-bond for the different *n*-water clusters to quantify cooperativity. Two of the linear water cluster chains and a cage are shown in Figure 4.
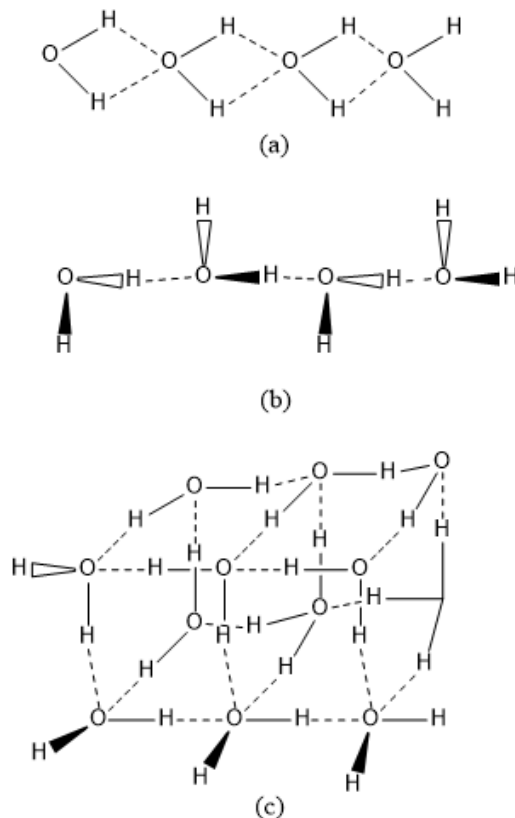
Figure 4 The (a, b) two linear configurations and (c) cage geometry used by Neela *et al.*[15] Figure reproduced from Neela *et al.*

In a 2015 paper by Saha and Sastry[41] (from the same research group) the same clusters were used, but they calculated an energy value termed the cooperative energy value, which is the difference between the total interaction energy and the pairwise interaction energy. Hence a negative value indicates cooperativity. Albrecht and Boyd[42] calculated the cooperativity energy contribution as the difference between the hydrogen bond energy per hydrogen bond (interaction energy divided by the number of H-bonds) and the interaction energy of a dimer. In addition, they constructed an unconventional trimer and tetramer shown in Figure 5. The trimer is made up of a double donor water molecule and two single acceptors. The trimer is in the form of a chain. The tetramer is made up of two double donors and two double acceptors and is still cyclic in this case. The trimer and tetramer are constructed to exhibit anti-cooperative behaviour. Methanol and formaldehyde clusters were also considered for investigating different cooperativity effects.
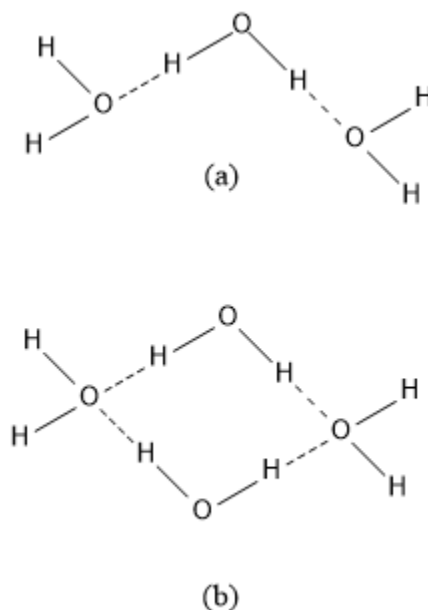
Figure 5 The unconventional (a) trimer and (b) tetramer constructed to show anti-cooperativity. Figure reproduced from Albrecht and Boyd.[42]

Marshall[43] extended the thermodynamic perturbation theory (TPT2) to include H-bond cooperativity in a 4-site water model (two acceptor sites and two donor sites). To do this they added a single adjustable parameter, namely hydrogen bond volume κ_{AB}, which made it possible to obtain an equation of state. The water-methanol water clusters are shown in Figure 6.
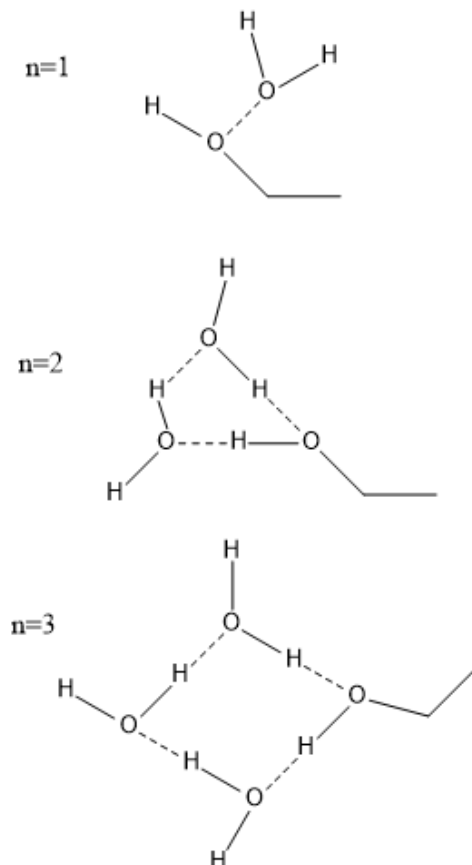
Figure 6 The water-methanol clusters using the same numbering as Marshall.[43] Figure reproduced from Marshall.

Ojamäe and Hermansson[44] investigated linear chains of varying length of water molecules, a pentamer cyclic water cluster and a water tetrahedron that consisted of a central water molecule and four water molecules bonded to it. They calculated the many-body interaction energy as E_{tot} and subtracted the energy of the same number of water monomers as the size of the water cluster under consideration. Interestingly, this paper was written 24 years after the paper by Hankins *et al.*, which used a similar energy calculation.

11

The calculation method used by Hankins *et al.* is also used by a few other authors[3,7,39,44] The energy approach is usually the first place to start when considering cooperativity in water clusters. The approach used by the above authors is localised only to the H-bond and generally does not consider whole water molecules or clusters.

Guevara-Vela *et al.*[45] investigated hydrogen bond cooperativity from the perspective of a real space Interacting Quantum Atoms (IQA)[46,47] and a QTAIM within small water clusters ((H_2O)$_n$, $n = 2 - 6$). They measured cooperative effects with $\Delta\Delta E$, which is defined as the difference between 1) the energy required to add a water molecule into the cluster, and 2) the formation energy of the intermolecular hydrogen bond in the water dimer. When the $\Delta\Delta E$ becomes negative, the inclusion of a water molecule in the system is more energetically favourable than an isolated hydrogen bond in a dimer and is therefore indicative of cooperativity. Due to the versatility of IQA, the research group was able to dig deep into the energetics of water clusters. Rong *et al.*[48] used a mathematical relation approach to investigate the origin of cooperativity. The water clusters considered ranged from ((H_2O)$_n$) $n = 1 - 20$. These authors used a cooperativity index to determine whether the cooperativity was positive or negative (negative cooperativity = anti-cooperativity). The cooperativity index is mathematically defined as the change of interaction energy per monomer unit as a function of the change in monomers within the molecular system or $\kappa = -(\partial E_n/\partial n)$. Boyd *et al.*[49] explored the atomic energies of different water cluster sizes, $n = 2 - 5$ using QTAIM. Moreover, they determined the molecular energy by taking the difference between the energy of the molecules and the number of monomers present within the molecule. They also determined the average H-bond energy, which is the formation energy divided by the number of H-bonds.

The method used by Guevara-Vela *et al.*[45] is similar to the approach taken in this dissertation, the only difference being the method of energy calculation used for the cooperative effects. The energetic values directly correlate with the analogous electronic values, which makes this an

attractive approach to cooperativity. Guevara-Vela *et al*. did not use a molecular-wide approach. The mathematical equation used by Rong *et al*.[48] incorporates more properties compared to the other methods. The method used by Boyd correlates well with the one used by our research group for the current study.

Koehler *et al*.[50] studied cooperativity within the tetramer water cyclic structure. These authors compared and calculated cooperativity using three different methodologies: 1) Cooperativity is calculated as an energy value derived from the difference between the interaction energy per H-bond for a tetramer and the interaction energy for a dimer. This is then divided by the interaction energy per H-bond for a tetramer. The answer is a value, which can be used to judge the cooperativity observed in the tetramer structure. The only caveat is that the dimer is used as a reference which the authors are trying to avoid because, according to them, the cooperativity of an H-bond should not depend on the system. 2) The non-additivity term is calculated as the addition of three- and four-body contributions and then divided by the interaction energy of the system (tetramer in this case). 3) The third and final coefficient is determined without a reference system: the sum of two-body, non-neighbour interactions, three-body, four-body and one-body deformation energy, which is then divided by the system's interaction energy.

Xu *et al*.[51] examined cooperativity within the context of hydrogen bond kinetics. They looked at the polarizability of water by using three solutions of pure water, aqueous NaCl and aqueous ethane. They investigated hydrogen bonds within the different solutions and examined the change in the kinetics of the H-bonds. They used molecular dynamics with the TIP4P/FQ model and took polarization into account. The breaking and forming of H-bonds correlate with the initial definition of cooperativity by Frank and Wen.[36]

Koehler *et al*. and Xu *et al*. used substantially different methods to explore cooperativity. The different approaches used by the two research groups give a different insight into this concept of cooperativity.

13

Han *et al.*[52] considered water clusters bonded with ethanol $((H_2O)_n, n = 1 - 5)$ to study the cooperative effects of hydrogen bonding within ethanol clusters as well as the cooperativity within pure water clusters. The n value here is the number of water molecules in the water cluster. The water-ethanol cluster consists of the known small water clusters each bonded with a single ethanol molecule. The cooperative effects observed for the mixed cluster are compared with those of pure water clusters. The cooperativity is quantified in two ways: 1) The mean H-bond strength is calculated by subtracting the electronic energy of both the water and the ethanol monomer from the total electronic energy. This subtracted value is then divided by the number of primary H-bonds (donor-acceptor fashion H-bonds). 2) The ratio of the donor covalent H-bond (O–H) redshift stretch and the redshift of the intermolecular H-bond (O–H$\cdots$O). This ratio is calculated from both the numerator and denominator redshift from a mixed water cluster or pure water. The cooperativity effects of the ethanol-water mixed cluster and pure water are then compared.

The comparison between these two types of clusters give an insight into the nature of H-bond cooperativity and the role that carbon plays. The influence of cooperativity on a molecular system is shown by the comparison of the pure and mixed clusters.

In 2000 Ludwig[53] wrote a review of liquid water (the theoretical representation of water as seen in nature) and showed the necessity of incorporating cooperativity in liquid water. Ludwig commented on the results, which point to cooperativity. The shortening of the oxygen atoms' interaction distances d(O$\cdots$O) in strong H-bond networks is due to H-bonding cooperativity. The charge transfer that takes place causes cooperativity with the following consequences: lengthening of the O-H covalent bond and shortening of the non-covalent H$\cdots$O H-bond, which result in the reduction of the overall separation distance between oxygen atoms d(O$\cdots$O). When the enthalpic component of water structures is taken into account, the cooperative bi-coordinate ring structures are favoured above the linear chain and star-like

structures. Ludwig's characteristics given for cooperativity are the foundation for cooperativity and are taken as a definitive result by all studies in various fields. Sastry[10] stated in his review paper that cooperativity is a non-additive effect, meaning that the sum of at least two pairs of interactions is larger than simple addition. The origin of H-bond cooperativity in water clusters is due to many-body interactions. The review by Mahadevi and Sastry[54] is much more up to date and focused on cooperativity. It discusses the cooperativity observed in various chemical systems that goes well beyond the cooperativity of only water clusters. The overview of cooperativity is fully explained and shown for different systems. The different possible origins of cooperativity within these various molecular systems are discussed as well. The review mentions the water cluster as a favourite for studying intermolecular interactions and the result of cooperativity. Gillian *et al.*[55] reviewed the results obtained from density functional theory (DFT) for water in its different forms (water clusters, ice structure and liquid water). There is a section that discusses the effects and results of cooperativity within small water clusters (H_2O_n, $n = 2 - 6$). The reader can consult these three reviews for a complete explanation of the concept of cooperativity in different chemical systems as this is beyond the scope of this literature study.

Hankins *et al.*[37] obtained negative values for the three-body potential for neighbouring water molecules in the trimer in addition to an overall increase in binding energy. The trimer linear chain orientated in the donor-acceptor fashion had the largest negative three-body potential. Xantheas[3] established that pairwise two-body interaction potentials can almost fully explain trimer and tetramer interaction energetic values, but from pentamer onwards the error will exceed 20% if three-body and higher non-additive terms are neglected. The most stable and highest increase in cooperative effects from dimer to pentamer occur when the water molecules are arranged in a donor-acceptor fashion. Ohno[38] found in their water clusters that the formation of one H-bond in the network leads to the enhancement of other H-bonds – the general concept of cooperativity. Four bands are observed with their magnitude equation: free O–H band, 4-

15

coordinated water band and two 3-coordinated water bands. These four bands correspond to different wave numbers. The O–H bands with the same magnitude for the equation have nearly the same wave number. The various answers to their equation found for the water clusters of size $n = 2 - 8$ are $M_{OH} = -1, 0, 1, 2, 3$ and 4. Magnitudes of -1 and 0 were found when an ether solution and a CCl_4 solution were introduced. The equation is rather a quantification taking cooperativity into account than a way to measure cooperativity. It was found that their equation works for any phase of water (i.e. liquid, ice).

Hankins' results are still used in various ways today even though this was the first SCF study on cooperativity in water clusters. Ohno's equation with relevant answers may possibly assist in finding a quick solution if a system is cooperative and the region of the wave number, but not the precise origin.

Ahirwar[39] found that the cooperativity energy value calculated corresponded to a decrease in H-bond energy as the cluster size increases. The lowest cooperativity value for a single H-bond corresponded to an H-bond within the heptamer water cluster. The 3D water clusters (prism, cage, book, heptamer and octamer) had significantly lower energy than the smaller 2D cyclic counterparts. It should also be noted that H-bond cooperativity is maximised for an interaction between an oxygen atom from a double H-bond donor and a hydrogen atom from a double H-bond acceptor. Interestingly, the cooperativity contributions calculated are similar for MP2 and CCSD levels of theory. Glendening[56] also found that three-body terms are primarily responsible for the cooperative effects or non-pairwise additivity stabilization in water clusters. The NEDA results showed that the dominating forces in the H-bond are electrostatic, polarization and charge transfer. The greatest cause of the cooperativity within the trimer and tetramer water cyclic water clusters is charge transfer and little polarization. Liu *et al.*[9] used the contraction of oxygen interaction distance (O···O) as proof of cooperative effects. The experimental results showed an exponential decrease in the separation distance between oxygen atoms for cyclic water clusters

16

ranging from dimer to pentamer. The trend they found experimentally agrees with theoretically predicted distances with MP2 and HF level of theory. The source of H-bond cooperativity is largely many-body effects. Neela *et al.*[15] found that the energy is much lower for the 3D water clusters compared to the 2D water chain. The cooperativity effects are much more evident when going from dimer to decamer ($n = 2 - 10$) than from decamer to eicosamer ($n = 10 - 20$). It can thus be concluded that a levelling-off or plateau is being reached or has already been reached at approximately $n = 10$ water cluster size. Moreover, they found that the H-bond strength is much greater in the 3D water clusters than it is in the 2D water clusters when considering the electron density at the bond critical point (BCP) (3,–1). In a paper by the same research group,[41] they calculated an energy value which they termed the cooperative energy value, which is the difference between the total interaction energy and the pairwise interaction energy. Hence a negative value indicates cooperativity and the authors reached the same conclusions as they did in their 2010 paper. Albrecht and Boyd[42] found that the cyclic water cluster exhibited cooperativity as the cluster size increased. These were the benchmarks against which the anti-cooperativity clusters are compared. The two anti-cooperativity water clusters are also compared. The double-donating trimer had half the stabilization increase than its cyclic counterpart. The tetramer, consisting of two double-donating and two double-accepting water molecules, was less stabilized and had less electron density at the bond critical points. The double-donating water molecules were more stabilized than the double-accepting water molecules. Additionally, when they compared the anti-cooperative trimer and tetramer, they found that the critical point electron density was lower for the tetramer than for the trimer, indicating that the four H-bonds were weaker than the two bonds formed in a linear trimer water chain. Lastly, the non-H-bonded hydrogens became destabilized and the oxygen atoms became more stabilized. The methanol cluster showed an increase in cooperativity as the cluster size increased which occurred in the water clusters. The methyl group displayed an insignificant increase in stability. The

17

formaldehyde clusters showed little cooperativity with cyclic clusters. The biggest difference in cooperativity occurred when the geometry of the clusters was changed to create different atomic interactions.

There is experimental evidence of the cooperativity phenomenon taking place within water clusters, making it an important property to gain a better understanding. It is therefore possible that experimental evidence can be obtained for an array of other systems other than water clusters. The effect of cooperativity within larger clusters is interesting and poses the question as to whether they are truly present in liquid water. Another possible interpretation of the results by Albrecht and Boyd is that the observed effects are not anti-cooperativity as the clusters do not become destabilized relative to the dimer – there is just a smaller increase in stability. The ambiguity of cooperativity is seen here in these authors' results.

Marshall[43] proved their extension of perturbation theory to be true by comparing the results with spectroscopy, neutron diffraction and molecular simulation data. The equation of state yielded by the extended perturbation theory had to be adjusted to fit water by substantially increasing the hydrogen bond volume. Ojamäe and Hermansson[44] found that the cooperativity effect increased with increasing chain length and observed the highest cooperativity in water molecules placed within the chain rather than at the edges. The cyclic pentamer water cluster had larger O–H stretching frequencies and non-additive frequency contributions compared to the linear chains. The polarization is the same for all water molecules in the cyclic pentamer but differs for the water molecules in the linear chain. However, the authors went further and defined strict cooperativity where all the many-body terms should match the two-body term sign. Furthermore, a negative sign means strict cooperativity and a positive sign means strict anti-cooperativity. This strict cooperativity is seen for all the linear water molecule chains as well as the pentamer ring. The tetrahedron only had cooperative effects and not strict cooperativity.

18

Guevara-Vela *et al.*[45] obtained numerous results proving the concept of cooperativity. The $\Delta\Delta E$ values are the most negative for trimer and tetramer, indicating that the cooperative effects are the strongest for these cyclic water clusters. Furthermore, they state that electron correlation is an important inclusion for cooperative effects. Cooperative effects of hydrogen bonding in small water clusters occur due to the partial cancellation of deformation and interaction energy. The cooperative effects of hydrogen bonding in water clusters are complemented by an increase in exchange repulsion (the sum of exchange energy and deformation energy). The increase of the exchange repulsion causes the electrostatic interpretation of H-bonds to become questionable. The delocalization indices of neighbouring oxygen atoms ($O\cdots O$), oxygen and hydrogen involved in an intermolecular H-bond ($O–H^{bonding}$) and neighbouring water molecules ($H_2O\cdots H_2O$) all increase with the size of the water cluster, thus cooperative effects are complemented by an increase in the number of delocalized electrons in the cyclic structures. As the water molecules increase there is a reduction in exchange, electron delocalization and electron density at the critical point for the covalent bond ($O–H^{bonding}$) forming part of the H-bond. The covalent character decreases so the stability of the intermolecular H-bond can increase. The cooperative effects of hydrogen bonding occur due to the formation of an exchange channel within the cyclic clusters. The polarization-assisted delocalization process is associated with cooperativity within cyclic water clusters. All these different properties contribute to the cooperative effects of the H-bond for small cyclic water clusters.

Rong *et al.*[48] found cooperativity with $(H_2O)_n$, $n = 1 – 20$. Exchange-correlation is the main contributor to the cooperative effect observed within water clusters. Moreover, the many-body energetic contribution also pointed to cooperative effects between water molecules. They found a linear relationship between total energy and Shannon entropy[57] as well as between total energy and Ghosh–Berkowitz–Parr entropy.[58] Boyd *et al.*[49] found a few cooperativity relationships within small cyclic water clusters. Charge transfer occurs between two water molecules,

19

according to Weinhold,[59] when the lone pair of the accepting oxygen atom interacts with the anti-bonding orbital of the O–H bond. When the anti-bonding orbital is occupied the O–H species is destabilized while the O is stabilized. This leads to an overall increase in stability, meaning that the cooperativity increases. The geometry effects associated with this are a decrease in O···O interaction length and an increase of O–H covalent bond distance, causing increased H-bond strength at the expense of a weakening O–H covalent bond. The dihedral angle of H–O···H moves closer to 180°. All of these mentioned effects due to charge transfer are observed within the water clusters. The hydrogen atoms pointing out of the cluster became destabilized. The change in atomic energy increased for all the atoms and tended to a maximum, which correlates with the exponential trend for cooperativity.

Guevara-Vela *et al.* showed that a truly cooperative system will exhibit several characteristics of cooperativity. There is an increase in stability, electron density and electron delocalization, covering three different aspects with which cooperativity takes place. According to our research group, the whole molecular system should be considered when investigating cooperativity using the Molecular Wide Electron Density (MOWED) approach.

Koehler *et al.*[50] noted that the cooperative effect is mainly due to the three-body contributions, which is calculated from induction energy, two-body and non-neighbouring interactions. The four-body term contributes to a total energy of only 1%. These authors also found elongation of the covalent O–H bond in the tetramer compared to the dimer, which according to them, results in large polarization and larger induction energy. Xu *et al.*[51] found that cooperativity occurs due to water polarizability. The polarizability of water causes the kinetics of H-bonds to be slower and causes the environment of the H-bond to have an effect. Han et al.[52] state that increased stability is correlated with an increased number of water molecules for both pure water clusters as well as ethanol-water clusters. Interestingly, they found larger cooperativity for ethanol-water clusters than for pure water clusters. The contributions to cooperativity in the ethanol clusters

originated from higher donor-acceptor fashion H-bonds, a shorter interaction distance for H-bonds, a longer O–H covalent bond length, lower binding energies and longer shifts of the O–H covalent stretching frequencies.

Conclusions

There are quite a number of ways in which authors have investigated the phenomenon of cooperativity within a variety of systems, but all the systems considered have one thing in common – the H-bond. Interaction energies have been used predominantly as an indicator of cooperativity as well as H-bond strength. Most of the time the authors normalized the values to be per water molecule or hydrogen bond so that a comparison can be made between diverse sizes of systems. The only problem that could possibly arise would be when comparing 2D cyclic and 3D water clusters since these convey cooperativity in different ways. As one can see, there are a few characteristics associated with cooperativity that are always found when investigating this phenomenon for H-bonds: decrease in energy, increased stability, shorter H-bond, longer covalent bond and longer stretching frequencies. An assumption that may be made is that cooperativity is responsible for the characteristics observed in water clusters due to its presence within the energetic and electronic parts – however, absolute quantification of the effect is difficult.

Problem statement

Cooperativity in water clusters is investigated from a variety of perspectives. All these perspectives have one thing in common: they only consider the two – four atoms involved in the H-bond. Little to no research has been done which considers the whole water cluster changing and adapting to atomic (localized) changes to ensure that the stability of the water cluster is optimal. In addition, although electron delocalization has been identified as the origin of

cooperativity (or is otherwise an important mechanistic consideration), measurement and interpretation of electron delocalization using reductionist, atomistic constructions is extremely difficult.

Aims and Objectives

The primary aim of the present study is to investigate the effect of cooperativity in water clusters from a molecular-wide perspective (MOWED) that stretches beyond the 2- or 3-atom paradigm. I hypothesize that the main mechanism for molecular-wide cooperativity is electron delocalization. The secondary aim is to investigate the stated hypothesis by looking at electron delocalization patterns within suitable water clusters. These aims will be pursued through the following objectives:

- Select suitable water cluster set for each of the two aims.
- Select a level of theory/basis set that will achieve the needed accuracy in the desired time.
- Select a suitable chemistry model to accurately optimize selected water clusters and produce corresponding wavefunctions for further analysis.
- Use software that can decompose the necessary molecular wide information needed for delocalization patterns.
- Analyse data and look for trends that show molecular wide phenomena.

Chapter Overviews

Overviews of the chapters here are intended to give the reader an idea of what to expect in this dissertation. The results are discussed in Chapter 3 to Chapter 5. Chapter 3 is the manuscript submitted to *Physical Chemistry Chemical Physics* journal. The dissertation provides the reader with a different perspective on cooperativity by taking a novel approach, namely the MOWED approach.

22

Chapter 2: The theoretical background is discussed in this chapter. It starts with Hartree-Fock theory and continues with its shortfalls. DFT is then discussed in some detail. The quantum nature of the electrons is also explained. The common basis sets used with DFT are explained with some mathematical descriptors. The chapter concludes with a description of the in-house developed software FALDI and FAMSEC. These two types of decomposition techniques are introduced and derived in detail to give the reader a clear understanding.

Chapter 3: The manuscript titled *Molecular-wide and electron density (MOWED)-based definition and quantification of cooperativity in cyclic water clusters* was submitted to the *Physical Chemistry Chemical Physics* journal. The idea of a molecular-wide perspective for cooperativity is introduced. The paper discusses a new perspective from which to consider cooperativity. The electronic energy is the main descriptor of the cyclic water clusters and includes all other properties. The cooperativity-induced effects equation is introduced to model a system illustrating these effects. The electronic energy then leads to the cornerstone of cooperativity, namely the number of electrons delocalized from a water fragment to the remaining fragments in the water cluster. The individual contributions from the intermolecular H-bond and fragments are focused on next to further demonstrate the electronic contributions from the whole water cluster to an H-bond within the water cluster. The FAMSEC energy components of the H-bond then show the degree to which they contribute to the stability of the water cluster. The 'highways' on which the electrons travelled are showcased next and new ones found are discussed. 1D cross-section is performed on the intermolecular H-bond to show the electronic contributions from other atoms in the water cluster. The 'highways' and 1D cross-section solidify the molecular-wide contribution of cyclic water clusters. The intramolecular electron counts are shown last. These electron counts include the electrons associated with a water fragment and delocalized within a water fragment. These electron counts show how water molecules delocalize electrons intramolecularly.

Chapter 4: The products resulting from cooperativity are explored. The atomic charges relating to the O and H atoms are considered first. The interaction energy is investigated as a total that consists of intramolecular and intermolecular interactions. The topological properties at the critical point are dealt with next to give an insight into what occurs at the critical point. Lastly, the geometrical descriptors are considered for the properties looked at previously in this chapter to find the relationship between intermolecular distance and energetic and electronic properties.

Chapter 5

3D hexamer water clusters are investigated using a similar methodology as Chapter 3. Firstly, the relative energies at various level of theories are compared to our level of theory. Secondly, the correlation between electronic energy and number of intermolecular delocalized electrons is explored. Intramolecular electron counts are then considered to find the relationship between intramolecular and intermolecular electron counts. Lastly, the 3D delocalization patterns are shown which serves as the most import result from this Chapter.

Chapter 6

This chapter contains conclusions and explains the most important results and future work that needs to be done.

References:

1 S. S. Xantheas, *J. Am. Chem. Soc.*, 1995, **117**, 10373–10380.

2 S. S. Xantheas, *J. Chem. Phys.*, 1995, **102**, 4505–4517.

3 S. S. Xantheas, *Chem. Phys.*, 2000, **258**, 225–231.

4 S. S. Xantheas and E. Aprà, *J. Chem. Phys.*, 2004, **120**, 823–828.

5 S. S. Xantheas and T. H. Dunning, *J. Chem. Phys.*, 1993, **99**, 8774–8792.

6 S. S. Xantheas and T. H. Dunning, *J. Chem. Phys.*, 1993, **98**, 8037–8040.

7 A. Rakshit, P. Bandyopadhyay, J. P. Heindel and S. S. Xantheas, *J. Chem. Phys.*, 2019, **151**, 214307–214318.

8 K. Liu, M. G. Brown, J. D. Cruzan and R. J. Saykally, *Science.*, 1996, **271**, 62–64.

9 K. Liu, J. D. Cruzan and R. J. Saykally, *Science*, 1996, **271**, 929–933.

10 K. Liu, M. G. Brown, C. Carter, R. J. Saykally, J. K. Gregory and D. C. Clary, *Nature*, 1996, **381**, 501–503.

11 T. R. Dyke, K. M. Mack and J. S. Muenter, *J. Chem. Phys.*, 2008, **66**, 498–510.

12 F. Weinhold, *J. Chem. Phys.*, 1998, **109**, 367–372.

13 I. Bakó and I. Mayer, *J. Phys. Chem. A*, 2016, **120**, 631–638.

14 V. S. Znamenskiy and M. E. Green, *J. Chem. Theory Comput.*, 2007, **3**, 103–114.

15 Y. I. Neela, A. S. Mahadevi and G. N. Sastry, *J. Phys. Chem. B*, 2010, **114**, 17162–17171.

16 Y. Tao, W. Zou, J. Jia, W. Li and D. Cremer, *J. Chem. Theory Comput.*, 2017, **13**, 55–76.

17 J. M. Guevara-Vela, E. Romero-Montalvo, V. A. Mora Gómez, R. Chávez-Calvillo, M. García-Revilla, E. Francisco, Á. M. Pendás and T. Rocha-Rinza, *Phys. Chem. Chem. Phys.*, 2016, **18**, 19557–19566.

18 G. Hincapié, N. Acelas, M. Castaño, J. David and A. Restrepo, *J. Phys. Chem. A*, 2010, **114**, 7809–7814.

19 L. Albrecht, S. Chowdhury and R. J. Boyd, *J. Phys. Chem. A*, 2013, **117**, 10790–10799.

20 R. K. Campen and J. D. Kubicki, *J. Comput. Chem.*, 2009, **31**, 963–972.

21 J. H. De Lange, D. M. E. Van Niekerk and I. Cukrowski, *J. Comput. Chem.*, 2018, **39**, 973–985.

22 J. H. De Lange and I. Cukrowski, *J. Comput. Chem.*, 2017, **38**, 981–997.

23 R. F. W. Bader, *Atoms in molecules: A quantum theory*, Clarendon Press, 1990.

24 G. N. Lewis, *J. Am. Chem. Soc.*, 1916, **38**, 762–785.

25 K. Fukui, T. Yonezawa and H. Shingu, *J. Chem. Phys.*, 1952, **20**, 722–725.

26 W. M. Latimer and W. H. Rodebush, *J. Chem. Phys.*, 1920, **42**, 1419–1433 .

27 G. R. Desiraju, *Acc. Chem. Res.*, 2002, **35**, 565–573.

28 L. Pauling and R. B. Corey, *Proc. Natl. Acad. Sci. U.S.A.*, 1951, **37**, 261–271.

29 J.-M. Lehn, *Angew. Chem. Int. Ed. Engl.*, 1988, **27**, 89–112.

30 E. Arunan, G. R. Desiraju, R. A. Klein, J. Sadlej, S. Scheiner, I. Alkorta, D. C. Clary, R. H. Crabtree, J. J. Dannenberg, P. Hobza, H. G. Kjaergaard, A. C. Legon, B. Mennucci and D. J. Nesbitt, *Pu. Appl. Chem.*, 2011, **83**, 1637–1641.

31 C. E. Dykstra, *Chem. Rev.*, 1993, **93**, 2339–2353.

32 P. Kollman, *J. Am. Chem. Soc.*, 1977, **99**, 4875–4894.

33 A. D. Buckingham and P. W. Fowler, *J. Chem. Phys.*, 1983, **79**, 6426–6428.

34 G. Nadig, L. C. Van Zant, S. L. Dixon and K. M. Merz, *J. Am. Chem. Soc.*, 1998, **120**, 5593–5594.

35 A. V. D. Vaart and K. M. Merz, Jr., *Int. J. Quant. Chem.*, 2000, **77**, 27–43.

36 H. S. Frank and W.-Y. Wen, *Discuss. Faraday Soc.*, 1957, **24**, 133–140.

37 D. Hankins, J. W. Moskowitz and F. H. Stillinger, *J. Chem. Phys.*, 1970, **53**, 4544–4554.

38 K. Ohno, M. Okimura, N. Akai and Y. Katsumoto, *Phys. Chem. Chem. Phys.*, 2005, **7**, 3005–30014.

39 M. B. Ahirwar, S. R. Gadre and M. M. Deshmukh, *J. Phys. Chem. A*, 2020, **124**, 6699–6706.

40 S. Maheshwary, N. Patel, N. Sathyamurthy, A. D. Kulkarni and S. R. Gadre, *J. Phys. Chem. A*, 2001, **105**, 10525–10537.

41 S. Saha and G. N. Sastry, *Mol. Phys.*, 2015, **113**, 3031–3041.

42 L. Albrecht and R. J. Boyd, *Comput. Theor. Chem.*, 2015, **1053**, 328–336.

43 B. D. Marshall, *J. Chem. Phys.*, 2017, **146**, 174104-174112.

44 L. Ojamaee and K. Hermansson, *J. Phys. Chem.*, 1994, **98**, 4271–4282.

45 J. M. Guevara-Vela, R. Chávez-Calvillo, M. García-Revilla, J. Hernández-Trujillo, O. Christiansen, E. Francisco, Á. M. Pendás and T. Rocha-Rinza, *Chem. Eur. J.*, 2013, **19**, 14304–14315.

46 M. A. Blanco, Á. M. Pendás and E. Francisco, *J. Chem. Theory Comput.*, 2005, **1**, 1096–1109.

47 E. Francisco, Á. M. Pendás and M. A. Blanco, *J. Chem. Theory Comput.*, 2006, **2**, 90–102.

48 C. Rong, D. Zhao, D. Yu and S. Liu, *Phys. Chem. Chem. Phys.*, 2018, **20**, 17990–17998.

49 L. Albrecht and R. J. Boyd, *J. Phys. Chem. A*, 2012, **116**, 3946–3951

50 J. E. H. Koehler, W. Saenger and B. Lesyng, *J. Comput. Chem.*, 1987, **8**, 1090–1098.

51 H. Xu, H. A. Stern and B. J. Berne, *J. Phys. Chem. B*, 2002, **106**, 2054–2060.

52 G. Han, Y. Ding, P. Qian, C. Zhang and W. Song, *Int. J. Quant. Chem.*, 2013, **113**, 1511–1521.

53 R. Ludwig, *Angew. Chem. Int. Ed.*, 2001, **40**, 1808–1827.

54 A. S. Mahadevi and G. N. Sastry, *Chem. Rev.* 2016, **116**, 2775–2825.

55 M. J. Gillan, D. Alfè, A. Michaelides, *J. Chem. Phys.*, 2016, **144**, 130901–130933.

56 E. D. Glendening, *J. Phys. Chem. A*, 2005, **109**, 11936–11940.

57 C. E. Shannon, *Bell Sys. Tech. J.*, 1948, **27**, 379–423.

58 S. K. Ghosh, M. Berkowitz and R. G. Parr, *Proc. Natl. Acad. Sci. U.S.A.*, 1984, **81**, 8028–8031.

59 F. Weinhold, *J. Mol. Struct. (THEOCHEM)*, 1997, **398–399**, 181–197.

Chapter 2

Theoretical Background

Introduction

Quantum chemistry is the overlap of chemistry and physics to explain chemical systems using quantum mechanics as the backbone and relating it to the knowledge of the 'traditional' chemist. Quantum chemistry is used in various fields today such as pharmaceuticals,[1] pyrometallurgy[2] and biochemistry[3] to model the behaviour of the chemical systems and obtain their physicochemical properties.

Theoretical models used to model chemical systems today consists of a wide range of level of theories which vary considerably in accuracy but increase in computational time as well. These models make it easier and quicker to find a possible direction to explore for a synthesis of an organic molecule for example. Modelling of chemical systems are inexpensive and shorter compared to lab work. There is, however, still a gap in quantum chemistry regarding the absolute results for a chemical system. The current models are closer to the true value than the original Hartree-Fock (HF) theory was. This work uses Density Functional Theory (DFT) as the level of theory, which builds upon the work of HF theory.

The main aim of this chapter is to give the reader a background on the different theoretical chemistry tools used within this research project. Beginning with the fundamentals: level of theory and basis set. Hartree Fock theory and Density Functional Theory (DFT) are explained in detail as the levels of theory followed by the basis set used. The basic framework for quantifying electron counts and charges QTAIM[4] is looked at, followed by FALDI,[5–9] cross-sections and finally FAMSEC.[10–13]

The derivation for Hartree-Fock theory and DFT is largely borrowed from the following quantum chemistry textbooks: A Chemist's Guide to Density Functional Theory,[14] Exploring Chemistry with Electronic structure Methods[15] and Essentials of Computational Chemistry: Theories and Models.[16]

Hartree Fock Theory

To explain the behaviour of a molecular system, it starts with the electronic Schrödinger equation:

$$E\Psi = \hat{H}\Psi = \frac{-\hbar^2}{2m}\nabla^2\Psi + V(x)\Psi \tag{1}$$

Where ψ is short for the full electronic wavefunction ($\Psi = \Psi_{elec}(\mathbf{r}_1, \mathbf{r}_2 \ldots \mathbf{r}_n)$) with the Born-Oppenheimer approximation. The first term is the kinetic energy of the electrons and nuclei and the second term is the potential energy part.

The energy (E) of the wave function equals the Hamiltonian operator ($\hat{H}$) of the wave function. The Hamiltonian operator is the addition of the kinetic and potential energy. The Schrödinger equation however cannot be solved for more than one electron simultaneously. Therefore, the Hamiltonian needs to change to accommodate only one electron:

$$\hat{H} = \sum_{i=1}^{N} \hat{h}_i \tag{2}$$

where N is the total number of electrons and $\hat{h}_i$ the Hamiltonian operator for one electron. The sum of all the one electron Hamiltonians of the molecular system then becomes the main Hamiltonian operator, which is also separable. The single electron Hamiltonian is defined as:

$$\hat{h}_i = -\frac{1}{2}\nabla_i^2 - \sum_{K=1}^{M} \frac{Z_k}{r_{ik}} \tag{3}$$

where M is the total number of nuclei, Z_k is the charge of nucleus k and r_{ik} is the distance between electron i and nucleus k. The one-electron Hamiltonian eigenfunctions should satisfy the one-electron Schrödinger equation. To illustrate the role of quantum-mechanical exchange, I start with the Hartree-products first.

$$\hat{h}_i\psi_i = \varepsilon_i\psi_i \tag{4}$$

Due to the separable nature of the Hamiltonian, it is possible to use the products of the one-electron eigenfunctions.

$$\Psi_{\text{HP}} = \psi_1 \psi_2 \cdots \psi_N \tag{5}$$

The subscript HP denotes the Hartree product. Making it possible to obtain a solution as a start. The eigenvalue can be obtained by using the operator introduced in Equation 2.

$$\Psi_{\text{HP}} = \psi_1 \psi_2 \cdots \psi_N$$
$$\Psi_{\text{HP}} = \left(\sum_{i=1}^{N} \varepsilon_i\right) \Psi_{\text{HP}} \tag{6}$$

There is no interelectronic repulsion with Equations 2 and 3 because both equations utilise a single electron Hamiltonian. The Hamiltonian does not compute the energies accurately enough; finding the orbitals (ψ) that minimise $\langle \Psi_{\text{HP}} | \hat{H} | \Psi_{\text{HP}} \rangle$ will improve the energy calculation. This is achieved by making each ψ an eigenfunction of the operator $\hat{h}_i$:

$$\hat{h}_i = -\frac{1}{2}\nabla_i^2 - \sum_{K=1}^{M} \frac{Z_k}{r_{ik}} + V_i\{j\} \tag{7}$$

where

$$V_i\{j\} = \sum_{i \neq j} \int \frac{\rho_j}{r_{ij}} \, d\boldsymbol{r} \tag{8}$$

The third term in Equation 7 [$V_i\{j\}$] represents the interaction potential of an electron with all other electrons in orbitals $\{j\}$, and ρ_j represents the charge density linked with electron j.

The problem that arises from using Equation 7 is that the desired solution to (ψ) which minimizes the energy is not a one-electron Hamiltonian. The solution to this is the idea suggested by Hartree: the self-consistent field (SCF) method. One then gives an initial guess for ψ to minimise the energy and takes the difference between the guess function and the previous energy, which is repeated until an arbitrary threshold yields a converged value. The Hartree-product wavefunction is, however, not a valid solution to the Schrodinger equation, it is not antisymmetric and clearly distinguishes between electrons. Practically speaking, the Hartree-product

31

wavefunction does not account for any correlation between electrons (which results from the wave-nature of the electron). A simple correction can be made, however, to ensure antisymmetry and electron indistinguishability – that of a Slater determinant, as discussed below.

Either electrons in the orbital are paired (i.e.one electron spin up and the other spin down) or parallel (i.e. both spin up and spin down) spin when there are two electrons placed in the orbital. The Pauli Exclusion Principle states that no two electrons can have the same quantum number – α or β – resulting in paired electrons with doubly occupied orbitals.

Take a Hartree-Product wave function with the same spin electrons yields:

$$^3\Psi_{HP} = \psi_a(1)\alpha(1)\psi_b(2)\alpha(2) \tag{9}$$

where superscript 3 denotes the Hartree-Product triplet state and ψ_a, ψ_b are two different orbitals that are orthonormal. The electronic wave function needs to comply with the Pauli exclusion principle to be valid. The wave function should have a change in sign to be considered valid or antisymmetric. The Pauli exclusion principle does not hold for the triplet state of the Hartree Product (Equation 9), this is shown with a variation operator $\hat{\omega}_{ij}$ that switches the coordination of electrons i and j:

$$\hat{\omega}_{12}[\psi_a(1)\alpha(1)\psi_b(2)\alpha(2)] = \psi_b(1)\alpha(1)\psi_a(2)\alpha(2)$$
$$\neq -\psi_b(1)\alpha(1)\psi_a(2)\alpha(2) \tag{10}$$

The Hartree-Product can be changed to be antisymmetric with a small iteration to Equation 9. The new function is called the Slater determinant:

$$^3\Psi_{SD} = \frac{1}{\sqrt{2}}[\psi_a(1)\alpha(1)\psi_b(2)\alpha(2) - \psi_a(2)\alpha(2)\psi_b(1)\alpha(1)] \tag{11}$$

formulated differently:

$$^3\Psi_{SD} = \frac{1}{\sqrt{2}}\begin{vmatrix} \psi_a(1)\alpha(1) & \psi_b(1)\alpha(1) \\ \psi_a(2)\alpha(2) & \psi_b(2)\alpha(2) \end{vmatrix} \tag{12}$$

more formally defined as:

32

$$\Psi_{SD} = \frac{1}{\sqrt{N!}} \begin{vmatrix} \chi_1(1) & \chi_2(1) & \cdots & \chi_N(1) \\ \chi_1(2) & \chi_2(2) & \cdots & \chi_N(2) \\ \vdots & \vdots & \ddots & \vdots \\ \chi_1(N) & \chi_2(N) & \cdots & \chi_N(N) \end{vmatrix} \tag{13}$$

where χ is the spin orbital obtained from the spatial orbital (ψ) and electron spin eigenfunction (α or β) product.

The Hartree Product is calculated the same as the Hartree-Fock orbitals: eigenfunctions of the product of one electron Hamiltonian operators. However, the Hartree Product now includes the average potential field effect of the other electrons with exchange effects on the Coulomb repulsion. The previous modification of the Hartree Product into the Slater determinant did not include exchange effects for paired electron spins.

The spin orbitals individual components were investigated until now, but the spin orbital is made from a combination of basis functions:

$$\chi_j = \sum_{i=1}^{N} a_{ij} \varphi_i \tag{14}$$

When Equation 14 is introduced into the equations mentioned above, it results in the Roothan equations – describing Hartree-Fock calculations as matrix algebraic equations.

The one electron Fock operator ($\hat{f}_i$) for electron i is defined as:

$$\hat{f}_i = -\frac{1}{2}\nabla^2 - \sum_{k}^{M} \frac{Z_k}{r_{ik}} + V_i^{HF}\{j\} \tag{15}$$

Similarly, when the one electron eigenfunction is defined in Equation 7. Making it possible to calculate the Hartree-Fock molecular orbitals (MO) by solving the secular equation as part of the Roothan approach:

$$\begin{vmatrix} F_{11} - ES_{11} & F_{12} - ES_{12} & \cdots & F_{1N} - ES_{1N} \\ F_{21} - ES_{21} & F_{22} - ES_{22} & \cdots & F_{2N} - ES_{2N} \\ \vdots & \vdots & \ddots & \vdots \\ F_{N1} - ES_{N1} & F_{N2} - ES_{N2} & \cdots & F_{NN} - ES_{NN} \end{vmatrix} = 0 \tag{16}$$

where S is the overlap matrix:

33

$$S = \begin{vmatrix} S_{11} & S_{12} & \cdots & S_{1N} \\ S_{21} & S_{22} & \cdots & S_{2N} \\ \vdots & \vdots & \ddots & \vdots \\ S_{N1} & S_{N2} & \cdots & S_{NN} \end{vmatrix} \tag{17}$$

or shorter defined as:

$$S_{ik} = \int \varphi_i \varphi_k \, d\tau \tag{18}$$

and $F_{\mu v}$ is the Fock matrix element; defined as:

$$F_{\mu v} = \left\langle \mu \left| -\frac{1}{2} \nabla^2 \right| v \right\rangle - \sum_{k}^{M} Z_k \left\langle \mu \left| \frac{1}{r_k} \right| v \right\rangle + \sum_{\lambda \sigma} P_{\lambda \sigma} \left[(\mu v | \lambda \sigma) - \frac{1}{2} (\mu \lambda | v \sigma) \right] \tag{19}$$

The final term on the right-hand side of Equation 19 shows the electron-electron repulsion made up of Coulomb repulsion $(\mu v | \lambda \sigma)$ and Exchange energy $(\mu \lambda | v \sigma)$; halved due to only half the electrons affected.

$P_{\lambda \sigma}$ is the density matrix element:

$$P_{\lambda \sigma} = 2 \sum_{i}^{occopied} a_{\mu i} a_{v i} \tag{20}$$

The coefficients $(a_{\mu i}, a_{v i})$ is the contribution from each basis function to molecular orbital i.

The same problem, one electron Hamiltonian, as mentioned above occurs when one solves the secular equation because the orbital coefficient $(a_{\mu i}, a_{v i})$ is needed to solve the density matrix P. Creating the problem of finding an answer (orbital coefficients) from the density matrix that is obtained from the Fock matrix element. In order to circumvent this one simply uses the SCF method mentioned earlier where, and initial guess is made for the orbital coefficients until the energies converge.

Hartree Fock theory is useful for obtaining a base level prediction for various chemical systems. It unfortunately has drawbacks such as omitting electron correlation due to the one electron fashion. Furthermore, the magnitude of approximations made lends itself to errors; with every electron existing within the domain of a nuclei. This leads to the influence being averaged over all

electrons with the same spin and omitting the effect of opposite spins. However, laying the foundation for computational models.

Density Function Theory

The density is calculated first followed by the wave function. From the start it is already different compared to Hartree Fock's theory which uses the inverse. As stated above there are a few shortcomings that should be addressed.

DFT is developed with two theorems from Hohenberg and Kohn in 1964. These two theorems have laid the foundation on which all forms of DFT are built on.

Theorem 1:

Electron density gives all the properties of a system meaning it can be used to determine the Hamiltonian operator:

$$\hat{H} = \hat{T} + \hat{V}_{ee} + \hat{V}_{ext} \tag{21}$$

where $\hat{T}$ is the kinetic energy operator, $\hat{V}_{ee}$ is the electron-electron repulsion operator and $\hat{V}_{ext}$ is the external potential operator, furthermore proving that the ground state electron density can only be described by $\hat{V}_{ext}$ as it uniquely defines $\hat{V}_{ext}$. The ground state electron density makes it possible then to obtain the Hamiltonian operator used to obtain the wave function and further the energy. The ground state energy is a functional of the ground state electron density meaning that the energy will then also be a ground state function:

$$E_0[\rho_0] = T[\rho_0] + E_{ee}[\rho_0] + E_{ne}[\rho_0] \tag{22}$$

The ground state energy function can then be divided into properties that depend on the system and others that do not:

$$E_0[\rho_0] = \int \rho_0(\mathbf{r}) V_{ne} d\mathbf{r} + T[\rho_0] + E_{ee}[\rho_0] \tag{23}$$

The first term is system dependant with second and third system independent. The second and third terms can then be combined to form the Hohenberg-Kohn functional:

$$E_0[\rho_0] = \int \rho_0(\mathbf{r})V_{ne}d\mathbf{r} + F_{HK}[\rho_0] \tag{24}$$

The Hohenberg-Kohn functional makes it possible to obtain the ground state wave function with an arbitrary density. The Hohenberg-Kohn functional without the ground state can be defined as:

$$F_{HK}[\rho] = T[\rho] + E_{ee}[\rho] = \langle \Psi|\hat{T} + \hat{V}_{ee}|\Psi\rangle \tag{25}$$

The Hohenberg-Kohn functional or universal functional is the basis for DFT. The Schrödinger equation's exact solution can be obtained in this manner if the Hohenberg-Kohn function is known exactly. This functional is independent from the system used. Furthermore, the kinetic energy $T[\rho]$ and electron-electron repulsion is contained within this functional; the explicit form of these two properties is not known.

The electron-electron repulsion can be defined as:

$$E_{ee}[\rho] = \frac{1}{2}\int\int \frac{\rho(r_1)\rho(r_2)}{r_{12}}dr_1dr_2 + E_{net}[\rho] = J[\rho] + E_{net}[\rho] \tag{26}$$

where $E_{net}[\rho]$ is the effect of all the non-classical interactions such as self-interaction correction as well as exchange and Coulomb correlation. $J[\rho]$ is the classical Coulomb contribution.

Second theorem:

The second theorem continues from the first, by using the variation principle - The lowest energy is only obtained when the ground state density is used. Expressed as:

$$E_0 \leq E[\tilde{\rho}] = T[\tilde{\rho}] + E_{ne}[\tilde{\rho}] + E_{ee}[\tilde{\rho}] \tag{27}$$

Meaning that if $\tilde{\rho}(r) \geq 0$ and $\int \tilde{\rho}(r)dr = N$ holds and is associated with some external potential $\hat{V}_{ext}$, then for any trial density $\tilde{\rho}(r)$, the energy value obtained from Equation 22 will be the upper limit for the ground state energy. The true ground state energy is only obtained when the true ground state density is used.

Any trial density $\tilde{\rho}(\mathbf{r})$ defines its own Hamiltonian $\hat{H}$ and thus its own wave function $\tilde{\Psi}$. This wave function can now be used as the trial wave function from the Hamiltonian generated from the true external potential $\hat{V}_{ext}$. Resuting in:

$$\langle\tilde{\Psi}|\hat{H}|\tilde{\Psi}\rangle = T[\tilde{\rho}] + V_{ee}[\tilde{\rho}] + \int \tilde{\rho}(\mathbf{r})V_{ext}d\mathbf{r} = E[\tilde{\rho}] \geq E_0[\rho_0] = \langle\Psi_0|\hat{H}|\Psi_0\rangle \qquad (28)$$

The variational principle can be seen in a different way due to the Hohenberg-Kohn. Starting with the variational approach:

$$E_0 = \min_{\Psi \to N}\langle\Psi|\hat{T} + \hat{V}_{ne} + \hat{V}_{ee}|\Psi\rangle \qquad (29)$$

Equation 29 searches over all the valid antisymmetric *N*-electron wave functions to obtain the one with the lowest value of the Hamiltonian operator (energy in this case) is the ground state wave function.

The search for the minimum should be performed in two steps to connect it to density functional theory. Firstly, search over the subset of the infinite antisymmetric wave functions Ψ^X that yields a corresponding ρ_X when squared (with the constraint of density integrating to the correct number of electrons). The wave function Ψ^X_{min} yielding the lowest energy for the corresponding density ρ_X is obtained. The second step eliminates the constraint and searches over all densities ρ_τ where τ = a, b, ..., *X*, ... to obtain the ground state energy. The lowest energy wave function resulting is then Ψ^τ_{min} from the first step. The method used for the minimization in density functional theory is known as the Levy constrained search defined as:

$$E_0 = \min_{\rho \to N}\left(\min_{\Psi \to \rho}\langle\Psi|\hat{T} + \hat{V}_{ne} + \hat{V}_{ee}|\Psi\rangle\right) \qquad (30)$$

where the inner and outer minimizations relate to the first and second step above, respectively.

The external potential energy is obtained from the density and independent from the wave function yielding that density. This holds for all wave functions allowing the kinetic and electron-electron repulsion to be separated:

37

$$E_0 = \min_{\rho \to N} \left(\min_{\Psi \to \rho} \langle \Psi | \hat{T} + \hat{V}_{ee} | \Psi \rangle + \int \tilde{\rho}(\mathbf{r}) V_{ne} d\,\mathbf{r} \right) \tag{31}$$

The universal functional can also be introduced:

$$F[\rho] = \min_{\Psi \to \rho} \langle \Psi | \hat{T} + \hat{V}_{ee} | \Psi \rangle \tag{32}$$

resulting in:

$$E_0 = \min_{\rho \to N} \left(F[\rho] + \int \tilde{\rho}(\mathbf{r}) V_{ne} d\mathbf{r} \right) \tag{33}$$

Any density introduced to Equation 33 will yield the energy and when minimization is done the ground state density as well as the ground state energy. Noteworthy, is that $F[\rho]$ differs from $F_{HK}[\rho]$ (Equation 25) in that $F_{HK}[\rho]$ is defined for all densities from an antisymmetric wave function. When the constrained search is performed with the ground state density ρ_0 there will only be one wave function associated with that ground state energy for the ground state density ρ_0 found.

Kohn-Sham Approach

The Kohn-Sham approach builds on the foundation of DFT laid down by Hohenberg and Kohn. Kohn and Sham give an approach for the unknown universal functional.

Following from Equation 33 the universal functional $F[\rho]$ contains the contribution from kinetic energy and electron-electron repulsion that is made up of the classical Coulombic interactions and non-classical self-interaction, exchange and electron correlation effects:

$$F[\rho(\mathbf{r})] = T[\rho(\mathbf{r})] + J[\rho(\mathbf{r})] + E_{net}[\rho(\mathbf{r})] \tag{34}$$

The only known variable is $J[\rho(\mathbf{r})]$; the explicit form of other two terms are unknown.

The problem that occurs here is the accurate determination of the kinetic energy; Kohn and Sham approached this problem by computing as much of the kinetic energy as possible. The remaining is then dealt with in an approximation manner.

Kohn and Sham start with the Hartree-Fock theory, where the wave function is a single slater determinant made up from N spin orbitals. Remember that the Slater determinant wave function is

a fictitious system that consists of N non-interacting electrons. It is therefore an exact wave function with no Coulomb interactions. The kinetic energy can be expressed exactly as:

$$T_{\text{HF}} = -\frac{1}{2} \sum_i^N \langle \chi_i | \nabla^2 | \chi_i \rangle \tag{35}$$

The HF spin orbitals in Equation 35 forms the lowest energy E_{HF} where χ_i is orthonormal.

$$E_{\text{HF}} = \min_{\phi_{\text{SD}} \to \text{N}} \langle \phi_{\text{SD}} | \hat{T} + \hat{V}_{ne} + \hat{V}_{ee} | \phi_{\text{SD}} \rangle \tag{36}$$

Both the equations above are needed to build on, in order to define the kinetic energy for density functional theory. Next is to set up a non-interacting reference system with Hamiltonian that has a local potential $V_S(\mathbf{r})$:

$$\hat{H}_s = -\frac{1}{2} \sum_i^N \nabla_i^2 + \sum_i^N V_s(\mathbf{r}_i) \tag{37}$$

Due to there not being any electron-electron interactions the Hamiltonian operator is for a non-interacting system. Resulting in a new ground state Slater determinant wave function (using Θ_s and φ instead of Ψ_{SD} and χ to show a new function different from the Hartree-Fock)

$$\Theta_s = \frac{1}{\sqrt{N!}} \begin{vmatrix} \varphi_1(1) & \varphi_2(1) & \cdots & \varphi_1(1) \\ \varphi_1(2) & \varphi_2(2) & \cdots & \varphi_1(2) \\ \vdots & \vdots & \ddots & \vdots \\ \varphi_1(N) & \varphi_2(N) & \cdots & \varphi_N(N) \end{vmatrix} \tag{38}$$

where the spin orbitals are determined as:

$$\hat{f}^{\text{KS}} \varphi_i = \varepsilon_i \varphi_i \tag{39}$$

where $\hat{f}^{\text{KS}}$ is the one electron Kohn-Sham operator defined as:

$$\hat{f}^{\text{KS}} = -\frac{1}{2} \nabla^2 + V_S(\mathbf{r}) \tag{40}$$

The orbitals established from Equations 38-40 is different from the Hartree-Fock ones and thus called Kohn-Sham orbitals. The need for the new different orbitals is due to the effective potentials $V_S(\mathbf{r})$ that causes the square of the orbitals to be the ground state density for the molecular system of interacting electrons.

$$\rho_s(\vec{r}) = \sum_i^N \sum_s |\varphi_i(\mathbf{r}, s)|^2 = \rho_0(\mathbf{r}) \tag{41}$$

The same problem where the kinetic energy can't be determined is seen here. One can compute as much as possible of the kinetic energy and approximate the rest as suggested by Kohn-Sham. Thus, use Equation 35 to predict the kinetic energy with the same density as for the interacting system, although Equation 35 uses no interactions.

$$T_S = -\frac{1}{2} \sum_i^N \langle \varphi_i | \nabla^2 | \varphi_i \rangle \tag{42}$$

Naturally the kinetic energy of the non-interacting and interacting system will not match even with the same density (e.g., $T_s \neq T$). Kohn-Sham had a work-around by separating $F[\rho(\mathbf{r})]$ (Equation 34):

$$F[\rho(\mathbf{r})] = T_s[\rho(\mathbf{r})] + J[\rho(\mathbf{r})] + E_{XC}[\rho(\mathbf{r})] \tag{43}$$

where E_{XC} is the exchange-correlation energy expressed as:

$$E_{XC}[\rho] \equiv (T[\rho] - T_s[\rho]) + (E_{ee}[\rho] - J[\rho]) = T_C[\rho] + E_{net}[\rho] \tag{44}$$

$T_C[\rho]$ represents a residual part added to the non-classical electrostatic contribution, $T_s[\rho]$ does not include this residual part. The exchange-correlation energy functional E_{XC} contains all the unknowns that are difficult to define. However, $E_{XC}[\rho]$ contains the potential energy non-classical effects due to self-interaction correction (exchange and correlation) and a small portion of the kinetic energy.

The energy equation for a non-interacting system is made up of two contributions namely the kinetic energy and the energy resulting from interaction with an external potential. The Hohenberg-Kohn theorem states that the energy must be a function of density. The same applies to the interaction with the external potential. It is difficult to fully quantify $T_s[\rho]$ because Equation 42 contains the Kohn-Sham orbitals but not the density.

Next it is necessary to define the orbitals in the non-interacting system uniquely; done by defining $V_S(\mathbf{r})$ with a Slater determinant containing the same density as the interacting system. The way to solve this is by using the energy expression of the interacting system but using the separations showed in Equation 43 and defining it in terms of the orbitals (Equations 41 and 42) as:

$$
\begin{aligned}
E[\rho(\mathbf{r})] &= T_s[\rho(\mathbf{r})] + J[\rho(\mathbf{r})] + E_{XC}[\rho(\mathbf{r})] + E_{ne}[\rho] \\
&= T_S[\rho] + \frac{1}{2}\int\int \frac{\rho(\mathbf{r}_1)\rho(\mathbf{r}_2)}{r_{12}}d\mathbf{r}_1 d\mathbf{r}_2 + E_{XC}[\rho] + \int V_{ne}\rho(\mathbf{r})d\mathbf{r} \\
&= -\frac{1}{2}\sum_i^N \langle\varphi_i|\nabla^2|\varphi_i\rangle + \frac{1}{2}\sum_i^N\sum_j^N \int\int |\varphi_i(\mathbf{r}_1)|^2 \frac{1}{r_{12}}|\varphi_j(\mathbf{r}_2)|^2 d\mathbf{r}_1 d\mathbf{r}_2 \\
&\quad + E_{XC}[\rho(\mathbf{r})] - \sum_i^N \int\sum_A^M \frac{Z_A}{r_{1A}}|\varphi_i(\mathbf{r}_1)|^2 d\mathbf{r}_1
\end{aligned}
\tag{45}
$$

The E_{XC} is again the only unknown resulting in the variational principle being used again as with Hartree-Fock approximations. The energy expression should be minimized with the constraint $\langle\varphi_i|\varphi_j\rangle = \delta_{ij}$ resulting in:

$$
\begin{aligned}
&\left(-\frac{1}{2}\nabla^2 + \left[\int \frac{\rho(\mathbf{r}_2)}{r_{12}}d\mathbf{r}_2 + V_{XC}(\mathbf{r}_1) - \sum_A^M \frac{Z_A}{r_{1A}}\right]\right)\varphi_i \\
&= \left(-\frac{1}{2}\nabla^2 + V_{\text{eff}}(\mathbf{r}_1)\right)\varphi_i = \varepsilon_i\varphi_i
\end{aligned}
\tag{46}
$$

where $V_{\text{eff}}(\mathbf{r}_1)$ is the same as $V_S(\mathbf{r})$ (seen in Equation 40). This is only a snippet from the end of the derivation from Parr and Weitao.[17]

$$
V_S(\mathbf{r}) \equiv V_{eff}(\mathbf{r}) = \int \frac{\rho(\mathbf{r}_2)}{r_{12}}d\mathbf{r}_2 + V_{XC}(\mathbf{r}_1) - \sum_A^M \frac{Z_A}{r_{1A}}
\tag{47}
$$

Once all the contributions for Equation 47 is known it can be inserted into Equation 45. This then leads to the ground state density and further ground state energy. Importantly $V_{\text{eff}}(\mathbf{r}_1)$ depends

on the density and orbitals due to the Coulomb term ($J[\rho(\mathbf{r})]$). The sane principle is followed again where the energy is calculated until there is a convergence.

Continuing with the exchange-correlation potential (V_{XC}) from the corresponding energy E_{XC}. The explicit form is not known for the exchange-correlation, where it is only possible to define it as the functional derivative E_{XC}:

$$V_{XC} = \frac{\delta E_{XC}}{\delta_\rho} \tag{48}$$

If the E_{XC} and V_{XC} were known exactly the exact solution would also be known.

There is a difference between the exchange and the correlation. These two concepts are quantified in Hartree-Fock theory but have a different meaning with Kohn-Shan equations.

Exchange and Correlation

It is important to now give a further explanation on exchange and correlation. Let's start with electrons that move in a correlated fashion meaning that all the electrons in real time affect each other. Thus, the big emphasis on using an interacting system and not a one-electron non-interacting one. The correlation can be calculated by starting with correlated probabilities: when there is an electron at r_1 this will impact the probability of finding an electron at $\mathbf{r}_2$.

$$\rho_2(\mathbf{r}_1, \mathbf{r}_2) = \rho(\mathbf{r}_1)\rho(\mathbf{r}_2)[1 + f_c(\mathbf{r})] \tag{49}$$

f_c is a correlation factor here.

The problem that arises in Hartree-Fock theory is that electrons with parallel spins are correlated whereas opposite spin are not. For a given two-electron wavefunction in a triplet state:

$$\left| {}^3\Psi(x_1 x_2) \right|^2 \neq \rho(\mathbf{r}_1)\rho(\mathbf{r}_2) \tag{50}$$

Remember Equation 9 (${}^3\Psi_{HP} = \psi_a(1)\alpha(1)\psi_b(2)\alpha(2)$) is the Hartree Product. Hartree-Fock theory does not describe instantaneous electron-electron repulsion between two electrons but

42

rather treats it in an average manner. Hartree-Fock theory only accounts for exchange or Fermi correlation but not Coulomb correlation.

To illustrate this problem further, another important probability to determine is the conditional probability, which is the probability of finding an electron at $\mathbf{r}_2$ if there is already an electron at $\mathbf{r}_1$:

$$\vartheta(r_1; r_2) = \frac{\rho_2(\mathbf{r}_1, \mathbf{r}_2)}{\rho(\mathbf{r}_1)} \tag{51}$$

Following this is the difference between the conditional and uncorrelated density at $\mathbf{r}_2$:

$$h_{XC}(r_1; r_2) = \frac{\rho_2(\mathbf{r}_1, \mathbf{r}_2)}{\rho(\mathbf{r}_1)} - \rho(\mathbf{r}_2) = \rho(\mathbf{r}_2)f(\mathbf{r}_1; \mathbf{r}_2) \tag{52}$$

where h_{XC} is the exchange-correlation electron hole.

$$h_{XC}(r_1; r_2) = h_x^{\sigma=\sigma} + h_c^{\sigma,\sigma} \tag{53}$$

Fermi Holes

$$\int h_X(\mathbf{r}_1; \mathbf{r}_2)\, d\mathbf{r}_2 = -1 \tag{54}$$

The Pauli exclusion principle causes electrons to be excluded around an electron. The Fermi hole is negative over all space and excludes a total of 1 electron. The Fermi hole is usually localized around the probe electron (at $\mathbf{r}_1$ in this case), on the other hand a correlated system will cause the hole to be delocalized over an entire molecular system.

Coulomb Holes

$$\int h_C(\mathbf{r}_1; \mathbf{r}_2)\, d\mathbf{r}_2 = 0 \tag{55}$$

Instantaneous (non-average) electron-electron repulsion causes a decrease in the probability of finding another electron with the probe electron at $\mathbf{r}_1$ but also an increase in probability of finding an electron. The Coulomb hole can be positive or negative but integrate to zero.

It is only through the combined evaluation of both Coulomb and Fermi holes that an accurate depiction of short- and long-range electron probabilities are observed, which itself only occurs when electrons are fully and dynamically correlated.

Basis Set

The theoretical background for basis sets is extracted from Quantum chemistry by Levine.[18] The first part serves as a mathematic description of a basis set and the second part explains the basis set used in this work.

The right basis set for any molecular system is of utmost importance to the success of any computational calculation. In essence, a basis set is a mathematical function used to describe the orbitals used to preform calculations on a molecular system. There exist two types of orbitals used namely: Gaussian type orbitals (GTO) and Slater type orbitals (STO). Where Gaussian type orbitals consists of a Gaussian curve or bell shape to describe an orbital and Slater uses the tail of the Gaussian curve enabling to calculate electrons further from the nucleus. The GTO is expressed as when centred on atom b:

$$g_{ijk} = N x_b^i y_b^i z_b^k e^{-\alpha r_b^2} \tag{56}$$

where i, j and k are non-negative integers, α is the orbital exponent, which is positive, and x_b^i, y_b^i and z_b^k are Cartesian coordinates with origin at nucleus b. Lastly, r_b is the distance to nucleus b. The function can be normalized yielding:

$$N = \left(\frac{2\alpha}{\pi}\right)^{\frac{3}{4}} \left[\frac{(8\alpha)^{i+j+k} i! \, j! \, k!}{(2i)! \, (2j)! \, (2k)!}\right]^{\frac{1}{2}} \tag{57}$$

Different integer values for i, j and k yields s,p,d,f etc. type Gaussian, i.e. $i + j + k = 0$ is s-type, $i + j + k = 1$ is p-type etc. The d-type Gaussian has six factors: x_b^2, y_b^2, z_b^2, $x_b y_b$, $x_b z_b$ and $y_b z_b$ as and example. The $3d$ orbital can be shown with five linear combinations $x_b y_b$, $x_b z_b$, $y_b z_b$, $x_b^2 - y_b^2$ and $3z_b^2 - r_b^2$ as the factors that have the same angular momentum as the five real $3d$ atomic

orbitals. The sixth factor is $x_b^2 + y_b^2 + z_b^2 = r_b^2$, which is the same as a 3*s* function, which is typically absent from the basis set. Furthermore, there are ten *f*-type Gaussians and similarly can be combined to have the same angular momentum as seven real 4*f* atomic orbitals.

The general form of the linear combinations of Cartesian coordinates can be expressed as:

$$Nr_b^l e^{-\alpha r_b^2}[(Y_l^m)^* \pm Y_l^m]/2^{\frac{1}{2}} \tag{58}$$

Sometimes the spherical Gaussian form is used:

$$Nr_b^{n-1} e^{-\alpha r_b^2}[(Y_l^m)^* \pm Y_l^m]/2^{\frac{1}{2}} \tag{59}$$

The atomic orbitals are expressed as a linear combination of slater orbitals to explain the molecular system.

The STO centred on atom *a* has the form:

$$Nr_a^{n-1} e^{-\zeta r_a} Y_l^m(\theta_a, \phi_a) \tag{60}$$

For non-linear molecules the real form of STO is:

$$Nr_a^{n-1} e^{-\zeta r_a}[(Y_l^m)^* \pm Y_l^m]/2^{\frac{1}{2}}(\theta_a, \phi_a) \tag{61}$$

The MO ϕ_i is shown as: $\phi_i = \sum_r c_{ri}\chi_r$, where χ_r's is the STO basis orbitals.

The only basis set used in the following work is aug-cc-pVTZ with B3LYP level of theory. The simplest basis set to start with is 6-311++g(d,p), where 6 refers to six functions contracted into 1 (core and valence electrons). The number first after the dash is for valence electrons where 3 functions are contracted into one with two additional functions added due to the two 1's after 3. The first plus sign refers to diffuse functions on the non-H-atoms and second plus diffuse functions for the H-atom. The g is simply Gaussian function. The *d* in the parentheses is the addition of a *d*-orbital to *p*-orbitals and similarly *p* the addition of a *p*-orbital for *s*-orbitals. These are polarization functions.

The basis set aug-cc-pVTZ is much larger than 6-311++g(d,p) as well as containing electron correlation. The first part aug (augmented) is the functions contracted into one, -cc is correlation

45

consistent and -pVTZ is polarization valence triple zeta. The number of zeta functions can vary from 1-5 (pVSZ, pVDZ etc.).

Quantum Theory of Atoms in Molecules

Quantum Theory of Atoms In Molecules[4] (QTAIM) was developed by Richard F. W. Bader. QTAIM explains chemical bonding, i.e., ED and atomic charge, from the topology. The atomic basins and bond paths are obtained using QTAIM. The zero-flux surface is used to describe atoms in the QTAIM framework. The complex quantum mechanical wavefunction is transformed with the zero flux to more easily understood data for a chemist. QTAIM gives a quantum mechanical definition of an atom in a molecule allowing general concepts to be explained in terms of quantum mechanics. It also assists preceding discussions and critically important for FALDI. Portions of the discussion are aided by Chapter 1 of An Introduction to the Quantum Theory of Atoms in Molecules.[19]

The gradient of the ED is used to obtain the atomic basin within QTAIM:

$$\nabla\rho(\mathbf{r}) = i\frac{\partial\rho}{\partial x} + j\frac{\partial\rho}{\partial y} + ki\frac{\partial\rho}{\partial z} \to \left\{\begin{matrix} = 0 \text{ (at critical point and at } \infty)) \\ \neq 0 \text{ (all other points)} \end{matrix}\right\} \tag{62}$$

where $\rho(\mathbf{r})$ is the ED. Each partial derivative will be 0 at a critical point. The critical points can be classified by rank (ω) and signature (σ) denoted as (ω, σ). The curvature of the ED in 3D space can be showed by the Hessian matrix at a critical point $\mathbf{r}$ to obtain the eigenvalues.

$$H(\mathbf{r}) = \begin{pmatrix} \dfrac{\partial^2\rho}{\partial x^2} & \dfrac{\partial^2\rho}{\partial x\partial y} & \dfrac{\partial^2\rho}{\partial x\partial z} \\ \dfrac{\partial^2\rho}{\partial y\partial x} & \dfrac{\partial^2\rho}{\partial x^2} & \dfrac{\partial^2\rho}{\partial y\partial z} \\ \dfrac{\partial^2\rho}{\partial z\partial x} & \dfrac{\partial^2\rho}{\partial z\partial y} & \dfrac{\partial^2\rho}{\partial x^2} \end{pmatrix} \tag{63}$$

The diagonalized Hessian matrix at critical point $\mathbf{r}$ is:

46

$$H(\mathbf{r}) = \begin{pmatrix} \dfrac{\partial^2 \rho}{\partial x^2} & 0 & 0 \\ 0 & \dfrac{\partial^2 \rho}{\partial x^2} & 0 \\ 0 & 0 & \dfrac{\partial^2 \rho}{\partial x^2} \end{pmatrix} = \begin{pmatrix} \lambda_1 & 0 & 0 \\ 0 & \lambda_2 & 0 \\ 0 & 0 & \lambda_3 \end{pmatrix} \tag{64}$$

Please note that H does not refer to the Hamiltonian operator here, but rather the Hessian matrix measured at **r**.

The eigenvalues can also be obtained from the Laplacian ($\nabla^2 \rho(\mathbf{r})$):

$$\nabla^2 \rho(\mathbf{r}) = i\frac{\partial^2 \rho}{\partial x^2} + j\frac{\partial^2 \rho}{\partial y^2} + k\frac{\partial^2 \rho}{\partial z^2} = \lambda_1 + \lambda_2 + \lambda_3 \tag{65}$$

The ED curvature has a negative value at a local minimum and a positive value at a local maximum; shown with (ω, σ). Rank (ω) is the number of non-zero curvatures. Signature (σ) is the sum of all the curvature signs:

$$\sigma = \sum_i^{\omega} \lambda_i / \|\lambda_i\| \tag{66}$$

There are then four possible combinations of rank and signature: (3,-3) there are 3 negative curvatures and ρ is a local maximum, a nuclear critical point; (3,-1) is a bond critical point (BCP) where there are 2 negative curvatures and one positive curvature. The ρ is a maximum in the two negative curvature eigenvector directions and a minimum in the third perpendicular axis; (3,+1) there are two positive curvatures which are ρ minimums and a ρ maximum in the perpendicular axis. This is a ring critical point. The last one is (3,+3) where ρ is a local minimum with 3 positive curvatures, this is a cage critical point.

The ED maxima's at the nuclei positions yields the topology seen. The topology encompasses the entire molecule but gets divided into mononuclear regions, Ω, which is atoms in the molecule (AIM). The atom in a molecule has a surface boundary that is a zero-flux surface in a gradient vector field within the ED surface of the molecule meaning that no gradient vectors ($\nabla(\rho(\mathbf{r}))$) cross this surface or mathematically defined as:

47

$$\nabla\rho(\mathbf{r}) \cdot \mathbf{n}(\mathbf{r}) = 0 \text{ for all } \mathbf{r} \text{ belonging to atomic basin } \Omega \tag{67}$$

where $\mathbf{r}$ is the position vector and $n(r)$ the unit vector normal to the surface of atomic basin Ω.

The atomic properties can thus be calculated extending from the definition boundary given to an atom. The expectation value of the molecule can be used to determine the atomic properties. For any given observable O:

$$\langle\hat{O}\rangle_{\text{molecule}} = \sum_{i}^{\text{all atoms}} \left(N \int_{\Omega_i} \left\{ \frac{1}{2}[\Psi^*\hat{O}\Psi + (\hat{O}\Psi)^*\Psi]d\tau' \right\} d\mathbf{r} \right) \tag{68}$$

$$\langle\hat{O}\rangle_{\text{molecule}} = \sum_{i}^{\text{all atoms}} \left(N \int_{\Omega_i} \rho_O d\mathbf{r} \right) = \sum_{i}^{\text{all atoms}} O(\Omega_i)$$

where the expectation value is the sum over all molecular space. The integration is over all 3D space as well denoted by $d\tau'$.

The total electron population can then be calculated by integrating ED over the entire atomic basin:

$$N(\Omega_i) = \int_{\Omega_i} \rho(\mathbf{r})d\tau \tag{69}$$

The total electron population in atomic basin A, $\Omega(A)$, is made up from localized and delocalized electrons. These are calculated using the (de)localization indices.

$$N(A) = \lambda(A) + \frac{1}{2}\sum_{B \neq A} \delta(A, B) \tag{70}$$

Where $\lambda(A)$ is the localization index for atomic basin A and $\delta(A, B)$ is the delocalization index between atomic basin A and atomic basin B. Only half the sum is used to ensure electrons are not counted twice when delocalized between atomic basins. The localized indices can be expressed as $\lambda(A)$:

48

$$\lambda(A) = \sum_i \sum_j \sqrt{n_i n_j} \, S_{ij}^A S_{ji}^A \tag{71}$$

and delocalized index ($\delta(A,B)$) expressed as:

$$\delta(A, B) = \sum_i \sum_j \sqrt{n_i n_j} (S_{ij}^A S_{ji}^B + S_{ij}^B S_{ji}^A) \tag{72}$$

where S_{ij}^A is the amount of overlap between atomic basin i and atomic j from atom A. The overlap elements S_{ij}^A is defined in matrix notation and called the atomic overlap matrix.

$$S_{ij}^A = \int_A \chi_i^*(\mathbf{r}) \chi_j(\mathbf{r}) d\mathbf{r} \tag{73}$$

The localization and delocalization index can also be calculated from the integration of the Fermi correlation function.[19] These indices and total count make it possible to interpret the complexity of the quantum mechanical nature for the atoms in a simple way. QTAIM forms an important building block to quantify the electronic nature of the atoms in the molecule.

Fragment, Atomic, Localized, Delocalized and Interatomic

Fragment, Atomic, Localized, Delocalized and Interatomic (FALDI)[5–9] utilises QTAIM-defined atomic basins (Ω) within a molecule to obtain the electronic populations as a total and which is (de)localised. FALDI uses the same theoretical framework that was developed for the Domain Averaged Fermi Hole (DAFH); developed by Ponec and co-workers.[20,21] The DAFH is based on the exchange-correlation electron hole that is linked with correlated movement of electrons. The DAFH is further explained here where previously only Fermi hole was used. The correlation function is the level of deviation for the pair density ($\rho_2(\mathbf{r}_1, \mathbf{r}_2)$) from the completely uncorrelated product of the first-order densities. FALDI is explained and proven in much more detail by de Lange et al.[5–9]

The correlation factor, conditional probability and electron hole equations are given again to aid the explanation for FALDI. The correlation function[22] for correlated electrons is expressed as:

$$C_f(\mathbf{r_1}, \mathbf{r_2}) = 2\rho_2(\mathbf{r_1}, \mathbf{r_2}) - \rho(\mathbf{r_1})\rho(\mathbf{r_2}) \tag{74}$$

The electron hole function at $\mathbf{r_2}$ affecting $\mathbf{r_1}$ is:

$$\rho^{\text{Hole}}(\mathbf{r_1}, \mathbf{r_2}) = \rho(\mathbf{r_1}) - \vartheta(\mathbf{r_1},;\mathbf{r_2}) \tag{75}$$

where $\vartheta(\mathbf{r_1},;\mathbf{r_2})$ is the conditional probability, which is the same as Equation 50, the probability of finding an electron at $\mathbf{r_2}$ if there is already one at $\mathbf{r_1}$, expressed as:

$$\vartheta(\mathbf{r_1},;\mathbf{r_2}) = \frac{\rho_2(\mathbf{r_1}, \mathbf{r_2})}{\rho(\mathbf{r_2})} \tag{76}$$

The electron hole function (Equation 74) gives the amount of electron density that is excluded at $\mathbf{r_1}$ due to the correlated movement with the electron at $\mathbf{r_2}$. When Equation 75 and 76 is substituted into 74 it yields:

$$C_f(\boldsymbol{r_1}, \boldsymbol{r_2}) = \rho_2(\boldsymbol{r_1}, \boldsymbol{r_2}) - \rho^{\text{Hole}}(\boldsymbol{r_1}; \boldsymbol{r_2})\rho(c) \tag{77}$$

The correlation function is now given in terms of the electron hole. The pseudo-dynamic probability density distribution[23] of an electron at $\mathbf{r_2}$ can be plotted with Equation 77 and varying $\mathbf{r_1}$ with constant $\mathbf{r_2}$.

The correlation function can be integrated over an atomic basin (Ω_i):

$$g_i(\boldsymbol{r_1}) = -\int_{\Omega_i} C_f(\boldsymbol{r_1}, \boldsymbol{r_2}) d\boldsymbol{r_2} \tag{78}$$

In matrix form it is expressed as:

$$g_i(\boldsymbol{r_1}) = -\sum_{\sigma\lambda}^{N} \chi_\sigma(\boldsymbol{r_1}) \chi_\lambda(\boldsymbol{r_1}) S_{\sigma\lambda}^{\Omega} \tag{79}$$

$S_{\sigma\lambda}^{\Omega}$ is again an element of the atomic overlap matrix as:

$$S_{\sigma\lambda}^{\Omega} = \langle \chi_\sigma | \chi_\lambda \rangle = \int_{\Omega_i} \chi_\sigma(\boldsymbol{r_1}) \chi_\lambda(\boldsymbol{r_1}) d\boldsymbol{r_1} \tag{80}$$

50

$g_i(\boldsymbol{r_1})$ provides the FALDI-defined *atomic electron density* (*atom*-ED), which is the same as the DAFH-defined function of the same symbol. *Atom*-ED distributions provide the contribution at **r** arising from the average electron population of an atomic basin. Notably, **r** can be within the atom's volume (localized contributions) or outside of the atom's volume (delocalized contributions).

The total electron population is calculated from the integration over the entire atomic basin or integration of $g_i(\boldsymbol{r})$ over the entire space:

$$N(\Omega_i) = \int_{\Omega_i} \rho(r) d\boldsymbol{r} = \int_{-\infty}^{\infty} g_i(r) d\boldsymbol{r} \tag{81}$$

The total electron population is partitioned into the localized electron density and delocalized electron density,

$$N(\Omega_i) = \lambda_i(\Omega_i) + \frac{1}{2} \sum_{\chi \neq i}^{M} \delta(\Omega_i, \Omega_\chi) \tag{82}$$

and

$$\lambda(\Omega_i) = \int_{\Omega_i} g_i(r) d\boldsymbol{r} \tag{83}$$

Delocalized density can also be expressed as:

$$\delta(\Omega_i, \Omega_j) = \int_{\Omega_i} g_i(\boldsymbol{r_1}) d\boldsymbol{r_1} + \int_{\Omega_j} g_j(\boldsymbol{r_2}) d\boldsymbol{r_2} = 2 \int_{\Omega_i} g_i(\boldsymbol{r_1}) d\boldsymbol{r_1} \tag{84}$$

The above is similar to the QTAIM functionals. The preceding parts will make use of the DAFH approach.

The localized and delocalized electron density can be obtained using the correlation functional (Equation 78):

$$g_i(\boldsymbol{r_1}) = \mathcal{L}_i(\boldsymbol{r}) + \sum_{j \neq i}^{M} \mathcal{D}_{ij}(\boldsymbol{r}) \tag{85}$$

The localized electron density is given by

51

$$\mathcal{L}_A(\boldsymbol{r}) = \sum_{ij} \chi_i^*(\boldsymbol{r}) \chi_j(\boldsymbol{r})(S^A S^A)_{ji} \tag{86}$$

and delocalized electron density is given by

$$\mathcal{D}_{AB}(\boldsymbol{r}) = \sum_{ij} \chi_i^*(\boldsymbol{r}) \chi_j(\boldsymbol{r})(S^A S^B + S^B S^A)_{ji} \tag{87}$$

The LIs and DIs count from QTAIM are normalized to the atomic population $N(A)$. FALDI localized and delocalized electron populations count the electrons. The indistinguishability of electrons causes an electron to be able to be delocalized among several atomic basins, resulting in inequal sharing of electrons. The delocalization, however, arises from the pair-wise correlation of electrons (i.e., the electron-pair density). If only electron-pairs that are equally split and distributed between two basins are counted, one arrives at the (orthodox) QTAIM-defined DIs. If one then further consider intact electron-pairs delocalized across multiple basins, one arrives at the FALDI-defined DIs. This contrasts QTAIM which assumes equal sharing between atomic basin A and B as stated above. Moreover, the overlap between two atomic basins' localized electron distribution is non-zero. The localized-delocalized overlap (LDO) approximation is used to differentiate between delocalization of core and non-bonded electrons and multi-centric effects over the entire molecular space. The LDO approximation is used for all the electron populations in this work. To describe the mechanism of the LDO approximation, a short detour to describe further decompositions of the (de)localized density distributions need to be taken.

Diagonalization of the localized electron density and delocalized electron density yields orthogonal functions that are called natural density functions (NDFs). The diagonalization is done with the overlap of atomic basin A and any other atomic basin X ($\mathbf{S}^A\mathbf{S}^X$) as:

$$S^A S^X U^{AX} = n^{AX} U^{AX} \tag{88}$$

where U^{AX} is the eigenvectors associated with the overlap of atomic basin A and X and n^{AX} is the corresponding eigenvalues or occupations. $\mathbf{S}^A\mathbf{S}^A$ would imply the overlap matrix describing

localized density of basin A, whereas $\mathbf{S}^A\mathbf{S}^B$ would imply the overlap matrix of electrons delocalized from basin A to basin B. The eigenvalues are calculated as:

$$n_i^{AX} = \sum_{jk}^{N_{MO}} U_{ji}^{AX}(\mathbf{S}^A\mathbf{S}^X)_{kj}U_{kj}^{AX} \tag{89}$$

where N_{MO} refers to the number of molecular orbitals. The localized and delocalized electron density distribution can be expressed in terms of eigenvectors and eigenfunctions. These distributions are expressed as the sum of the occupations multiplied by the density of a helper function,

$$\mathcal{L}_A(\boldsymbol{r}) = \sum_i^{N_{MO}} n_i^{AA}[\phi_i^{AA}(\boldsymbol{r})]^2 \tag{90}$$

where

$$\phi_i^{AA}(\boldsymbol{r}) = \sum_j^{N_{MO}} \chi_j(r)U_{ji}^{AA} \tag{91}$$

$n_i^{AA}[\phi_i^{AA}(\boldsymbol{r})]^2$ is referred to as theNDF. Note, these are not the same as natural orbitals.

The delocalized electron density distribution is calculated as:

$$\mathcal{D}_{AB}(\boldsymbol{r}) = \sum_i^{N_{MO}} n_i^{AB}[\phi_i^{AB}(\boldsymbol{r})]^2 \tag{92}$$

and the QTAIM defined delocalization index is expressed as:

$$\delta_{QTAIM}(A,B) = \sum_i^{N_{MO}} n_j^{AB} \tag{93}$$

Localized distributions generated using Equation 85 are generally not exclusively localized to an atomic basin, and significant portions of the total (orthodox) LI is described as electrons found in other basins (i.e., delocalized). The total LO measures the degree of overlap between localized distributions from two atomic basins.

The overlap between localized electron density and NDF fields is expressed as:

53

$$s\left(\mathcal{L}_A^i; \mathcal{L}_B^j\right) = \sqrt{n_i^{AA} n_j^{BB} [U^{AA} U^{BB}]_{ij}} \tag{94}$$

The overlap is normalized to 1 and expressed with the square root of the occupation of the NDF's

$\sqrt{n_i^{AA} n_j^{BB}}$. Due to localization electron density ($\mathcal{L}_A^i$) the overlap is simply the same as its

occupation. The overlap between $\mathcal{L}_A^i$ and delocalized electron density distribution NDF $\mathcal{D}_A^i$ can be

calculated similarly by using the eigenvalues and eigenvectors of $\mathbf{S}^A \mathbf{S}^B$ which is n_j^{AB} and $\mathbf{U}^{AB}$,

respectively.

To calculate the total LO, one uses the overlap of ith NDF from atomic basin A with all other

localized electron density NDF's expressed as:

$$LO\left(\mathcal{L}_A^j\right) = \sum_{X \neq A}^{M_{atoms}} \sum_j^{N_{MO}} s(\mathcal{L}_A^j; \mathcal{L}_X^j) \tag{95}$$

The occupation is calculated when the occupation of the NDF (n_j^{AA}) is larger than total localization

overlaps ($LO\left(\mathcal{L}_A^j\right)$), otherwise the NDF is completely overlapped by other localized electron

density distribution with contributions to the same MOs equating to an occupation of zero or

mathematically illustrated as:

$$n_i'^{AA} = \begin{cases} n_i^{AA} - LO(\mathcal{L}_A^i) & n_i^{AA} > LO(\mathcal{L}_A^i) \\ 0 & n_i^{AA} \leq LO(\mathcal{L}_A^i) \end{cases} \tag{96}$$

The prime indicates the occupation of the ith NDF that is LO-free. The adjusted occupations from

Equation 95 are substituted into Equation 90 to get a LO-free localized electron density distribution

$$\mathcal{L}_A'(r) = \sum_i^{N_{MO}} n_i'^{AA} [\phi_i^{AA}(r)]^2 \tag{97}$$

The localized electron density distribution can be integrated over all space to yield a localization

index, which is LO-free

$$\lambda_{\text{LO-free}}(A) = \int_{-\infty}^{\infty} \mathcal{L}_A'(r) dr \tag{98}$$

54

The occupation removed through Equation 95 is delocalized electron density, which is included when using orthodox LI. Therefore, the amount taken away should be added to the delocalized electron density distribution:

$$n'\left(\mathcal{L}_A^i \rightarrow \mathcal{D}_{A,B}^j\right) = w'\left(\mathcal{L}_A^i; \mathcal{D}_{A,B}^j\right)\left(n_i^{AA} - n_i'^{AA}\right) \tag{99}$$

The weighting factor is defined as:

$$w'\left(\mathcal{L}_A^i; \mathcal{D}_{A,B}^j\right) = \frac{s\left(\mathcal{L}_A^i; \mathcal{D}_{A,B}^j\right)}{\sum_j \left(\mathcal{L}_A^i; \mathcal{D}_{A,B}^j\right)} \cdot \frac{\sum_k s\left(\mathcal{L}_A^i; \mathcal{L}_B^k\right)}{LO\left(\mathcal{L}_A^i\right)} \tag{100}$$

with the overlap of $\mathcal{L}_A^i(\boldsymbol{r})$ and $\mathcal{D}_{A,B}^j(\boldsymbol{r})$ as a fraction of the total overlap of $\mathcal{L}_A^i(\boldsymbol{r})$ with all NDFs of $\mathcal{D}_{A,B}^j(\boldsymbol{r})$. The overlap of $\mathcal{L}_A^i(\boldsymbol{r})$ and $\mathcal{L}_B^j(\boldsymbol{r})$ is given as a fraction of the total overlap between $\mathcal{L}_A^i(\boldsymbol{r})$ and all other localized electron density distribution.

The LO-free delocalized electron density distribution can be presented as:

$$\mathcal{D}_{A,B}'(\boldsymbol{r}) = \sum_j^{NMO} n_j^{AB}\left[\phi_j^{AB}(\boldsymbol{r})\right]^2 + \sum_j^{NMO}\sum_i^{NMO}\left(n'\left(\mathcal{L}_A^j \rightarrow \right.\right.$$
$$\left.\left. \mathcal{D}_{A,B}^j\right)\left[\phi_j^{AA}(\boldsymbol{r})\right]^2 + n'\left(\mathcal{L}_B^j \rightarrow \mathcal{D}_{A,B}^j\right)\left[\phi_j^{BB}(\boldsymbol{r})\right]^2\right) \tag{101}$$

The first term is related to the overlap of atomic basin *A* and atomic basin *B* and the second term is the amount of density removed from localized electron density distribution due to LO-overlap. When the LO-free delocalized electro density distribution is integrated over the entire space (same as seen with LO-free localization) obtains the LO-free localization index

$$\delta_{\text{LO-free}}(A, B) = \int_{-\infty}^{\infty} \mathcal{D}_{A,B}'(\boldsymbol{r})d\boldsymbol{r} \tag{102}$$

This concludes the method for LO-free. The localized-delocalized overlap (LDO) method is similar by using the localized electron density distribution overlap of the ith NDF of atomic basin *A* with all the other atomic basins' NDFs. The LDO method calculates additionally the overlap between localized and delocalized NDFs. The LDO method uses the same conditions as seen in Equation 95 but instead uses a double prime to differentiate LDO from LO

$$LDO(\mathcal{L}_A^i) = \sum_{X \neq A}^{M_{atoms}} \sum_{j}^{N_{MO}} s(\mathcal{L}_A^i; \mathcal{L}_X^j) + \sum_{X}^{M_{atoms}} \sum_{Y \neq A}^{M_{atoms}} \sum_{j}^{N_{MO}} s(\mathcal{L}_A^i; \mathcal{D}_{X,Y}^j) \qquad (103)$$

Similarly, the LDO-free localization electron density distribution index ($\lambda_{\text{LDO-free}}(A)$) as well as the LDO-free delocalization electron density distribution index ($\delta_{\text{LDO-free}}(A,B)$) can be calculated by integrating over all space.

The $\lambda_{\text{LDO-free}}(A)$ index only (within the LDO approximation and notwithstanding any integration errors) includes electrons exclusively within atomic basin A, all other localized electron densities within atomic basins not equal to A are excluded. These electrons include core and non-bonded (e.g., lone pairs) electrons. The delocalization index of LDO ($\delta_{\text{LDO-free}}(A,B)$) accounts for all delocalized electrons in any way between atomic basins. It is important to note the subscript for each index as this show whether it is classical description (unadjusted) – QTAIM – or LO-free or LDO-free. There can be referred to a specific NDF with $\lambda_{\text{LDO-free}}^2(A)$, which is the 2nd NDF and an LDO-free localization index of atomic basin A.

1D Cross-Section

Cross-section at a point **r** makes it possible to decompose the electronic contribution made to that point **r** from the different atomic basins within the molecular system. The cross-section yields vital information for a point **r** that does not form part of a bond path. Making it possible to explain strange interactions such as the of H in biphenyl.[24] To obtain an in-depth understanding of the intermolecular H-bonds within the water clusters (cyclic + 3D) investigated in this work, the origin of electron density to the intermolecular H-bonds should be explained. Large parts of the discussion is from Cukrowski *et al.*[10]

The cross-section is usually calculated from the BCP or simply CP(-3,1). This is done because the most valuable information is obtained where the highest concentration of density is found. The 2nd order partial derivative is determined along the path of the λ_2-eigenvector. The 2nd order partial

derivative reveals then if a contribution concentrates (negative 2nd order partial derivative), depletes (positive 2nd order partial derivative), or remove (negative 1st order derivative for electron density) electron density. The three different contributions are also called bonding, non-bonding and anti-bonding, respectively. The contributions that concentrate density assists the formation of a DB at the point **r** whereas non-bonding and anti-bonding decreases the strength and electron density for the BP at **r**. One should differentiate here that the nature of the contribution to **r** is only applicable at **r** not a uniform assumption for all points in the molecular system.

The different contributions to point **r** in space can be summed:

$$\rho_{\text{tot}}(\mathbf{r}) = \rho_{concentrating}(\mathbf{r}) + \rho_{depleting}(\mathbf{r}) + \rho_{removing}(\mathbf{r}) \tag{104}$$

The type of contribution can be obtained from the equation with the 2nd order partial derivatives but the presence or absence of a CP(3,-1) is not known. The gradient of the total electron density yields the answer to this, making it possible to rewrite Equation 104:

$$\partial\rho_{\text{tot}}(\mathbf{r}) = \partial\rho_{concentrating}(\mathbf{r}) + \partial\rho_{depleting}(\mathbf{r}) + \partial\rho_{removing}(\mathbf{r}) \tag{105}$$

The sum of the terms in Equation 104 must equal zero for a CP(3, -1) to be present. The contribution from removing or non-bonding is negligible small. The concentrating (bonding) and depleting (non-bonding) contributions only remain and considering that the sum of $\partial(\mathbf{r}) = 0$. The two contributions should then be equal but opposite in sign when a CP(3, -1) is present. The interplay between the concentrating and depleting is complex making it difficult to interpret.

de Lange *et al*[9] introduced the CP(**r**) function to make it easier to calculate:

$$CP(\mathbf{r}) = -sign(\partial\rho_{depleting}(\mathbf{r}))[\partial\rho_{concentrating}(\mathbf{r}) + \partial\rho_{depleting}(\mathbf{r})$$
$$+ \partial\rho_{removing}(\mathbf{r})] \tag{106}$$

The CP(**r**) function yields the slope of the total electron density with the sign corrected depending on the sign of the slope for removing (non-bonding) electron density contribution. The $-sign(\partial\rho_{depleting}(\mathbf{r}))$ factor ensures that the CP(**r**) function is negative everywhere except for regions where the sum of absolute values of $\partial\rho_{concentrating}(\mathbf{r})$ and $\partial\rho_{depleting}(\mathbf{r})$ are larger than

$\partial \rho_{removing}(\mathbf{r})$ or when the sum has an opposite sign to $\partial \rho_{removing}(\mathbf{r})$. Similarly, the CP($\mathbf{r}$) function also equals zero at a CP(3,-1) when the contributions are summed. There is always a region along λ_2-eigenvector close to the CP(3,-1) where CP($\mathbf{r}$) is positive in one or both directions. Different chemical systems studies using the CP($\mathbf{r}$) function[9] revealed the multi-centric nature involved with atoms interacting even when no DB is present, leading to a different view on chemical bonds and the way it should be described.

Fragment Attributed Molecular Energy System Change

Fragment attributed molecular system energy change (FAMSEC)[11–13,25] main aim is to quantify the energetic effect of a 3D placement molecular fragment on a molecule or molecular system. FAMSEC does not break any chemical bonds of the structure to study the effects of the specific fragment. The derivation of FAMSEC stems from the IQA framework.[26,27]

The derivation starts from the IQA primary energy components ($E_{add}^X, E_{self}^X, E_{int}^{XY}$) where the energy of a molecule is partitioned into the atomic energy contributions:

$$E = \sum_X E_{add}^X \tag{107}$$

where E is the energy of a molecule and E_{add}^X the additive atomic energy of any atom X. The additive energy of an atom A can be decomposed within the IQA framework to self-atomic energy and diatomic interaction energies between the atom A and any other atom X in the molecule.

$$E_{add}^A = E_{self}^A + \sum_{X \neq A} 0.5 E_{int}^{AX} \tag{108}$$

where E_{add}^A is the additive energy of atom A, E_{self}^A (one-body compound) is the self-energy of atom A and $\sum_{X \neq A} 0.5 E_{int}^{AX}$ (two-body component) is the diatomic interaction energy. The additive of the molecule is then calculated as:

$$E = \sum_{X} E_{\text{self}}^{X} + 0.5 \sum_{X} \sum_{Y \neq X} E_{\text{int}}^{XY} \tag{109}$$

where $0.5 \sum_{X} \sum_{Y \neq X} E_{\text{int}}^{XY}$ is the interaction energy contribution from all unique atomic interactions within the molecular system. When the molecular system changes from *ref* → *fin* state the interactions between atoms within the molecule will be different due to the 3D placement changing for the atoms under consideration. To quantify the difference between *ref* and *fin* state ~~we will consider two~~ fragments G and $\mathcal{H}$ is considered. Fragment G consists of atoms *A* and *B* involved in a classical intramolecular interaction in the *fin* state within a molecular system. Fragment $\mathcal{H}$ consists of all the remaining atoms within the molecular system. The change from *ref* → *fin* for fragment G can be written as:

$$\Delta E_{\text{self}}^{G} = \Delta E_{\text{self}}^{A} + \Delta E_{\text{self}}^{B} = \left({}^{\text{fin}}E_{\text{self}}^{A} - {}^{\text{ref}}E_{\text{self}}^{A} \right) + \left({}^{\text{fin}}E_{\text{self}}^{B} - {}^{\text{ref}}E_{\text{self}}^{B} \right) \tag{110}$$

The self-energy for fragment G is the same as the deformation energy of the fragment. The combined interaction energy for both fragments G and $\mathcal{H}$ when going from *ref* → *fin* is expressed as:

$$\begin{aligned}
\Delta \sum_{X \in \mathcal{H}} E_{\text{int}}^{GX} &= {}^{\text{fin}}\sum_{X \in \mathcal{H}} E_{\text{int}}^{GX} - {}^{\text{ref}}\sum_{X \in \mathcal{H}} E_{\text{int}}^{GX} \\
&= {}^{\text{fin}}\left(\sum_{X \in \mathcal{H}} E_{\text{int}}^{AX} + \sum_{X \in \mathcal{H}} E_{\text{int}}^{BX} \right) - {}^{\text{ref}}\left(\sum_{X \in \mathcal{H}} E_{\text{int}}^{AX} + \sum_{X \in \mathcal{H}} E_{\text{int}}^{BX} \right)
\end{aligned} \tag{111}$$

The Equation is the same for the interfragment interaction energy component ($\Delta E_{int}^{G,\mathcal{H}}$), which is between atoms of fragment G and fragment $\mathcal{H}$. The 3D placement of atoms $X \in \mathcal{H}$ is different meaning that the geometry differs impacting the density distribution within atomic basins and net atomic charge. All these differences will affect the interaction energy meaning that they are accounted for even though not explicitly calculated.

Atoms *A* and *B* are not involved in classical intramolecular interaction in the *ref* state, but they still interact with each other regrades of the 3D placement. The change in interaction energy between them is accounted for with:

$$\Delta E_{\text{int}}^{\text{AB}} = {}^{\text{fin}}E_{\text{self}}^{\text{A}} - {}^{\text{ref}}E_{\text{self}}^{\text{B}} \tag{112}$$

The change in interaction energy is the same as the interfragment interaction energy ($\Delta E_{\text{int}}^{\mathcal{G}}$). The combination of Equations 110, 111 and 112 yields the attributed molecular system energy change:

$$\Delta E_{\text{attr-mol}}^{\mathcal{G}} = \Delta E_{\text{self}}^{\mathcal{G}} + \Delta E_{\text{int}}^{\text{AB}} + \Delta \sum_{\text{X} \in \mathcal{H}} E_{\text{int}}^{\mathcal{G}\text{X}} \tag{113}$$

or written more generally for any size molecular fragments $\mathcal{M}$ and $\mathcal{N}$:

$$\Delta E_{\text{attr-mol}}^{\mathcal{M}} = \Delta E_{\text{self}}^{\mathcal{M}} + \Delta E_{\text{int}}^{\mathcal{M}} + \Delta E_{\text{int}}^{\mathcal{M},\mathcal{N}} \tag{114}$$

where $\Delta E_{\text{int}}^{\mathcal{M}}$ is the change in interaction energy for the intrafragment interactions and $\Delta E_{\text{int}}^{\mathcal{M},\mathcal{N}}$ is the change in interaction energy for the interfragment interactions, which includes all diatomic interactions between fragment $\mathcal{M}$ and $\mathcal{N}$.

The terms in Equation 113 considers all the interactions made between atoms as well as the change from *ref* → *fin* state and the IQA defined primary energy terms. The sum of the terms from Equation 113 gives the contribution molecular fragment $\mathcal{G}$ makes to the whole molecule when changing from *ref* → *fin* state, therefore the contribution is defined as *mol*-FAMSEC. The first two terms in Equation 113 gives the energetic change observed within the fragment and it is defined as localized $\mathcal{G}$ energy change ($E_{\text{attr-loc}}^{\mathcal{G}}$) denoted as *local*-FAMSEC. Moreover, expressed as:

$$\Delta E_{\text{attr-loc}}^{\mathcal{G}} = \Delta E_{\text{self}}^{\mathcal{G}} + \Delta E_{\text{int}}^{\text{AB}} \tag{115}$$

One can express Equation 112 more compact as:

$$\Delta E_{\text{attr-mol}}^{\mathcal{G}} = \Delta E_{\text{attr-loc}}^{\mathcal{G}} + \Delta \sum_{\text{X} \in \mathcal{H}} E_{\text{int}}^{\mathcal{G}\text{X}} \tag{116}$$

or in general form:

60

$$\Delta E^{\mathcal{M}}_{\text{attr}-\text{mol}} = \Delta E^{\mathcal{M}}_{\text{attr}-\text{loc}} + \Delta \sum_{X \in \mathcal{H}} E^{\mathcal{MN}}_{\text{int}} \tag{117}$$

It is important to note here that $E^{\mathcal{G}}_{\text{attr}-\text{loc}}$ is not the same electron energy change ($\Delta E = {}^{\text{fin}}E - {}^{\text{ref}}E$) because electronic energy accounts for a lot more energy changes in the molecule not found with $E^{\mathcal{G}}_{\text{attr}-\text{loc}}$.

References:

1 A. H. Mazurek, Ł. Szeleszczuk and D. M. Pisklak, Pharmaceutics, 2020, **12**, 415.

2 Y. Li, Z. Wei, Q. Xiao, H. Gao and S. Song, *Minerals Engineering.*, 2018, **121**, 205–211.

3 J. Řezáč, B. Lévy, I. Demachy and A. De La Lande, *J. Chem. Theory Comput.*, 2012, **8**, 418–427.

4 R. F. W. Bader, *Atoms in molecules: A quantum theory*, Clarendon Press, 1990.

5 J. H. De Lange and I. Cukrowski, *J. Comput. Chem.*, 2017, **38**, 981–997.

6 J. H. De Lange and I. Cukrowski, *J. Comput. Chem.*, 2018, **39**, 1517–1530.

7 J. H. De Lange, D. M. E. Van Niekerk and I. Cukrowski, *Phys. Chem. Chem. Phys.*, 2019, **21**, 20988–20998.

8 J. H. De Lange, D. M. E. Van Niekerk and I. Cukrowski, *J. Comput. Chem.*, 2018, **39**, 973–985.

9 J. H. De Lange, D. M. E. Van Niekerk and I. Cukrowski, *J. Comput. Chem.*, 2018, **39**, 2283–2299.

10 I. Cukrowski, *Comput. Theor. Chem.*, 2015, **1066**, 62–75.

11 I. Cukrowski, F. Sagan and M. P. Mitoraj, *J. Comput. Chem.*, 2016, **37**, 2783–2798.

12 I. Cukrowski, G. Dhimba and D. L. Riley, *Phys. Chem. Chem. Phys.*, 2019, **21**, 16694–16705.

13 I. Cukrowski, D. M. E. Van Niekerk and J. H. De Lange, *Struct. Chem.*, 2017, **28**, 1429–1444.

14 W. Koch and M. C. Holthausen, *A Chemist's Guide to Density Functional Theory*, Wiley, 1st edn., 2001, 3–89.

15 J. B. Foresman, A. E. Frisch and I. Gaussian, *Exploring chemistry with electronic structure methods*, Gaussian, Incorporated, 1996, 465–490.

16 C. J. Cramer, *Essentials of computational chemistry: Theories and models*, Wiley, 2005, 249–298.

17 R. G. Parr and Y. Weitao, *Density-functional theory of atoms and molecules*, Oxford University Press, 1995, 3–69.

18 I. N. Levine, *Quantum chemistry*, Pearson, Boston, Seventh edition., 2014, 442–449.

19 C. F. Matta and R. J. Boyd, in *The Quantum Theory of Atoms in Molecules*, eds. C. F. Matta and R. J. Boyd, Wiley-VCH Verlag GmbH & Co. KGaA, Weinheim, Germany, 2007, 1–32.

20 R. Ponec, *J. Math. Chem.*, 1997, **21**, 323–333.

21 R. Ponec, *J. Math. Chem.*, 1998, **23**, 85–103.

22 R. McWeeny, *Rev. Mod. Phys.*, 1960, **32**, 335–369.

23 E. Francisco, A. M. Pendás and A. Costales, *Phys. Chem. Chem. Phys.*, 2014, **16**, 4586–4597.

24 T. G. Bates, J. H. Lange and I. Cukrowski, *J. Comput. Chem.*, 2021, **42**, 706–718.

25 I. Cukrowski, J. H. De Lange, A. S. Adeyinka and P. Mangondo, *Comput. Theor. Chem.*, 2015, **1053**, 60–76.

26 M. A. Blanco, Á. M. Pendás and E. Francisco, *J. Chem. Theory Comput.*, 2005, **1**, 1096–1109.

27 Á. M. Pendás, E. Francisco and M. A. Blanco, *Faraday Discussions*, 2007, **135**, 423–438.

Chapter 3

Molecular-wide and electron density (MOWED)-based definition and quantification of cooperativity in cyclic water clusters

Reproduced the article as submitted to *Physical Chemistry Chemical Physics* journal.

Supplementary Information supplied in Appendix I

Ignacy Cukrowski: Writing, Editing, Conceptualization
Stéfan Zaaiman: Writing, Editing, Conceptualization, data generation, graph generation
Shahnawaz Hussain: Software development (MOWeD-LAC, MOWeD-LFC)
Jurgens H. de Lange: Writing, Editing, Conceptualization

Molecular-wide and electron density (MOWED)-based definition and quantification of cooperativity in cyclic water clusters

Ignacy Cukrowski,[*a] Stéfan Zaaiman,[a] Shahnawaz Hussain[a,b] Jurgens H. de Lange[*a]

[a] *Department of Chemistry, Faculty of Natural and Agricultural Sciences, University of Pretoria, Lynnwood Road, Hatfield, Pretoria 0002, South Africa*
[b] *Elective student at the University of Pretoria. Permanent position: a student in the Department of Computer Science and Engineering at the Indian Institute of Technology, Kharagpur, India*

Abstract

From the MOWED-based approach, the origin of cooperativity is synonymous with physics- and quantum-based processes of electron delocalization throughout a molecular cluster. Intermolecular H-bonds in water clusters make the electron transport possible by building electron density bridges between molecules. The vast majority of electrons 'travelling on a density highway' ($\cdots$O–H$\cdots$O–H$\cdots$O–H$\cdots$) linking all water molecules is provided by O-atoms. The Fragment, Atomic, Localized, Delocalized and Interatomic (FALDI)-based electron density decomposition scheme revealed that the O-atom driven cooperativity is limited, as $8.42e$ must remain localized to H_2O to preserve the 'covalent' O–H bonds in a constellation of nuclei known as a water molecule. The count of delocalized electrons by each O-atom and H_2O in a cyclic hexamer is approaching $1.49e$ and $1.56e$, respectively, meaning that about $9.3e$ are shared by six water molecules. The intermolecular electron delocalization, i.e. cooperativity, is energy-minimising process that fully explains non-additive increase in stability of water clusters observed with an increase in their size. The Fragment Attributed Molecular System Energy Change (FAMSEC)-based method showed that fragments containing three O-atoms stabilize cyclic water clusters 5 times more than intermolecular H-bonds. A non-linear model equation proposed quantified cooperativity itself (statistical H_2O in a symmetric, homodromic cyclic cluster cannot delocalize more than $1.58e$) as well as predicted the limiting values the cooperativity-induced properties can reach with an increase in the size of cyclic structures. The qualitative and quantitative electron delocalization-based concept of cooperativity should be equally applicable to homo- and hetero-molecular clusters.

Keywords: cooperativity; cyclic water clusters; molecular-wide and electron density (MOWED)-based approach; the Fragment, Atomic, Localized, Delocalized and Interatomic (FALDI)-based electron density decomposition scheme, The Fragment Attributed Molecular System Energy Change (FAMSEC)-based method

1. Introduction

Properties of water clusters fascinate physicochemical and theoretical chemists for many decades and this continues to date.[1–9] This is not surprising as to the best of our knowledge, life is inseparably linked with water and the search for water in our solar system and beyond continues. In principle, water might be regarded as one among simplest molecules but many properties of water might be considered as anomalous. To this effect, in 'countless' contributions, the formation and properties of water clusters were investigated to shed some light on cooperativity between water molecules. Not surprisingly, cooperativity effects are understood to be ultimately linked with intermolecular hydrogen bond formation linking neighbouring water molecules[1-40] as structurally the O–H⋯O bridge is the only obvious difference between a non-interacting free water molecule and H_2O in a water cluster. This is such an entrenched concept that many contributions state this directly in their titles: (i) '… *Estimating the hydrogen bond strength and cooperativity in water clusters*',[2] (ii) '… *hydrogen bond cooperativity in water hexamers*',[10] (iii) '*Hydrogen-bond cooperative effects in small cyclic water clusters*',[11] and '*Origin of cooperativity in hydrogen bonding*',[12] to mention just a few examples.

A distinguishable feature of 'cooperativity' is non-additivity of cooperativity-linked effects and, as an example; '*nonpairwise*' effects with respect to the C_s dimer[13] were investigated in cyclic trimers. Cooperativity is also seen as manifesting itself as non-additivity of H-bond energies and this is due to mutual enhancement of H-bonds[14,15] such that '*the overall binding energy is greater than the sum of dimer binding energies*'.[16] *Non-additivity* of cooperativity effects was observed not only in water clusters but also in general, e.g., in resonance assisted hydrogen bonds in merged structures of malondialdehide,[17] in mixed water-ethanol clusters,[18] or methanol and formaldehyde clusters.[19]

Many cooperativity effects in water clusters were investigated computationally for decades with a focus on the properties of the O–H⋯O region of intermolecular H-bonding. Restricting ourselves

to the title cyclic water clusters, shorter O-O distances,[20–23] longer donor O–H bond lengths,[23,24] greater shifts of the donor O–H bond stretching frequencies than the C_s dimer,[15,25,26] increasing stability of O-atoms and decreasing stability of H-atoms[27] of the O–H$_{bonding}$ fragment and many more trends in topological properties on an increase of the cyclic water structure were reported.[11,19]

From papers dedicated to cooperativity, the concept of '*cooperativity*' is regarded as of high importance, but it is clear that it is neither a quantum nor physics-based property of a molecular system. The cooperativity was classified into several types, such as *'(a) many body interaction, (b) secondary interaction, (c) chelate effects, and (d) cooperativity and anticooperativity induced by conformation change'* and the type (a) was seen as the origin of hydrogen bond cooperativity in small clusters.[28] In search for the origin of cooperativity, a several information-theoretic quantities were examined and correlated against the interaction energy per building block with a final conclusion arrived at stating that '*the interactions governing the existence and validity of the cooperativity effect is rather complicated*'.[29] Considering linear chains of water clusters, the origin of non-additivity in hydrogen bonds was found to originate solely from classical electroststics.[12] It appears that the descriptive concept of cooperativity fits perfectly the term of a '*unicorn*' coined by Frenking and Krapp.[41] They suggested that chemists developed many unicorns with hope to '*bring law and order, health and good fortune, fame and satisfaction to chemists who would otherwise be lost in a pandemonium of experimental observations*.' To link this with the theme of this contribution, we all use cooperativity to explain many phenomena, many of us study it but nobody really knows where to place cooperativity in terms of universal laws of physics.

Our aim is to define and measure cooperativity, using cyclic water clusters as model systems, within well-established and quantifiable physics- and quantum-based descriptions of chemical bonding. In this contribution, we depart from classical approach where major focus is on the intermolecular H-bonding. To achieve our aims, we will treat all atoms on equal footing and treat water cyclic structures as a constellation of nuclei that spontaneously drive electron density (ED)

arrangement such that the system reaches the minimum energy. This physical process is due to '*only two forces operative in chemistry, the Feynman force exerted on the nuclei and the Ehrenfest force exerted on the electrons*'.[42] We investigate cooperativity from the perspective of the unified molecular-wide and electron density (MOWED)-based concept of chemical bonding.[43] We will make use of three tools incorporated in the MOWED-based approach, namely:

(i) The Fragment, Atomic, Localized, Delocalized and Interatomic (FALDI)-based electron density decomposition scheme [44–46] involving entire space occupied by a molecular system.

(ii) The Fragment Attributed Molecular System Energy Change (FAMSEC) family of methods[47,48] used to provide a qualitative and quantitative description of the impact made by any size of a molecular environment (immediate, distant, or molecular-wide) on intra and intermolecular interactions.

(iii) 1D cross-section of the electron density distribution.[49] This simple protocol provides detailed information on atoms and atom-pairs contributions to the total ED at a selected **r** coordinate in the 3D space occupied by a molecular system.

Finally, we propose here a mathematical expression dedicated to quantifying cooperativity and predicting its limiting value on the increase of a cyclic water cluster. This expression is easily modifiable and it works equally well to evaluate any cooperativity-related effect for any size of a cyclic water cluster.

2. Computational methods

All calculations were performed in Gaussian 09 Rev. D.01[50] in the gas phase with a keyword 'opt=verytight' at the B3LYP level of theory with Grimme's[51] empirical correction for dispersion using a keyword 'empiricaldispersion=GD3'. The Dunning triple zeta basis set, aug-cc-pVTZ, which is augmented by diffuse functions, was used throughout. Coordinates of all optimized structures are given in Table S1 of the Electronic Supporting Information (ESI). Frequency

calculations were performed for the optimized structures and no imaginary frequency were present. Topological, QTAIM[52] molecular graphs, atomic overlap matrices and IQA[53,54] calculations were performed in AIMAll[55] using B3LYP-generated wavefunctions. The IQA energy terms, and interaction energies in particular, were found to be highly comparable to those obtained at the CCSD/BBC1 level.[56] FAMSEC and FALDI data were calculated using in-house software, and FALDI isosurfaces were visualized using VMD.[57] FALDI codes were incorporated in MOWED-LAC (molecular-wide electron delocalization and localization atomic counts) and MOWED-LFC (molecular-wide electron delocalization and localization fragment counts) applications; these two applications are made freely available[58] and if required any assistance will be provided.

3. Theoretical background

3.1. The FALDI density decomposition scheme

The FALDI-based density decomposition scheme[44–46] provides electron population and (de)localization counts as well as 3D distributions of (de)localization patterns that can be visualized in real-space. The total electron density at any coordinate $\mathbf{r}$ within the 3D space occupied by an n-atom molecular system is made of specifically defined contributions as:

$$\rho(\mathbf{r}) = \sum_{A}^{n} g_{A}(\mathbf{r}) = \sum_{A}^{n} \mathcal{L}_{A}(\mathbf{r}) + \sum_{A}^{n-1} \sum_{B=A+1}^{n} \mathcal{D}_{A,B}(\mathbf{r}) \tag{1}$$

where $g_{A}(\mathbf{r})$ is the contribution made by electrons in atomic basin A, Ω_{A}, to the total electron density at $\mathbf{r}$ (*atom*–ED distribution), $\mathcal{L}_{A}(\mathbf{r})$ stands for the contribution made by electrons localized to Ω_{A} (*loc*–ED distribution) and $\mathcal{D}_{A,B}(\mathbf{r})$ represents the contribution made by electrons delocalized between all unique basin-pairs (Ω_{A},Ω_{B}) (*deloc*–ED distribution). Note that $g_{A}(\mathbf{r})$ is identical to the same descriptor used in Domain-Averaged Fermi Hole analyses (DAFH)[59–61] and, as for DAFH, FALDI terms are also subjected to isopycnic transformations.[62] Atomic basins are

68

usually chosen to be defined in QTAIM terms, using the topological condition of zero-flux surfaces.[52]

$g_A(\mathbf{r})$ will generally be non-zero, even when $\mathbf{r}$ is outside of basin's real-space volume of atom A, i.e., outside Ω_A, due to the wave-like nature of electrons leading to the phenomenon of electron delocalization. The FALDI decomposition is exhaustive so that, when $g_A(\mathbf{r})$ is integrated over all molecular space, it is equivalent to integrating the electron density over the atomic basin:

$$N(A) = \int_{\Omega_A} \rho(\mathbf{r})d\mathbf{r} = \int_{\infty} g_A(\mathbf{r})d\mathbf{r} \tag{2}$$

where the atomic electron population $N(A)$ is the total number of electrons found, on average, in atomic basin Ω_A. The *atom*–ED distribution, $g_A(\mathbf{r})$, is therefore the real-space and molecular-wide distribution of $N(A)$. Similar relationships can be constructed for *loc*–ED distributions, $\mathcal{L}_A(\mathbf{r})$:

$$LI_{LDO}(A) = \int_{\Omega_A} g_A(\mathbf{r})d\mathbf{r} = \int_{\infty} \mathcal{L}_A(\mathbf{r})d\mathbf{r} \tag{3}$$

so that the localization index (LI_{LDO}) counts the number of electrons described by $g_A(\mathbf{r})$ that are distributed over Ω_A, or, equivalently, the total number of electrons localized to atomic basin Ω_A (as described by $\mathcal{L}_A(\mathbf{r})$). Lastly, electrons described by $g_A(\mathbf{r})$ can also be delocalized to other basins,

$$^{A}DI_{LDO}(A,B) = \int_{\Omega_B} g_A(\mathbf{r})d\mathbf{r} = \int_{\infty} {}^{A}\mathcal{D}_{A,B}(\mathbf{r})d\mathbf{r} \tag{4}$$

so that $^{A}DI_{LDO}(A,B)$ counts the number of electrons found, on average, in Ω_A that can also be found in Ω_B, i.e. electrons delocalized from Ω_A into Ω_B. Note that the superscript 'A' in Eq. 4 indicates the contribution that diatomic delocalized electrons make to the electron population of atom A, $N(A)$. The total diatomic delocalization can be described then as:

$$DI_{LDO}(A,B) = \int_{\Omega_B} g_A(\mathbf{r})d\mathbf{r} + \int_{\Omega_A} g_B(\mathbf{r})d\mathbf{r} = \int_{\infty} \mathcal{D}_{A,B}(\mathbf{r})d\mathbf{r} \tag{5}$$

and $DI_{LDO}(A,B) = {}^{A}DI_{LDO}(A,B) + {}^{B}DI_{LDO}(A,B)$. Eqs. 3 and 4 therefore uniquely describe the total electron population of an atom in terms of molecular-wide (de)localized electron distributions:

$$N(A) = \int_{\infty} \mathcal{L}_A(\mathbf{r})d\mathbf{r} + \sum_{B \neq A}^{n-1} \int_{\infty} {}^{A}\mathcal{D}_{A,B}(\mathbf{r})d\mathbf{r}$$

$$= LI_{LDO}(A) + \sum_{B \neq A}^{n-1} {}^{A}DI_{LDO}(A,B) \tag{6}$$

Note that FALDI-defined LIs and DIs differ significantly from orthodox, QTAIM-defined LIs and DIs.[46] Whereas orthodox LIs and DIs count (de)localized electron-*pairs*, normalized to the atomic electron population $N(A)$, FALDI-defined LIs and DIs count (de)localized *electrons*. This subtle difference has quite long-ranging consequences in the description of electron (de)localization patterns. An equal split of electron pair(s) between two atomic basins is assumed in QTAIM-defined DIs so that ${}^{A}DI_{QTAIM}(A, B) = {}^{B}DI_{QTAIM}(A, B) = \frac{1}{2}DI_{QTAIM}(A, B)$. However, due to the indistinguishability of electrons, an electron pair itself can be delocalized amongst multiple basins, resulting in an unequal sharing of electrons. QTAIM-defined LIs therefore not only count exclusively localized electron pairs – such as core electrons or highly localized lone-pair electrons – but also include electron pairs that are not exclusively localized to an atomic basin (and can thus be found in other atomic basins as well). Accordingly, there is a non-zero overlap between the localized electron distributions of two atomic basins. FALDI corrects for this phenomenon by employing the localized-delocalized overlap (LDO) approximation, which takes into account delocalization of core and non-bonded electrons as well as multi-centric effects by fully accounting for electron distributions over the entire molecular space. Practically speaking, FALDI's LDO-free LIs (DIs) tend to be much smaller (larger) than their QTAIM counterparts, and DIs in particular can be unequally distributed, i.e., the atomic contributions to LDO-free diatomic $DI_{LDO}(A,B)$ are unequal, ${}^{A}DI_{LDO}(A, B) \neq {}^{B}DI_{LDO}(A, B) \neq \frac{1}{2}DI_{LDO}(A, B)$. All *loc*– and

70

deloc–ED distributions discussed in this work, as well as all LIs and DIs are calculated using the LDO approximation; accordingly, the 'LDO' subscript, as used in Eqs. 3–6, will be omitted further for brevity.

FALDI's *atom–*, *loc–* and *deloc–*distributions are additive and can be conveniently combined to form fragment $\mathcal{F}$ distributions by accounting for selected atomic basins' contributions. The total electron population of a *k*-atom fragment $\mathcal{F}$ can be decomposed as:

$$N^{\text{total}}(\mathcal{F}) = N^{\text{self}}(\mathcal{F}) + N^{\text{deloc}}(\mathcal{F},\mathcal{R})$$

$$= N^{\text{loc}}(\mathcal{F}) + N^{\text{deloc}}(\mathcal{F},\mathcal{F}) + N^{\text{deloc}}(\mathcal{F},\mathcal{R}) \tag{7}$$

The fragment's electron population is therefore the sum of electrons that can be found only in the space occupied by the fragment $\mathcal{F}$ (a 'self'-fragment electron population, $N^{\text{self}}(\mathcal{F})$) and electrons delocalized with the remainder of the molecule, $N^{\text{deloc}}(\mathcal{F},\mathcal{R})$. Notably, the self-fragment $N^{\text{self}}(\mathcal{F})$ population includes all atom-localized electrons $N^{\text{loc}}(A)$ (and $N^{\text{loc}}(\mathcal{F}) = \sum N^{\text{loc}}(A)$, where $A \in \mathcal{F}$) as well as electrons delocalized amongst atoms of the fragment, $N^{\text{deloc}}(\mathcal{F},\mathcal{F})$. $N^{\text{deloc}}(\mathcal{F},\mathcal{R})$, on the other hand, counts electrons that can be found in both fragments, i.e. in the *k*-atom fragment $\mathcal{F}$ and somewhere within the remainder $\mathcal{R}$ of the molecule. It is calculated by summing the atomic contributions (and only those made by atoms within the *k*-atom fragment $\mathcal{F}$) to diatomic DIs involving all other atoms in the molecule:

$$N^{\text{deloc}}(\mathcal{F},\mathcal{R}) = \sum_{A \in \mathcal{F}}^{k} \sum_{B \in \mathcal{R}}^{n-k} {}^{A}\text{DI}(A, B) \tag{8}$$

It might be very useful and informative to investigate electron delocalization patterns throughout a molecular system by computing delocalized electrons counts between molecular fragments, such as functional groups. To this effect, for the *k*-atom fragment $\mathcal{F}$ and *l*-atom fragment $\mathcal{H}$ one can write

$$\text{DI}(\mathcal{F},\mathcal{H}) = \sum_{A\in\mathcal{F}}^{k} \sum_{B\in\mathcal{H}}^{l} \text{DI}(A, B) \qquad (9)$$

where contributions made by individual atoms are accounted for, as DI(A,B) = ^{A}DI(A,B) + ^{B}DI(A,B). Eqs. 8 and 9 are related, in that $\text{DI}(\mathcal{F},\mathcal{H}) = N^{\text{deloc}}(\mathcal{F},\mathcal{H}) + N^{\text{deloc}}(\mathcal{H},\mathcal{F})$ and typically, $N^{\text{deloc}}(\mathcal{F},\mathcal{H}) \neq N^{\text{deloc}}(\mathcal{H},\mathcal{F})$. This means that $N^{\text{deloc}}(\mathcal{F},\mathcal{H})$ measures the degree to which electrons from the k-atom fragment $\mathcal{F}$ are delocalized within the l-atom fragment $\mathcal{H}$, whereas $\text{DI}(\mathcal{F},\mathcal{H})$ measures the total electron count due to delocalization of electrons between atoms of both fragments, i.e., the count of electrons shared by the two fragments.

3.2. A Fragment Attributed Molecular System Energy Change (FAMSEC) protocol

The concept of FAMSEC[47] was born from a need of understanding and quantifying changes taking place throughout a molecular system on a chemical event. A chemical event can be anything that results in new placement of nuclei in a 3D space and associated with this event a change in the electron density distribution. An example of a 'simple' chemical event is:

(i)   A structural change leading to a new conformer of a molecule with a new set of intramolecular interactions (among them, classical intramolecular NH···N or NH···O hydrogen bonds and steric –CH···HC– or HO···OH clashes), or

(ii) The formation of molecular clusters through intermolecular interactions, such as intermolecular OH···O, between water molecules in clusters considered in this work.

Changes taking place along the reaction energy profile (REP) constitute complex chemical events leading to the formation of new products. In order to explain a reaction mechanism and associated consecutive energy changes along the reaction pathway, a REP-FAMSEC protocol was designed.[48] Both approaches, FAMSEC and REP-FAMSEC, pinpoint n-atom molecular fragments $\mathcal{G}$ (in the latter case, a molecule might be treated as $\mathcal{G}$) that drive a chemical change the most by

quantifying the interaction energies between fragments and the energy contributions made by these fragments to the energy of a molecular system on a chemical event.

The molecular-wide and electron density-based approach to chemical bonding requires harvesting data from all corners of a molecular system. This is accomplished due to exhaustive energy partitioning schemes implemented in QTAIM[52] and IQA[53,54] where entire molecular space is occupied by atoms without voids between them. This means that the electronic energy of a molecular system E in the IQA energy-partitioning scheme

$$E = E_{\text{IQA}} = \sum_A E_{\text{add}}^A \qquad (10)$$

is made of additive atomic energies E_{add}^A defined as a sum of the self-atomic energy, E_{self}^A, and halved interaction energies between atom A and remaining atoms B in a molecule,

$$E_{\text{add}}^A = E_{\text{self}}^A + 0.5 \sum_{B \neq A} E_{\text{int}}^{A,B} \qquad (11)$$

The diatomic interaction energy $E_{\text{int}}^{A,B}$ is conveniently partitioned in the IQA scheme further to the exchange-correlation term, $V_{\text{XC}}^{A,B}$, that accounts for the interaction energy due to purely quantum effects (often synonymous with a covalent component of a diatomic interaction) and a classical Coulomb component of the diatomic interaction, $V_{\text{cl}}^{A,B}$,

$$E_{\text{int}}^{A,B} = V_{\text{XC}}^{A,B} + V_{\text{cl}}^{A,B} \qquad (12)$$

Making use of the IQA-defined principle energy components of a molecular system, the *mol-FAMSEC* term was designed to quantify energy contribution made by any fragment G by accounting for molecular-wide contributions made by all atoms of a molecular system and it is defined as:

$$mol\text{-FAMSEC} = \Delta E_{\text{self}}^G + \Delta E_{\text{int}}^G + \Delta E_{\text{int}}^{G,\mathcal{R}} \,. \qquad (13)$$

The first two terms in Eq. (13) quantify changes in a) self-atomic energies of atoms constituting the selected *n*-atom fragment G (ΔE_{self}^G) and b) intra-fragment interaction energies, i.e. ΔE_{int}^G and it accounts for changes in all unique diatomic interactions between atoms of G on the

73

transformation of a molecular system from the initial (*init*) to final (*fin*) state.. This means that the energy change localized to the 3D space occupied by atoms of a selected molecular fragment is quantified by these two energy terms and this can be written as

$$loc\text{-FAMSEC} = \Delta E_{\text{self}}^{G} + \Delta E_{\text{int}}^{G} . \tag{14}$$

The remaining atoms of a molecular system constitute a molecular fragment $\mathcal{R}$ and the last term in Eq. (13), $\Delta E_{\text{int}}^{G,\mathcal{R}}$, accounts for changes in the strength of all diatomic interactions between atoms of G and atoms of $\mathcal{R}$ on a change from the *init* $\rightarrow$ *fin* state.

Finally, one must note that to compute the changes in the energy terms shown in Eq. 13, a reference state is required and it is selected according to the scientific question posed. To this effect, if one is interested in by how much the interactions between oxygen and two hydrogen atoms in a water molecule changed, e.g. on the cyclic tetramer formation, then the G fragment is made of atoms belonging to a single water molecule, $G = \{O1,H2,H3\}$, and the $\Delta E_{\text{int}}^{G}$ can be computed vs. either:

1. A separate and non-interacting water molecule, when a total change in the strength of intra-molecular interactions in the cyclic structure is of interest, or

2. A water molecule in a dimer, or

3. A water molecule in a cyclic water cluster

and one can examine the $\Delta E_{\text{int}}^{G}$ term (or e.g., the energy of an atom E_{add}^{A}) computed vs. different reference states to find out which energy terms follow the trend in cooperativity defined in the following section.

4. Results and discussion

Cyclic water clusters (see Figure 1) are used to study the cooperativity effects. In this work, the water molecule is used as a single 'statistical' fragment $\mathcal{F}$ of an *n*-water cluster.
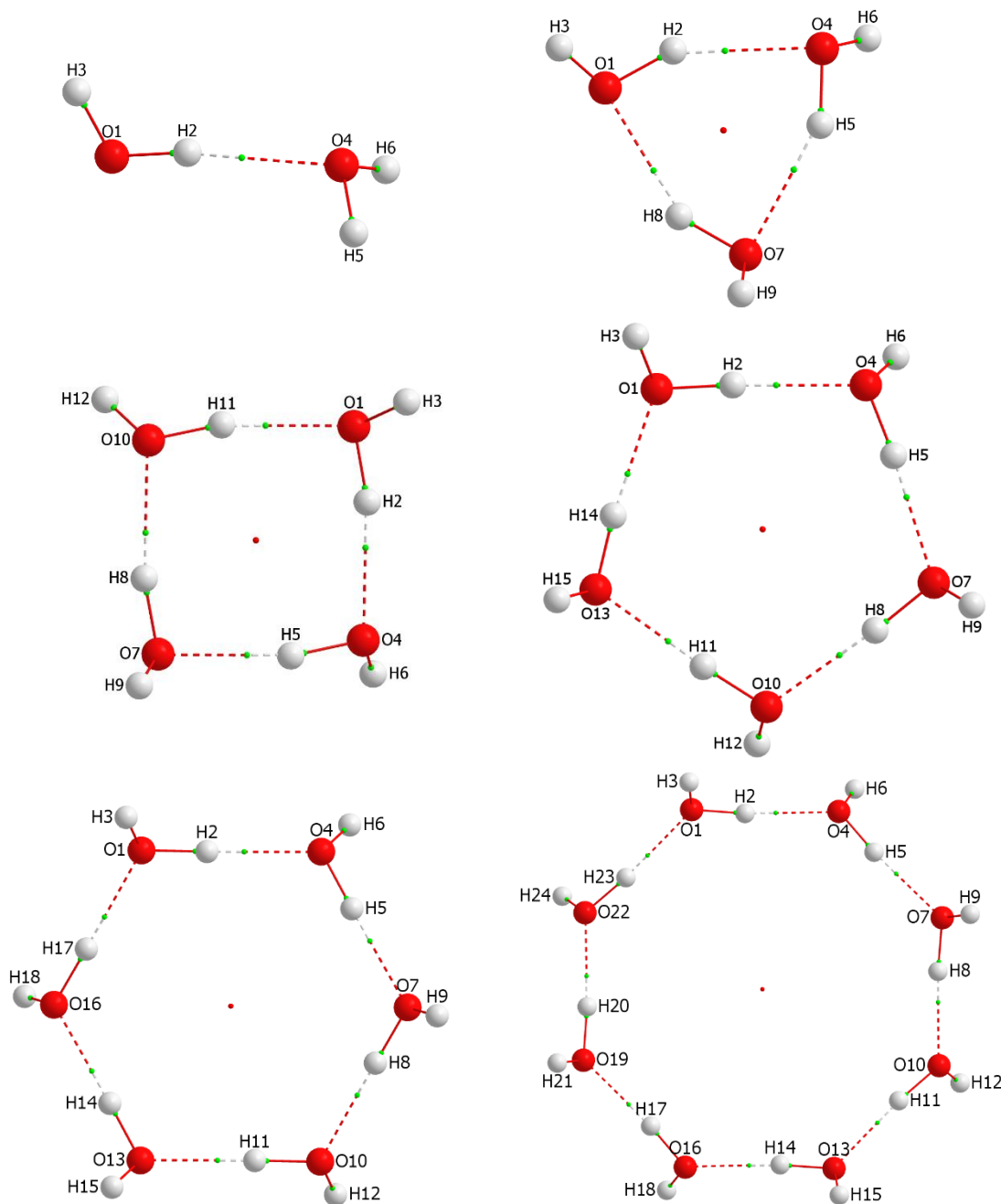
Figure 1 Cyclic water clusters investigated in this study, $(H_2O)_n$, n = 2-6, 8.

To ease interpretation of results, atoms in each consecutive water molecule $\mathcal{F}1$, $\mathcal{F}2$, $\mathcal{F}3$, etc. are numbered consistently as On, H(n+1) and H(n+2) such that:

(i)   The numbering of On-atoms differs by 3 (O1, O4, O7, etc.),

(ii)   The generic H(n+1) atom (i.e., H2, H5, H8, etc. in the consecutive water molecules of a cyclic cluster) forms the intermolecular H-bond with the neighbouring water molecule, and

(iii)   The generic H(n+2) atom in each water molecule (i.e., H3, H6, H9, etc.) is always pointing out of the ring.

Due to the symmetry of the cyclic water clusters, the properties of the 'first' H-bond between $\mathcal{F}$1 and $\mathcal{F}$2 in the cluster (O1–H2···O4) were used as an average for all H-bonds in the cluster.

The same was applied to the averaged per water molecule properties of On, H(n+1) and H(n+2) atoms. Although the dimer is not a cyclic structure, it was used as the smallest cluster where water molecules are linked via classical H-bond. Finally, non-interacting separate water molecules served as a reference state throughout the entire investigation.

4.1. MOWED-based concept of cooperativity

In this work, we depart from a classical approach, which is based on a major role played by intermolecular H-bonding used to explain a poorly defined concept of cooperativity between molecules. Instead, we propose a novel molecular-wide and electron density (MOWED)-based concept of cooperativity with well-defined physics-based foundation. In other words, we propose to link an abstractive concept of cooperativity with well-defined concepts of quantum physics/chemistry.

Our starting point is the fact that the most fundamental and general property of a molecular system is its electronic energy that, in turn, depends on the electron density distribution throughout the entire molecular system. In other words, the physics-based interactions and quantum effects among all atoms determine the distribution of ED and the relative placement of nuclei of a system in such a way that the final global equilibrium structure has the lowest energy possible. Furthermore, and importantly, all the properties of a molecular system can be derived from the molecular-wide distribution of ED. This was stressed already decades ago by Hohenberg and

Kohn,[63] as well as Bader.[52] As the electronic energy E of a molecular system encompasses all physico-chemical properties, E and some of its components were used in this work to explore cooperativity from a molecular-wide perspective. This means that contributions from all water molecules and each atom of a system were accounted for regardless of their significance and a kind of their contribution made to the total final property of a system. In order to link an impact made by cooperativity on E of a system, we computed a change in the electronic energy of a statistical water molecule in an n-H_2O cyclic cluster as - Eq. 15,

$$\Delta E(n\text{-}H_2O \text{ cluster}) \text{ per } H_2O = {}^W\Delta E(n) = \{E(n\text{-}H_2O \text{ cluster}) - nE(H_2O)\}/n \qquad (15)$$

The ${}^W\Delta E(n)$ term in Eq. 15 is the averaged change in the electronic energy of a water molecule in a cyclic n-water cluster. The change is computed relative to $E(H_2O)$, i.e. the energy of a free, non-interacting water molecule. The ${}^W\Delta E(n)$ values obtained for the cyclic water clusters using Eq. 15 are seen as circles in Figure 2.
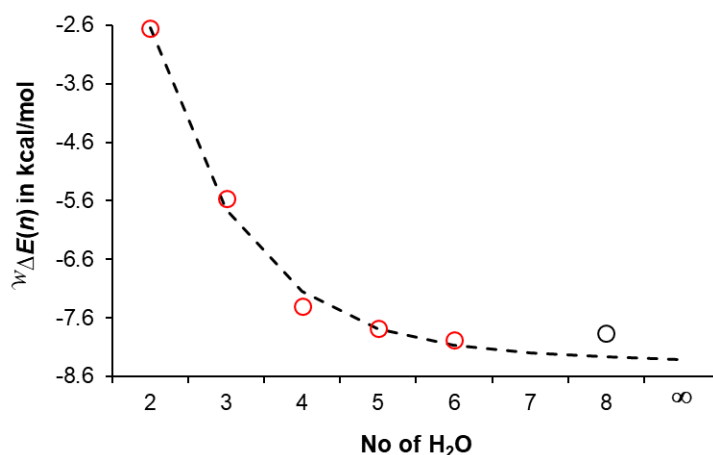
Figure 2. Relative to a free, non-interacting water molecule, an average increase in the stability of a statistical water molecule in n-H_2O cyclic clusters. The ${}^W\Delta E(n)$ values for $2 \leq n \leq 6$ (red circles) were used to generate the trend (seen as a dashed line). ${}^W\Delta E(8)$ computed for the octamer is shown as a black circle.

The non-linear decrease in the energy, hence also a non-linear increase in stability of a statistical water molecule, is observed on an incremental increase in the number of water molecules in a cluster. This also shows non-additivity of water molecules' electronic energy on a water cluster

77

formation. It is then very clear that the trend observed in Figure 2 correlates very well with the general concept of non-additivity of hydrogen bonding and we interpret this as a computationally quantifiable energy output of cooperativity phenomenon taking place in cyclic water clusters.

4.1.1. New equation for quantifying cooperativity-driven $^{W}\Delta E(n)$

To fit the data marked as red circles in Figure 2 (they represent data computed for energy-optimised cyclic water clusters) a dedicated new equation is proposed – see Eq. 16; it is a modified sigmoid function with two additional and unitless parameters α and β,

$$^{W}\Delta E(n) = \, ^{W}\Delta E(n_{\mathrm{ref}})\left[1 + \beta\left(1 - e^{-\alpha(n-n_{\mathrm{ref}})}\right)\right] \qquad (16)$$

The $^{W}\Delta E(n)$ term theoretically predicts, relative to a free, non-interacting water molecule, the decrease in E of a statistical water molecule in n-H_2O cyclic clusters and for $n \to \infty$ this represents the largest possible energy-minimizing contribution of cooperativity. The parameter α describes the initial steepness of the trend; the larger α is, the steeper the trend becomes. The β parameter is a multiplier that can be used to predict the largest possible decrease in the electronic energy of a water molecule in a n-H_2O cluster relative to the average E of a water molecule in a reference cluster. Note that the water dimer as well as a cyclic water cluster can be used as a reference state for Eq. 16.

The black circle seen in Figure 2 represents a datum point obtained for the octamer cyclic water cluster. This datum point was not considered for the calculations using Eq. 16 as the geometry of the system departs from planarity (as otherwise conserved throughout all other structures – Figure 1) and it visibly and significantly departs from the trend shown in Figure 2. The trend observed for the electronic energy decreases non-linearly and a constant value is reached when $n \to \infty$. Note that for $n \to \infty$, Eq. 16 simplifies to $^{W}\Delta E(n)(n\to\infty) = \, ^{W}\Delta E(n_{\mathrm{ref}})[1 + \beta]$ as the $e^{-\alpha(n-n_{\mathrm{ref}})}$ term $\to$ 0.

As an example and to illustrate applicability of Eq. 16, let us use a water dimer as a reference state for which $^{W}\Delta E(n_{ref}) = -2.651$ kcal/mol. From fitting computed energies (red circles in Figure 2), we obtained from Eq. 16 parameters $\alpha = 0.791$ and $\beta = 2.137$ used to calculate the dashed trend line in Figure 2. Hence:

1) The cooperativity-induced largest decrease in the electronic energy of a water molecule in a dimer (used as a reference) on the formation of an infinitely large cyclic water cluster is predicted to be $^{W}\Delta E(n_{ref}) \times \beta = -2.651 \times 2.137 = -5.665$ kcal/mol.

2) Theoretically and under standard conditions, a water molecule in a cyclic cluster cannot be stabilized more (relative to a free non-interacting water molecule) than $^{W}\Delta E(n_{ref}) \times \beta + ^{W}\Delta E(n_{ref}) = -5.665 + (-2.651) = -8.316$ kcal/mol and, in our opinion, this is of a fundamental significance.

Eq. 16 predicts that the maximum decrease in the electronic energy of a water molecule in the cyclic hexamer is -7.979 kcal/mol. This suggests that there is still some room to increase stability of a water molecule by about 0.34 kcal/mol. Notably, however, Eq. 15 gave us $^{W}\Delta E(8)$ = -7.068 kcal/mol for the optimized cyclic water octamer and this differs significantly from the trend-predicted value of -8.226 kcal/mol from Eq. 16. The largest deviation from the trend seen in Figure 2 is most likely due to the cyclic octamer being not as planar as the other cyclic water structures. It is important to stress that the lowest energy conformer of octamer, i.e., the eight-water cluster, is the 3D structure of cube.[24] Interestingly, the hexamer is also not the lowest energy conformer, but energetically it is much closer to the lowest energy conformer containing six water molecules, namely the 3D prism conformer. Instability of the cyclic water clusters larger than hexamer explains why the energy-optimisation protocols generate 3D rather than less stable planar cyclic water clusters.

4.1.2. A generalized expression for quantifying changes in properties of cyclic clusters

The trend seen as a dashed line in Figure 2 shows how cooperativity generates a non-linear decrease of E of a statistical molecule of a chemical system with an increase in the size of the system. It is our strong view that cooperativity is a product of underlying changes in physical and quantum properties of atoms and molecules in a molecular system. Hence, without a doubt, the phenomenon called cooperativity can be linked directly with the changes in the ED distribution among all atoms of water molecules in cyclic clusters considered. In other words, we strongly advocate linking a general concept of cooperativity with fundamental and rigorously derived measurable properties of Quantum Chemistry and Physics, namely the changes in (de)localization patterns of electron density on the increase of a molecular system. It makes then perfect sense to generate a holistic picture of cooperativity and cooperativity effects through quantum chemical topology (QCT)[64-66] methods, among them QTAIM, IQA, FALDI, and FAMSEC. In this contribution, our focus is on cooperativity as being a physics/quantum-based product of increasing counts of electrons delocalised throughout a molecular system with each addition of a component (molecule) to the system. To this effect, we will make extensive use of FALDI that was designed to quantify (de)localization of electrons among atoms of a molecular system. Notably, our concept of cooperativity is not restricted to a homogeneous molecular system made of the same kind of molecules.

To monitor changes in physical/quantum properties of cyclic water clusters, the proposed Eq. 16 was re-written to a general form that is suitable for modelling trends in cooperativity-induced changes in any property $y(n)$ of a molecular system, namely

$$y(n) = y(n_{\text{ref}})\left[1 + \beta\left(1 - e^{-\alpha(n - n_{\text{ref}})}\right)\right] \tag{17}$$

By replacing the $^W\Delta E(n)$ and $^W\Delta E(n_{\text{ref}})$ in Eq. 16 with relevant terms applicable to a physical/structural/quantum property under investigation one can generate a theoretical trend for a selected property of a system with fitted unitless α and β parameters. It is also obvious that the

80

reference state in Eq. 17 can be changed to meet requirements relevant to the specific property of interest. For instance, while the dimer is the most suitable reference state for most properties, it is unsuitable for measuring electron delocalization patterns stretching beyond neighbouring water molecules. Furthermore, having the fitted β parameter, one should be able to predict the maximal change in a selected property of a molecular system.

Although not considered in this work, one should be able to predict, relative to a selected reference state with n-water molecules in a cyclic structure, the limiting strength of a classical H-bond on $n \to \infty$, as measured by the IQA-defined interaction energy between generic H and O atoms forming an intermolecular H-bond, $\Delta E_{int}^{H,O}(n \to \infty) = \Delta E_{int}^{H,O}(n_{ref}) \times \beta$. We also expect that the α and β parameters will be useful when quantitatively comparing cooperativity effects in different systems, such as ammonia and acetone clusters, water clusters with non-cyclic geometries, or mixed clusters containing different types of molecules.

In the following sections, our focus will be on quantifying cooperativity and the cooperativity-related changes in selected properties of cyclic structures investigated. Qualitative and quantitative pictures of cooperativity and related properties will be presented. Trends in the total number of electrons delocalized by a statistical water molecule (and its atoms) among all water molecules in a cluster will be analysed following the MOWED-based concept of chemical bonding.[43] A simple attempt will be made to quantify the strength of intermolecular bonding induced by e-sharing between molecules. This will be compared against the strength of a classical and Lewis-defined single C–C covalent bond. The role played by the intermolecular O–H⋯O H-bonds will be explored in terms of facilitating the transport of electrons between water molecules. Finally, the origin and mechanism of e-delocalization throughout a cyclic structure will be explored through trends and patterns in the intramolecular (de)localization processes.

4.2. Quantifying cooperativity

4.2.1. Intermolecular delocalization of electrons by a water molecule in a cluster

In accord with a well-known Lewis concept, the chemical single, double and triple covalent bonds are formed when 1, 2 and 3 e-pairs are shared by the two neighbouring atoms. It is also well accepted that the physical/quantum processes of electron sharing and interference of the wavefunctions always stabilize a molecular system. In other words, a polyatomic system made of bonded atoms is expected to have a lower electronic energy than the combined energies of separate atoms. The Lewis concept of local diatomic e-pairs sharing (they are delocalized within the atomic volumes of the two atoms) is expanded holistically in the MOWED-based concept of chemical bonding to the entire 3D space occupied by a system.

The first electron count looked at is the number of electrons delocalized by a statistical water molecule $\mathcal{F}$ to all atoms of the remaining water molecules (treated as a molecular fragment $\mathcal{M}$) in a cluster. This intermolecular delocalization is denoted as $N^{\mathrm{deloc}}(\mathcal{F},\mathcal{M})$ and it was computed for each water molecule in each cluster using FALDI protocols. A significant increase in the count of delocalised by $\mathcal{F}$ to $\mathcal{M}$ electrons, $N^{\mathrm{deloc}}(\mathcal{F},\mathcal{M})$, was found - see circles in Figure 3.
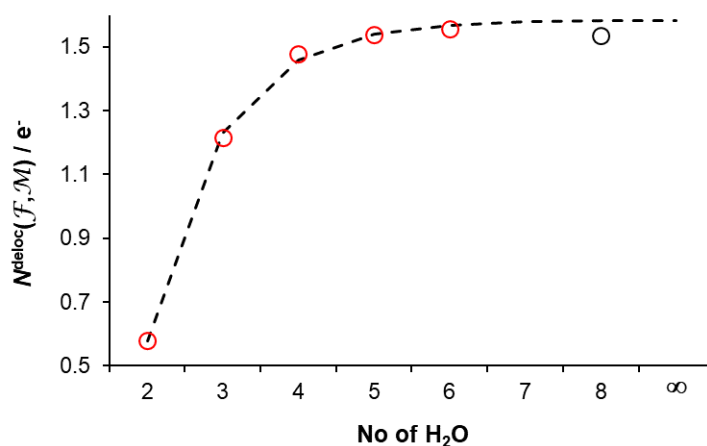
Figure 3. The trend in the number of electrons delocalized by a single water molecule to all atoms of the remaining water molecules in a cluster, $N^{\mathrm{deloc}}(\mathcal{F},\mathcal{M})$. The circles represent computed data and the dashed line is the fitted trend using Eq. 18.

On average, each water molecule in the dimer (smallest water cluster) delocalizes $0.579e$ among all atoms of the other water molecule. Naturally, this is significantly less than a classical intramolecular single covalent bond of $1e$ shared by an atom with its neighbouring atom in a

singly-bonded (i.e. $2e$ shared in total) homonuclear diatomic molecule, as suggested by Lewis over 100 years ago.[67] The difference between $N^{\text{deloc}}(\mathcal{F},\mathcal{M})$ computed for dimer and trimer is $0.636e$ showing a sharp 110% increase in the count of electrons delocalized by a water molecule with the formation of the first possible cyclic water cluster. Frenking[68] has reported recently that the formation of a covalent bond A-B is due to the interference of the wave functions of A and B and already singly occupied orbital can interfere constructively and form a bond. It is then clear that each water molecule makes comparable covalent-type contribution to intermolecular bonding with other water molecules by sharing $1.214e$ in trimer. The number of electrons delocalized by $\mathcal{F}$ with all other atoms in the hexamer water cluster is $1.557e$. This is almost a three-fold increase in the number of electrons delocalized relative to $0.579e$ delocalised by a water molecule in the dimer. From the above it follows that more than 9.3 electrons are shared among six water molecules in the cyclic hexamer. Mathematically, this count of delocalised electrons is equivalent to at least 4.5 single, ~2.5 double and 1.5 triple classical carbon-carbon covalent bonds.

It is known from an experiment[26] that water clusters are formed spontaneously but still water molecules move 'freely' in a liquid or gas phase as well as between them, e.g., evaporation and condensation of water. To shed some light on the ease with which water molecules can dissociate from clusters a decrease in the electronic energy of a statistical water molecule in a cluster was normalized per the count of electrons shared among all molecules in the cluster. It has been found that the $^{W}\Delta E(n)$ / (total count of e-shared) ratio is (i) -2.650 kcal/mol / $1.157e = -2.29$ kcal/mol per $1e$-shared obtained for a water molecule in a dimer and (ii) -7.979 kcal/mol / $9.341e = -0.854$ kcal/mol per $1e$-shared obtained for a water molecule in a hexamer. This finding, on one hand, reveals that intermolecular sharing of electrons provides a significant energy-minimizing contribution. On the other hand and in agreement with common sense, it shows that energetically intermolecular e-sharing is about an order of magnitude weaker when compared with classical covalent C-bonds; on average, a dissociation energy of a single C–C bond is about 90 kcal/mol,[69]

hence 45 kcal/mol per 1e-shared. This is an expected difference given that water-water interactions are closed-shell interactions with significantly less wavefunction overlap than open-shell classical covalent bonds. Moreover and importantly, we found that the normalised per a single shared electron energy-stabilizing effect on a cluster formation is most significant in a dimer and becomes weaker with an increase in the size of a cyclic structure. This does not mean, however, that it is easier to dissociate or separate a statistical water molecule when it is in larger water clusters.

The FALDI generated data for $N^{\mathrm{deloc}}(\mathcal{F},\mathcal{M})$ were fitted using Eq. 18. Using the water dimer as a reference state, the $\alpha = 1.040$ and $\beta = 1.737$ parameters, needed to theoretically predict the count of delocalized electrons in an n-size cyclic cluster, were obtained.

$$N^{\mathrm{deloc}}(\mathcal{F},\mathcal{M})(\mathrm{n}) = N^{\mathrm{deloc}}(\mathcal{F},\mathcal{M})(2)\left[1 + \beta\left(1 - e^{-\alpha(n-2)}\right)\right] \qquad (18)$$

The fitted trend, i.e., the dashed line follows the empty circles in Figure 3 quite well and, in theory, a statistical water molecule $\mathcal{F}$ in an infinitely large cyclic cluster cannot, relative to a dimer, increase the count of electrons shared by more than $N^{\mathrm{deloc}}(\mathcal{F},\mathcal{M})(\mathrm{dimer}) \times \beta = 1.005e$. Summing up the predicted maximal increase of 1.005e and the computed number of 0.578e shared by H_2O in a dimer suggests that, relative to a free water molecule, a fragment $\mathcal{F}$ in an infinitely large cyclic water cluster cannot delocalize more than 1.583e.

Being a global approach, the MOWED-based analysis is 'hiding' some details when local events are concerned. For instance, a statistical water molecule, on average, delocalizes in total 1.479 and 1.557 electrons to the remaining water molecules in cyclic tetramer and hexamer, respectively, but this does not mean that the neighbouring water molecules provide to each other the same count of electrons. Starting from a dimer, a definite and well-defined pattern persists throughout all cyclic structures, namely the water molecule considered as H-donor (our generic $H_2O1 = \mathcal{F}1$ water molecule) is delocalizing significantly less electrons to the adjacent water

molecule seen as a H-acceptor (our generic $H_2O4 = \mathcal{F}2$ water molecule) when compared with the

e-sharing in the opposite direction, i.e., from H_2O4 to H_2O1. For instance, FALDI predicts that (i) H_2O1(H-donor) delocalizes about 0.465 and 0.547 electrons to H_2O4(H-acceptor) in water dimer and hexamer, respectively, and (ii) H_2O4(H-acceptor) delocalizes about 0.692 and 0.909 electrons to H_2O1(H-donor) in water dimer and hexamer, respectively.

One must realize, however, that on a global scale each water molecule in a cyclic structure acts as an H-donor and H-acceptor when immediate neighbours are concerned. Furthermore, to have a full and MOWED-based picture one must not ignore e-density shared between distant water molecules and, considering cyclic hexamer we found from FALDI that the generic $\mathcal{F}1$ water molecule is delocalizing 0.547, 0.038. 0.013, 0.048, and 0.909 electrons to $\mathcal{F}2$, $\mathcal{F}3$, $\mathcal{F}4$, $\mathcal{F}5$, and $\mathcal{F}6$ water molecules, respectively, and this amounts to the total count of delocalized electrons of 1.557 that applies to each water molecule in the cyclic hexamer.

4.2.2. Intermolecular delocalization of electrons by atoms of a water molecule in a cluster

To gain deeper insight on intermolecular ED distribution patterns, we change a focus from a statistical water molecule $\mathcal{F}$ to its atoms. According to FALDI, H-atoms not involved in the intermolecular H-bonding (our generic H3 atom) share a rather minute count of electrons with remaining molecules reaching about 4 me in hexamer. On the other hand, H-atoms directly involved in intermolecular H-bonding, as exemplified by density bridges (DB, classical bond paths) between e.g., H2 and O4, delocalize significantly more electrons (43 and 63 me in dimer and hexamer, respectively).

One must note, however, that majority of delocalized electrons by a generic H2-atom is shared with a proton acceptor O4 (42 and 60 me in a dimer and hexamer, respectively). It is then very clear that the intermolecular e-delocalization involves, in terms of a number of e contributed, predominantly O-atoms of cyclic water clusters. As expected, the trend seen in Figure 3 is also

85

observed for the data denoted as $N^{\text{deloc}}(O1, \mathcal{M})$ where $\mathcal{M}$ represents all other water molecules (from $\mathcal{F}2$ to $\mathcal{F}n$) – see Figure S1 in the ESI. Just for the purpose of comparison and using hexamer as an example, the generic $\mathcal{F}1$ water molecule and O1-atom are delocalizing respectively 1.557 and 1.490e with $\mathcal{M}$, meaning that O-atoms contribute ~96% to the total count of delocalized electrons in a hexamer.

4.3. Cooperativity and the role played by a classical intermolecular H-bond

4.3.1. Delocalization and e-sharing patterns

Typically, for a 3-atom representation of an H-bond (DH···A, D = H-atom donor; A = H-atom acceptor) is used to explore its properties and its strength in the studies of inter- and intramolecular hydrogen bonding and this includes cooperativity among water molecules. Although highly localised, the standard approach that is focusing on an intermolecular classical H-bond (O1–H2···O4) is valuable as it can be used to reveal mechanism of electron sharing among atoms involved in the H-bond formation. To this effect, we found from FALDI that the O1–H2 group in a cyclic hexamer delocalizes to O4 (the proton acceptor) 0.488e with a dominant contribution coming from O1 $\rightarrow$ O4 delocalization count of 0.428e. Interestingly, O4 delocalizes nearly twice as much, 0.865e in total to the O1–H2 group of the proton donor: (i) the majority of delocalized 0.485e goes to the H2-atom directly involved in the intermolecular classical H-bonding and (ii) significant count of electrons of 0.379 is delocalized to O1. Interestingly, the two O-atoms share 0.807e combined whereas H2 and O4 share significantly less, 0.545e combined; this gives about 1.35e shared, in total, among the three atoms on the intermolecular H-bond formation in a hexamer. A similar pattern is observed in remaining clusters where (i) O-atoms share significantly more electrons than atoms directly involved in H-bonding, (ii) O1 delocalizes to O4 more than O4 to O1 and (iii) O4 delocalizes more electrons to H2 than to O1.

Restricting our knowledge to the data and patterns discussed above might create an impression that the atoms O1–H2···O4 of a classical H-bond:

(i)   Either constitute a unique assembly of atoms that is not involved in bonding of any significance with other parts of a molecular system; hence, the rest of a molecular system is simply ignored in description of H-bonding, or

(ii)   Interactions with other parts of a molecular system (if any) are presumed to be not significant enough such that the 3-atom description provides a significant and sufficient description of H-bonding.

From a molecular-wide perspective, contributions to a property of a system coming from all possible sources are considered and quantified without any presumption made on their significance – all contributions are treated on equal footing. Hence, from the MOWED-based approach it is of interest and importance to find out e-counts between atoms involved in the classical intermolecular H-bonding treated as a molecular fragment $\mathcal{G} = \{O1–H2···O4\}$ and other fragments of cyclic structures. Initially, water molecules that do not have common atoms with $\mathcal{G}$ in a cyclic hexamer were treated as a separate molecular fragment $\mathcal{H} = \{\mathcal{F}3, \mathcal{F}4, \mathcal{F}5, \mathcal{F}6\}$. We discovered that $\mathcal{G}$ and $\mathcal{H}$ share nearly twice as many electrons (2.65e) than atoms involved in the intermolecular O1–H2···O4 H-bonding (1.35e). Moreover, the count of electrons delocalised by the fragment $\mathcal{G} = \{O1–H2···O4\}$ to the fragment $\mathcal{H} = \{\mathcal{F}3, \mathcal{F}4, \mathcal{F}5, \mathcal{F}6\}$ is 1.591e, which again is more than the count of electrons shared among atoms of the O1–H2···O4 H-bond. Also $\mathcal{H}$ is delocalizing more than 1e to $\mathcal{G}$ (1.06e). Importantly, these e-counts are nearly entirely due to e-sharing among O-atoms of a cyclic cluster.

To gain a deeper insight on molecular-wide e-sharing we computed the count of electrons shared by the fragment $\mathcal{G} = \{O1–H2···O4\}$ with individual water molecules not having a common

atom with $\mathcal{G}$. We found that the total number of 2.65e is shared unequally between $\mathcal{G}$ and the $\mathcal{F}$3, $\mathcal{F}$4, $\mathcal{F}$5, and $\mathcal{F}$6 fragments (water molecules) and each fragment-pair $\{\mathcal{G},\mathcal{F}\text{n}\}$ made significant, hence not negligible, contribution of:

1) 0.949e shared between $\mathcal{G}$ and $\mathcal{F}$3 = {O7,H8,H9}; i.e. 35.8% of the total e-shared count.

2) 0.093e shared between $\mathcal{G}$ and $\mathcal{F}$4 = {O10,H11,H12}; i.e. 3.5% of the total e-shared count.

3) 0.109e shared between $\mathcal{G}$ and $\mathcal{F}$5 = {O13,H14,H15}; i.e. 4.1% of the total e-shared count.

4) 1.501e shared between $\mathcal{G}$ and $\mathcal{F}$6 = {O16,H17,H18}; i.e. 56.6% of the total e-shared count.

Furthermore, the counts of shared electrons between $\mathcal{G}$ and the closest water molecules ($\mathcal{F}$3 and $\mathcal{F}$6) reveal that a classical H-bond shares much more e-density with $\mathcal{F}$6 (1.50e, one could say with a water molecule placed at the back of the intermolecular H-bond) than with $\mathcal{F}$3 (0.949e, a water molecule placed in the front of a classical intermolecular H-bond).

4.3.2. Energy contribution to the cyclic structure

It is commonly accepted that e-sharing is synonymous with chemical bonding and the more electrons are shared the stronger bonding is. From the FALDI-based analysis, it follows that O-atoms of all cyclic water clusters delocalize more electrons throughout the entire cluster than the count of e-shared in the 3D space occupied by the O1–H2···O4 atoms forming intermolecular H-bonding. Also, O1,O4-atoms delocalize more electrons than H2···O4 atoms. These observations lead us to the following hypothesis: '*Since the majority of electrons shared among water molecules was delocalised by O-atoms of cyclic structures, O-atoms should be seen as a major contributor to cooperativity and responsible for the decrease in the energy of the clusters*'.

If the above hypothesis holds then it means that our 100-years concept of H-bonds in terms of their decisive energy stabilizing contributions is incorrect. In order to shed some light to the above hypothesis and, if possible, to validate it, we have made use of the FAMSEC approach where one

can quantify energy contribution made by any set of atoms on the *init* → *fin* state transformation of a molecular system. The proposed Eq. 16 allows one to predict, relative to a separate and non-interacting water molecule, a decrease in the energy of a water molecule when involved in a cluster formation. This means that we have used a free water molecule as an *initial* (or reference state) and exactly the same approach has been implemented in computing *mol*-FAMSEC terms. Using a hexamer as an example, the energy contribution of 3-atom fragments to the final energy of a cyclic hexamer was computed relative to the six non-interacting free water molecules. As one would expect, due to decades-old knowledge pertaining to the formation of intermolecular H-bonds, atoms involved in the intermolecular H-bonding do stabilize a molecular system and, as an example, the *mol*-FAMSEC term for the fragment $G = \{O1–H2\cdots O4\}$ in the cyclic hexamer was found to be –115 kcal/mol. This is a very significant contribution but it is nowhere close to what three neighbouring O-atoms contribute to the stability of clusters. In general, 3-atom O-containing fragments in *n*-water cyclic clusters contribute over 5 times more to the stability of a molecular system, e.g., *mol*-FAMSEC = –597 kcal/mol was computed for the {O1,O4,O7} fragment in cyclic water hexamer.

4.3.3. The H⋯O density bridges as 'highways' of sharing delocalized electrons

In general, any FALDI distribution (whether atom-localized density or atom-pair delocalized density) can be visualized in 3D space throughout a molecular system. Visualizing FALDI distributions in this manner can reveal insights towards the mechanism of electron (de)localization. Selected FALDI distributions generated for clusters investigated in this work are shown in Figure 4. It is clearly seen in Figure 4 that:

a) Even distant water molecules, i.e., the $\{\mathcal{F}1,\mathcal{F}3\}$, $\{\mathcal{F}1,\mathcal{F}4\}$ and $\{\mathcal{F}1,\mathcal{F}5\}$ water-pairs, share electrons between each other and the main transport channel is via H⋯O density bridges throughout a cyclic structure.

b) Quite surprisingly, the main density contributors, i.e., O-atoms, besides utilizing classical DBs, can also share density directly (i.e. through-space) - see isosurfaces showing *e*-sharing through the O1···O7 channel linking directly $\mathcal{F}1$ and $\mathcal{F}3$ in tetramer and O1···O10 channel linking $\mathcal{F}1$ and $\mathcal{F}4$ in hexamer. From this would follow that intermolecular DBs (bond paths) seen on molecular graphs do provide a 'privileged' QM-means of density sharing (as suggested by Pendas et al[70]) but they are not a unique way of *e*-sharing.

c) We found that, where applicable, isosurfaces computed for {$\mathcal{F}1,\mathcal{F}2$}, {$\mathcal{F}1,\mathcal{F}3$} and {$\mathcal{F}1,\mathcal{F}4$} are essentially identical in all water clusters.
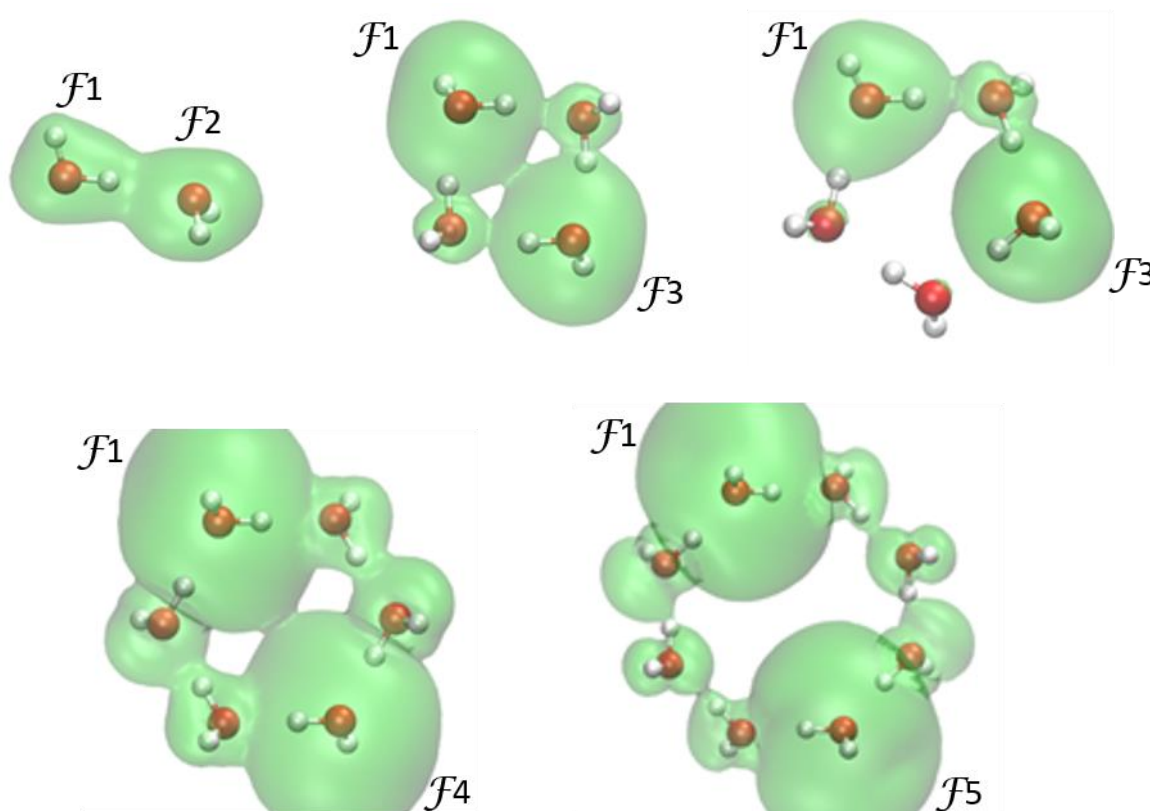
Figure 4. Visualizations of selected FALDI 3D density distributions computed for cyclic water clusters showing a mode of *e*-sharing throughout a molecular system between $\mathcal{F}1$ and the indicated water molecule presented as $\mathcal{F}$n. The 3D distributions are shown at isosurfaces of 0.001, 2E–05, 2E–05, 1.5E–07, and 1.E–08 au for dimer, tetramer, pentamer, hexamer, and octamer, respectively.

Density bridges on molecular graphs seen as dotted lines with small blue spheres representing critical points on DBs (see Figure 1) are linking two neighbouring water molecules and can be

seen as a part of a classical O1–H2···O4 H-bond (O1–H2←DB→O4). Intuitively, one assumes that these 'privileged' QM-means of density sharing are designed to exchange electrons between neighbouring water molecules. However, this has to be proved and to this effect we employed our methodology called a 1D-cross section[49] and applied it on a cyclic tetramer with the origin of the cross section set at the critical point between $\mathcal{F}1$ and $\mathcal{F}2$, i.e., CP(H2,O4). Significant delocalised electron density contributions made by atom-pairs at the CP(H2,O4) are included in Table 1 and selected results from the 1D-cross section are shown in Figures S2–S5 in the ESI. All these contributions are concentrating density at the CP(H2,O4) and its immediate vicinity; hence, they all are of a bonding and energy-stabilizing nature.[45,71]

Table 1. Atom-pairs that made major (significant) contribution to the total delocalized electron density (*deloc*-ED) at the critical point CP(H2,O4) on a density bridge between $\mathcal{F}1$ and $\mathcal{F}2$ in the cyclic water tetramer.

Contribution to the total *deloc*-ED			
At CP(H2,O4)		%-fraction	
Atom-pairs	ρ / au	**Individual**	**Cumulative**
O1,H2	0.0090	33.13	33.13
H2,O4	0.0047	17.32	50.45
O1,O4	0.0036	13.21	63.66
O4,H6	0.0034	12.56	76.22
O4,H5	0.0022	7.90	84.12
O1,H3	0.0014	5.13	89.25
O4,O7	0.0011	4.06	93.31
O1,H11	0.0003	1.19	94.50
O4,O10	0.0003	1.18	95.69
O1,O10	0.0003	0.95	96.64
H3,O4	0.0003	0.94	97.58

Data in Table 1 reveals that the three atom-pairs of a classical O1–H2···O4 H-bond made most significant contributions to the delocalized ED (*deloc*-ED) at the CP(H2,O4). This is expected as these atoms are in the closest vicinity of the CP(H2,O4). However, their contributions account only for 63.7% of the total *deloc*-ED meaning that a staggering 36% came from other atom-pairs

91

not formally involved in the O1–H2···O4 H-bond. Data included in Table 1 involves atom-pairs that contributed about 1% or more and excluding atoms O1, H2 and O4 of the hydrogen bond, there are eight such atom-pairs. To recover 99.9% of the delocalized ED at the CP(H2,O4) requires accounting for 26 atom-pairs in the cyclic tetramer. These results clearly show the importance of the MOWED-based approach in interpreting interactions in cyclic water structures and by extrapolation, in any molecular system under investigation. The above results correlate well with our previous report showing that DBs can form from multiple exchange channels often between non-neighbouring atoms.[71]

It is important to stress that all the 24 atom-pairs that contributed 99.9% of the delocalized ED discussed above made it in constructive (concentrating) manner meaning that the second partial derivative computed on their contributions along the second eigenvector, λ_2-eigenvector, at the CP(H2,O4) and its vicinity was negative – this is clearly seen in Figure S2 and S5 in the ESI. Traces seen in Figures S3-S4 in the ESI also show that regardless of the %-contribution made, the shape of the distribution of the delocalized density around the CP(H2,O4) is the same as found for the O1,H2 atom-pair, which made the most significant, i.e., 33% to the total *deloc*-ED at the CP(H2,O4).

In summary, it is then clear that the 'privileged' QM channel between H2 and O4 provides the most effective mode of transport through which electrons are delocalised among all atoms of a molecular system. The O–H···O 'highway' of sharing delocalized electrons throughout a system might be the most effective due to the unique combination of electron-rich O-atoms and the H-atom that delocalizes its single electron completely and without any trace of localised density found within the atomic volume of H. From this unique property of H-atom of non-localizing density when involved in the intermolecular H-bonding, one might speculate that electrons from all close and further neighbours of the generic H2-atom are not experiencing any significant

92

attraction in terms of being retained (localized to H2) hence they can travel freely on this highway

from one fragment to another. This insight could only be gained from MOWED-based approach.

### 4.4. Intra-molecular (de)localization of electrons

A separate water molecule $\mathcal{F}$ has $N(\mathcal{F}) = 10e$ in total and all of these electrons are denoted as

$N^{\text{self}}(\mathcal{F})$ because they are not shared with any other molecule or atom outside $\mathcal{F}$; hence, it can be

seen as a count of self-electrons of a molecule. Formally, $10e$ is made of $8e$ of O-atom and $2e$

coming from both H-atoms. Moreover, the total count of $N^{\text{self}}(\mathcal{F})$ is made of electrons delocalized

among atoms of a fragment $\mathcal{F}$, $N^{\text{deloc}}(\mathcal{F},\mathcal{F})$ (in this case a non-interacting water molecule) and the

total count of electrons localized to a specific atom of $\mathcal{F}$ (they cannot be found anywhere else but

within an atomic volume of an atom constituting a water molecule), $N^{\text{loc}}(\mathcal{F})$ - Eq. 19.

$$N^{\text{self}}(\mathcal{F}) = N^{\text{deloc}}(\mathcal{F},\mathcal{F}) + N^{\text{loc}}(\mathcal{F}) \tag{19}$$

Hence, following Lewis concept of bonding and disregarding any electronegativity differences

and resonance effects, a free water molecule should have $N^{\text{self}}(O)$ made of $N^{\text{loc}}(O) = 6e$ plus

$N^{\text{deloc}}(O) = 2e$ and for each H-atom $N^{\text{deloc}}(H) = 1e$. According to FALDI-based calculations and as

expected, there are no electrons localised to a H-atom in a water molecule, $N^{\text{loc}}(H) = 0$ as its

electron is shared with the O-atom. While the classical Lewis model qualitatively accounts for

electronegativity differences (as well as multi-centric resonance through conceptual valence bond

theory), it struggles to do so quantitatively. FALDI recovers the Lewis model, as well as any

charge-transfer and additional electron delocalization that occurs due to electronegativity

difference and multi-centric effects - each H-atom shares with O-atom only $0.423e$ rather than a

single electron. This means that each H-atom permanently 'lost' over $0.5e$ in favour of the O-atom

and, as a consequence, the electron population of O-atom increased from $8e$ in a free O-atom to

$9.14e$ when O-atom formed two O–H bonds in a free and non-interacting water molecule.

93

Interestingly, however, a single O–H bond in non-interacting H_2O shares 2.07 electrons, which is very close to the Lewis $2e$ single covalent bond dogma, and this is a product of 1.649 and 0.423 electron contributions made by O- and H-atom, respectively.

Naturally, when water clusters are formed, the intramolecular (de)localization patterns in the water molecule must change as, due to cooperativity, it shares electrons with all other water molecules in a cluster. Water dimer is unique as this is not a cyclic structure; hence, electrons are shared between two distinctive water molecules: 1) the one that plays the classical role of an H-donor (our generic $\mathcal{F}1$) and the other, $\mathcal{F}2$, is commonly seen as a proton acceptor. It is then expected that the $N^{\text{self}}(\mathcal{F})$ count will decrease upon formation of the dimer, but not equally. FALDI data showed that the electron count found exclusively in the H-donor water molecule is $N^{\text{self}}(\mathcal{F}1\text{-}donor) = 9.558e$ whereas for the H-acceptor water molecule $N^{\text{self}}(\mathcal{F}4\text{-}acceptor) = 9.285e$. It is then clear that $\mathcal{F}4$-acceptor is delocalizing to a H-donor, $\mathcal{F}1$-donor, significantly more, ~$0.23e$. Considering cyclic structures, each water molecule acts as a H-donor and H-acceptor meaning that each $\mathcal{F}$ will have exactly the same count of $N^{\text{self}}(\mathcal{F})$. Indeed and as expected due to cooperativity induced increase in the count of shared electrons among water molecules in a cluster, the averaged $N^{\text{self}}(\mathcal{F})$ count decreases with an increase in the size of a cyclic structure – see circles in Figure 5.
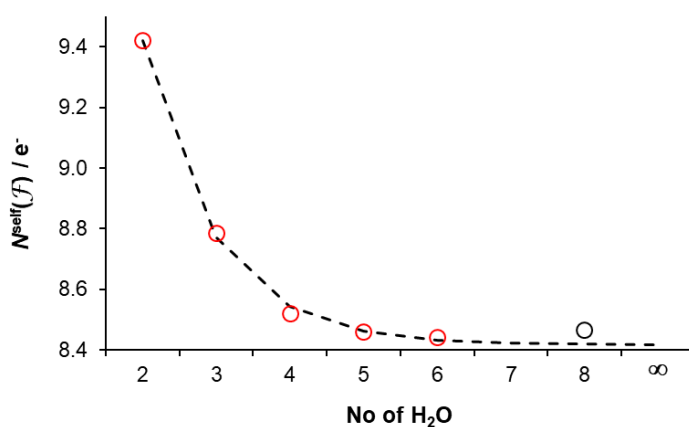
Figure 5 The trend in the number of electrons found only in a statistical water molecule with an increase in the size of a cyclic water cluster, $N^{\text{self}}(\mathcal{F})$. The circles represent computed FALDI data, and the dashed line is the fitted trend using Eq. 20.

94

The trend (dashed line in Figure 5) was obtained from Eq. 20 from which we obtained parameters $\alpha = 1.042$ and $\beta = -0.107$.

$$N^{self}(\mathcal{F})(n) = N^{self}(\mathcal{F})(2)\left[1 + \beta\left(1 - e^{-\alpha(n-2)}\right)\right] \tag{20}$$

Using these parameters and the averaged $N^{self}(\mathcal{F})$ value of $9.421e$ obtained for a water dimer, one can theoretically predict that a statistical water molecule in a cyclic structure has a lower limit of localized to itself electrons, $N^{self}(\mathcal{F}) = 8.417e$. This means that a statistical water molecule in a symmetric, homodromic cyclic cluster cannot delocalize more than $N^{deloc}(\mathcal{F},\mathcal{R}) = 1.583e$. (recall that the non-interacting separate water molecule has the $N^{self}(\mathcal{F})$ count of $10e$). This value describes the limit of cooperativity a cyclic structure can rich showing a trade-in between intermolecular bonding (it decreases E of a system) and intramolecular increase in the self-atomic energies. Using the *classic*-FAMSEC approach[47] we found that the self-energy of $\mathcal{F}$ and the *loc*-FAMSEC energy term (it accounts for changes in self-atomic and intramolecular interaction energies on the transition from a non-interacting water molecule to that in a cluster) does indeed increase with the size of a cyclic structure – selected data are included in Table S2 in the ESI. Relative to non-interacting water molecule, the largest increase in self-atomic energies is observed for O-atoms from a water dimer ($^{dimer}\Delta E_{self}(O1) = 11$ kcal/mol) to a cyclic octamer ($^{octamer}\Delta E_{self}(O1) = 34.8$ kcal/mol) and this can be attributed to the increasing number of delocalised electrons by O-atoms. Considering a statistical H3-atom, its self-atomic energy hardly changed as bonding pattern for the H3-atom has not changed – it is not involved in intermolecular interactions accompanied by the formation of new ED-bridges.

Notably, the decrease in the $N^{self}(\mathcal{F})$ count by about $1e$ seen in Figure 5 (from $9.42e$ in a dimer to $8.44e$ in a hexamer) is a product of several interesting (de)localization patterns taking place in a statistical water molecule when it becomes a member of an increasing in size cyclic water

95

structure. A detailed count of the physical (de)localization process taking place on the increase in the cluster size from a dimer to octamer is presented in Table S3 in ESI. Focusing on most important contributions made by a statistical water molecule $\mathcal{F}1$ and its atoms on the change from a dimer to hexamer we note that a statistical:

a) O1-atom is decreasing the count of its localized electrons by $0.58e$.

b) The O1,H2 atom-pair decreased the number of shared electrons by $0.36e$, from $1.90e$ in a dimer to $1.54e$ in a hexamer showing that the Lewis dogma must be treated in a highly flexible fashion when atoms become involved in the intermolecular interactions.

c) The O1,H3 atom-pair shares about $2e$, as predicted by a Lewis-based concept of a single covalent bond, and this is due to H3 not being involved in an additional significant intermolecular interaction. This is also recovered by the $N^{\text{deloc}}(\text{H3},\mathcal{M})$ term that reached $0.004e$, i.e., the count of electrons delocalised by H3 to all remaining water molecules in a water cluster.

d) The O1,O4 atom-pair increased the number of shared electrons up to about $0.8e$.

e) A water molecule $\mathcal{F}1$ increased the count of delocalised electrons mainly because of the contribution made by O1-atom; it increased from $0.555e$ in a dimer to $1.490e$ in a hexamer.

All the above clearly shows that the O-atoms are in a driving sit when the cooperativity phenomenon goes, i.e., delocalizing electrons between water molecules of cyclic structures. As there are no localized electrons on H-atoms, the increased electron count of O-atoms is being depleted with an increase in the water cluster from a dimer to octamer. Importantly, the number of shared electrons between O- and H-atoms of a statistical water molecule decreased significantly meaning that the covalent character of the single O–H bond also decreased significantly. We conclude that that the cooperativity, as measured by the number of delocalised electrons, must approach a limiting value and this is simply due to preserving a constellation of nuclei that is commonly known as a water molecule.

5. Conclusions

Cooperativity is inherently a molecular-wide concept, in that it cannot be defined without consideration of system-wide properties. Classical chemical language such as describing bonding (and especially hydrogen bonding) in terms of 2- or even 3-centre events therefore cannot provide a rational and exhaustive description of a non-local property such as cooperativity.

In this work, we redefine cooperativity in terms of molecular-wide physics and especially embracing the non-locality of quantum mechanics, captured and defined simultaneously by the wave-nature of particles. However, to retain chemical interpretability and to lower the language barrier between holistic physics and reductionist chemistry, we place the concept of electron delocalization at the centre and forefront of our cooperativity model. By using modern techniques in theoretical quantum chemistry, we are able to cast non-local and non-additive properties into atomic and molecular fragment resolutions.

We suggest that cooperativity in cyclic water clusters (such as the observation that the molecular energy decrease non-additively with an increase in water cluster size) arise from increasing electron delocalization across both the H-bonded atoms themselves (i.e. OH···O) as well as across neighbouring and non-neighbouring water molecules, i.e., throughout entire molecular system. Since electron delocalization itself is an energy-lowering phenomenon synonymous with bonding (whether through orbital expansion, reduction of electron-electron repulsion, minimization of Hellman and Feynman forces or whatever other lexicological school one ascribes to), our model of cooperativity suggests a clear mechanism for non-additive stabilization through molecular-wide electron delocalization.

To describe, test and explore our model, we derived a non-linear model equation that fits two unitless parameters to any molecular or atomic property of interest, relative to a suitable reference. Using our equation, we showed that i) we can predict the theoretical maximum, i.e. the limiting and cooperativity-induced value the property can reach ii) predict the rate of change of the property

97

with increasing water cluster size and iii) show where structural changes lead to deviations of the property from an otherwise ideally cooperative system.

When we fit our equation to the molecular energy, we recover the expected non-additive stabilization and show that the maximum obtainable stabilization per water molecule (in an infinitely large cyclic water cluster and relative to a water dimer) is –5.7 kcal/mol. We show that this value is mostly reached in the cyclic hexamer but is otherwise not exactly obtainable due to non-planar structures in larger cyclic clusters.

We then turned to the property central to our model of cooperativity – intermolecular electron delocalization. We showed that the number of electrons shared between a single water molecule with all other atoms in a cyclic water cluster increases non-additively with cluster size, from $0.579e$ in a water dimer to a theoretical maximum of $1.583e$. This almost 3-fold increase in electrons delocalized, arising from a single molecule but at a molecular-wide scale, is the primary reason for any cooperativity effect. We also look at the same effect of electron delocalization from different angles and resolutions: i) while delocalization between neighbouring water molecules are both largest and show the largest increase with cluster size, delocalization between non-neighbouring water molecules are non-negligible, ii) oxygen atoms are the primary sources of intermolecular delocalized electrons, and iii) while atoms of a classical H-bond (OH⋯O) in hexamer share a large quantity electrons (i.e. $1.35e$), the same atoms share almost double the number of electrons (i.e. $2.65e$) with all other water molecules in this cyclic cluster. We also expressed our concept of cooperative electron sharing in terms of energy changes upon formation of any cluster and showed that the oxygen atoms are indeed the primary drivers of stabilization.

Finally, we provide some insights on the electronic mechanism of cooperativity. We show that the maximum theoretical limit on molecular electron delocalization might arise from an energy balance between a water molecule's 'self' electron population (i.e. the count of atom-localized electrons and intramolecular delocalized electrons combined) and its intermolecular delocalized

electron population count. The two electron counts change inversely with cluster size, suggesting that fragment-localized electrons impose a limit on the total number of electrons that can be shared in an energetically efficient manner with the rest of the system. We note that, in a molecular environment dominated by oxygen-oxygen electron delocalization, hydrogen atoms play an interesting role: H-atoms contain no localized electrons and contribute insignificantly to intermolecular electron delocalization. Rather, these atoms delocalize most of their electrons intramolecularly to their covalently-bonded oxygen atoms, increasing O-atoms' total electron delocalization count. Using cross-sections of the electron density and visualizations of delocalized electron distributions, we show that density bridges between water molecules act as 'highways' for intermolecular delocalization (for both neighbouring and non-neighbouring water molecules) – in the tetramer, 36% of the total electron delocalization at the CP(H2,O4) arises from distant water molecules. The resultant 'privileged exchange channels' should therefore not be interpreted as local density bridges connecting neighbouring water molecules, but rather a continuous, molecular-wide path for cooperative electron delocalization between predominantly oxygen atoms.

Conflicts of interest

The authors declare no conflict of interest.

Acknowledgments

References

1   D. Ben-Amotz, Science, 2022, 376, 800-801.

2   M. B. Ahirwar, S. R. Gadre and M. M. Deshmukh, *J. Phys. Chem. A*, 2020, **124**, 6699−6706.

3   A. Simon, M. Rapacioli, E. Michoulier, L. Zheng, K. Korchagina and J. Cuny, *Mol. Sim.* 2019, **45**, 249–268.

4   A. Rakshit, P. Bandyopadhyay, J. P. Heindel and S. S. Xantheas, *J. Chem. Phys.* 2019, **151**, 214307.

5   J. C. Howard and G. S. Tschumper, *WIREs Comput. Mol. Sci.,* 2014, **4**, 199−224.

6.   C. Pérez, M. T. Muckle, D. P. Zaleski, N. A. Seifert, B. Temelso, G. C. Shields, Z. Kisiel, B. H. Pate, Science, 2012, **336**, 897–901.

7   F. N. Keutsch, J. D. Cruzan and R. J. Saykally, *Chem. Rev.*, 2003, **103**, 2533–2577.

8   R. Ludwig, *Angew. Chem. Int. Ed.* 2001, **40**, 1808–1827.

9   J. M. Ugalde, I. Alkorta and J. Elguero, *Angew. Chem. Int. Ed.*, 2000, 39, 717–721.

10   L. Albrecht, S. Chowdhury and R. J. Boyd, *J. Phys. Chem. A*, 2013, **117**, 10790−10799.

11   J. M. Guevara-Vela, R. Chávez-Calvillo, M. García-Revilla, J. Hernández-Trujillo, O. Christiansen, E. Francisco, Á. M. Pendás, and T. Rocha-Rinza, *Chem. Eur. J.*, 2013, **19**, 14304–14315.

12   J. Nochebuena, C. Cuautli and J. Ireta, *Phys. Chem. Chem. Phys.,* 2017, **19**, 15256–15263.

13   O. Mó, M. Yáñez and J. Eiguero, *J. Chem. Phys.*, 1992, **97**, 6628–6638.

14   S. S. Xantheas, *J. Chem. Phys.*, 1994, **100**, 7523–7534.

15   S. S. Xantheas, *Chem. Phys.*, 2000, **258**, 225–231.

16   M. J. Gillan, D. Alfè and A. Michaelides, *J. Chem. Phys.*, 2016, **144**, 130901.

17   E. Romero-Montalvo, J. M. Guevara-Vela, A. Costales, Á. M. Pendás and T. Rocha-Rinza, *Phys. Chem. Chem. Phys.,* 2017, **19**, 97–107.

18   G. Han, Y. Ding, P. Qian, C. Zhang, and W. Song, *Int. J. Quantum Chem.*, 2013, **113**, 1511–1521.

19   L. Albrecht and R. J. Boyd, *Comput. Theoret. Chem.*, 2015, **1053**, 328–336

20   S. S. Xantheas and T. H. Dunning, Jr., J. Chem. Phys. 1993, 99, 8774–8792.

21   K. Liu, J. D. Cruzan, R. J. Saykally, *Science*, 1996, **271**, 929–933.

22   K. Liu, M. G. Brown, J. D. Cruzan, R. J. Saykally, *Science*, 1996, **271**, 62–64.

23   F. Weinhold, *J. Mol. Struct. (Theochem)*, 1997, **398-399**, 181-197.

24   S. Maheshwary, N. Patel, N. Sathyamurthy, A. D. Kulkarni and S. R. Gadre, *J. Phys. Chem. A*, 2001, **105**, 10525–10537.

25   L. Ojamäe and K. Hermansson, *J. Phys. Chem.*, 1994, **98**, 4271–4282.

26 K. Ohno, M. Okimura, N. Akai and Y. Katsumoto, *Phys. Chem. Chem. Phys.*, 2005, **7**, 3005–3014.

27 L. Albrecht and R. J. Boyd, *J. Phys. Chem. A*, 2012, **116**, 3946−3951.

28 A. S. Mahadevi and G. N. Sastry, *Chem. Rev.*, 2016, **116**, 2775−2825.

29 C. Rong, D. Zhao, D. Yu and S. Liu, *Phys. Chem. Chem. Phys.*, 2018, **20**, 17990–17998.

30 G. Hincapié, N. Acelas, M. Castaño, J. David, and A. Restrepo, *J. Phys. Chem. A*, 2010, **114**, 7809–7814.

31 B. D. Marshall, *J. Chem. Phys.,* 2017, **146**, 174104.

32 E. D. Glendening, *J. Phys. Chem. A*, 2005, 109, 11936–11940.

33 J. E. H. Koehler and W. Saenger, *J. Comput. Chem.*, 1987, **8**, 1090–1098.

34 K. Liu, M. G. Brown, J. D. Cruzan, R. J. Saykally, J. K. Gregory, and D. C. Clary, Nature, 1996, 381, 501–503.

35 Y. I. Neela, A. S. Mahadevi and G. N. Sastry, *J. Phys. Chem. B*, 2010, **114**, 17162–17171.

36 S. Saha and G. N. Sastry, *Mol. Phys.*, 2015, 113, 3031–3041.

37 S. S. Xantheas, *J. Chem. Phys.*, 1995, **102**, 4505–4517.

38 S. S. Xantheas and E. Aprà, *J. Chem. Phys.*, 2004, **120**, 823–828.

39 V. S. Znamenskiy and M. E. Green, *J. Chem. Theory Comput*., 2007, **3**, 103–114.

40 J. M. Guevara-Vela, E. Romero-Montalvo, V. A. M. Gómez, R. Chávez-Calvillo, M. García-Revilla, E. Francisco, Á. M. Pendás, and T. Rocha-Rinza, *Phys. Chem. Chem. Phys.*, 2016, **18,** 19557–19566.

41 G. Frenking and A. Krapp, *J. Comput. Chem.*, 2007, **28**, 15–24.

42 R. F. W. Bader, *J. Phys. Chem. A*, 2009, **113**, 10391–10396.

43 I. Cukrowski, *WIREs Comput. Mol. Sci.*, 2022, **12**, e1579.

44 J. H. de Lange and I. Cukrowski, *J. Comput. Chem.*, 2017, **38**, 981–997.

45 J. H. de Lange, D. M. van Niekerk and I. Cukrowski, *J. Comput. Chem.*, 2018, **39**, 973–985.

46 J. H. de Lange and I. Cukrowski, *J. Comput. Chem.*, 2018, **39**, 1517–1530.

47 I. Cukrowski, *Comput. Theoret. Chem.*, 2015, **1066**, 62–75.

48 I. Cukrowski, G. Dhimba and D. L. Riley, *Phys. Chem. Chem. Phys.*, 2019, **21**, 16694–16705

49 I. Cukrowski, J. H. de Lange JH, A. S. Adeyinka and P. Mangondo, *Comput. Theoret. Chem.*, 2015, **1053**, 60–76.

50 M. J. Frisch, G. W. Trucks, H. B. Schlegel, G. E. Scuseria, M. A. Robb, J. R. Cheeseman, G. Scalmani, V. Barone, B. Mennucci, G. A. Petersson, H. Nakatsuji, M. Caricato, X. Li,

H. P. Hratchian, A. F. Izmaylov, J. Bloino, G. Zheng, J. L. Sonnenberg, M. Hada, M. Ehara, K. Toyota, R. Fukuda, J. Hasegawa, M. Ishida, T. Nakajima, Y. Honda, O. Kitao, H. Nakai, T. Vreven, J. A. Montgomery, J. E. Peralta, F. Ogliaro, M. Bearpark, J. J. Heyd, E. Brothers, K. N. Kudin, V. N. Staroverov, R. Kobayashi, J. Normand, K. Raghavachari, A. Rendell, J. C. Burant, S. S. Iyengar, J. Tomasi, M. Cossi, N. Rega, N. J. Millam, M. Klene, J. E. Knox, J. B. Cross, V. Bakken, C. Adamo, J. Jaramillo, R. Gomperts, R. E. Stratmann, O. Yazyev, A. J. Austin, R. Cammi, C. Pomelli, J. W. Ochterski, R. L. Martin, K. Morokuma, V. G. Zakrzewski, G. A. Voth, P. Salvador, J. J. Dannenberg, S. Dapprich, A. D. Daniels, O. Farkas, J. B. Foresman, J. V. Ortiz, J. Cioslowski and D. J. Fox, Gaussian 09, Revision D.1; Gaussian, Inc.: Wallingford, CT, 2009.

51   S. Grimme, *Wiley Interdiscip. Rev. Comput. Mol. Sci*. 2011, **1**, 211–228.

52   R. F. W. Bader, *Atoms in Molecules. A Quantum Theory*, Clarendon Press, Oxford, 1990.

53   M. A. Blanco, Á. M. Pendás and E. Francisco, *J. Chem. Theory Comput.*, 2005, **1**, 1096–1109.

54   E. Francisco, Á. M. Pendás, M. A. Blanco, *J. Chem. Theory Comput*., 2006, **2**, 90–102.

55   T. A. Keith, *AIMAll (Version 19.02.13)*, 2019, http://aim.tkgristmill.com.

56   I. Cukrowski, *Phys. Chem. Chem. Phys.*, 2019, **21**, 10244–10260.

57   W. Humphrey, A. Dalke and K. Schulten, *J. Molec. Graphics,* 1996, **14**, 33–38.

58   I. Cukrowski, J. H. de Lange and S. Hussain, MOWeD-LAC (Molecular-wide electron (de)localization atomic counts) and MOWeD-LFC (Molecular-wide electron (de)localization fragment counts) software applications, 2023. Available at https://bit.ly/link-to-mowed-software

59   R. Ponec, *J. Math. Chem.*, 1997, **21**, 323–333.

60   R. Ponec, *J. Math. Chem.*, 1998, **23**, 85–103.

61   P. Bultinck, D. L. Cooper and R. Ponec, *J. Phys. Chem. A*, 2010, **114**, 8754–8763.

62   J. Cioslowski, *Int. J. Quantum Chem.*, 1990, **24**, 15–28.

63   P. Hohenberg and W. Kohn, *Phys. Rev.*, 1964, **136**, B864–B871.

64   A. F. Silva, M. A. Vincent, J. L. McDonagh, and P. L. A. Popelier, *Chem. Phys. Chem.*, 2017, **18**, 3360–3368.

65   S. J. Davie, P. I. Maxwell and P. L. A. Popelier, *Phys. Chem. Chem. Phys.*, 2017, **19**, 20941–20948

66   P. L. A. Popelier, *Structure and Bonding. Intermolecular Forces and Clusters, Springer*, Heidelberg, Germany, 2005, vol. **115**, pp. 1–56.

67   G. N. Lewis, *J. Am. Chem. Soc.*, 1916, **38**, 762–785.

68   G. Frenking, *Mol. Phys.*, 2023, **121**, DOI: 10.1080/00268976.2022.2110168

69   S. J. Blanksby and G. B. Ellison, *Acc. Chem. Res.*, 2003, **36**, 4, 255–263.

70   Á. M. Pendas, E. Francisco, M. A. Blanco, and C. Gatti, *Chem. Eur. J.*, 2007, **13**, 9362–9371.

71   J. H. de Lange, D. M. E. van Niekerk, I. Cukrowski, *J. Comput. Chem.*, 2018, **39**, 2283–2299.

TOC

Cooperativity is synonymous with intermolecular delocalization of electrons throughout cyclic water clusters. Electrons provided mainly by O-atoms 'travel on a density highway' (···O–H···O–H···O–H···) using H-bond built density bridges linking water molecules.

Chapter 4

Cooperativity-Induced Effects

Introduction

It is clear from Chapters 1 and 3 that cooperativity leads to a non-linear decrease in the electronic energy of the system with the incremental addition of water molecules. It was also shown in Chapter 3 that the electronic energy decrease is linked with the increasing intermolecular delocalization of electrons. The biggest and most significant result noted in the previous chapter was that the molecular-wide effect taking place within the water cluster yielded the delocalization of electrons taking place from 1) the H-bond to other atoms and 2) from fragment $\mathcal{F}$ to all other fragments in the water cluster. It was concluded that the highways on which the electrons travel around the cyclic water cluster exist to ensure that stability is optimal for every water molecule or fragment $\mathcal{F}$.

Various geometrical, electronic and energetic changes can be observed as the cyclic water structures are stabilized through cooperativity. These results are a product of cooperativity within the water cluster known as *cooperativity effects*. The cooperativity effects include properties such as atomic charge, FAMSEC energetic components, topological properties and geometrical descriptors (i.e. intermolecular distance) – that is, any molecular or local property that *results from* but is not necessarily a *cause of* cooperativity. This chapter revolves around these changes due to cooperativity within the water cluster. This chapter therefore serves as a companion to Chapter 3.

The atomic charges of the oxygen and H-bond hydrogen atoms are discussed first, followed by an investigation of FAMSEC-defined interaction energies with their components (exchange-correlation and electrostatic interaction energy). The interaction energy is first looked at with the whole molecule as the focus (i.e. the total interaction energy), followed by its intermolecular and intramolecular contributions. The di-atomic contributions for intra-molecular interactions are shown as well. The third property investigated is the topological properties at the (H2,O4) critical point, and the last property considered is a set of selected geometrical descriptors, that is,

the link between intermolecular distance and all the changes due to cooperativity (i.e. electronic energy, electron counts, interaction energy) for the water clusters.

The general equation (see Equation 3 in Chapter 3) to fit the computed data is again used in this chapter, although it models different molecular, atomic and fragment properties. Note that the cyclic water clusters are the same as the ones used in the previous chapter, reproduced in this chapter in Figure 1 below for easy reference.
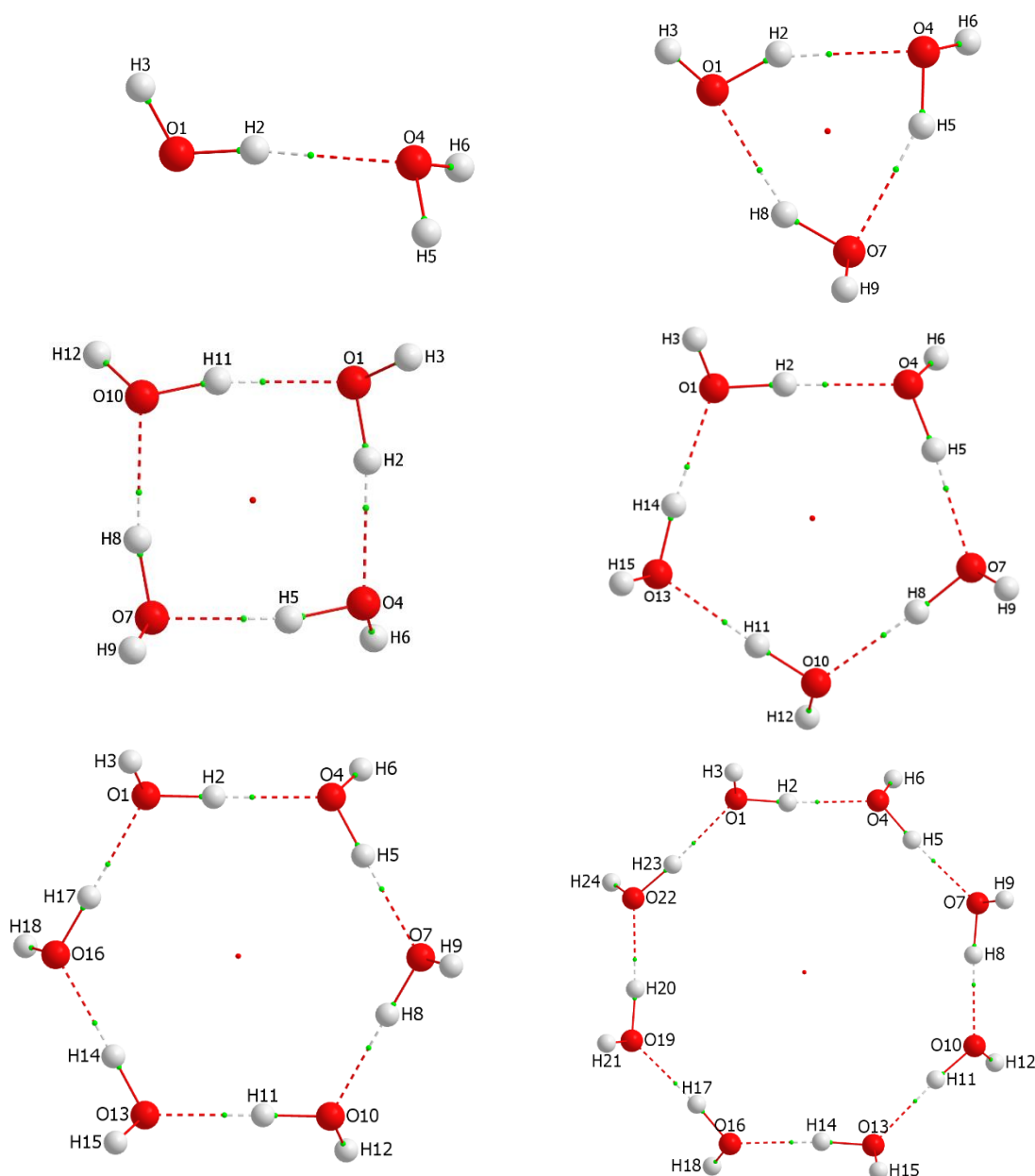
Figure 1 The cyclic water clusters investigated $(H_2O)_n$ $n = 2–6, 8$

To reiterate the numbering system used, water molecules are numbered consistently as On, H(n+1) and H(n+2) such that (i) the numbering of On-atoms differs by 3 (O1, O4, O7, etc.), (ii) the generic H(n+1) atom (i.e. H2, H5, H8, etc. in the consecutive water molecules of a cyclic cluster) forms the intermolecular H-bond with the neighbouring water molecule, and (iii) the generic H(n+2) atom in each water molecule (i.e. H3, H6, H9, etc.) always points out of the ring.

Atomic Net Charges

Changes in atomic net charge can be seen as a cooperativity effect – the net changes in the total number of delocalized and localized electrons of an atom will often not be equal, leading to an increase or decrease in the total electron population of the atom. Hence cooperativity-induced changes in electron delocalization will often result in charge transfer as observed in changes in atomic charges.

The net atomic charge is calculated from QTAIM[1] using $Q(A) = Z(A) - N(A)$, where Z(A) is the number of protons for atom A and N(A) is the number of electrons. The change in the atomic charge of an atom is calculated by $\Delta Q(A) = N^{\text{total}}(A)(\text{monomer}) - N^{\text{total}}(A)(n\text{-H}_2\text{O})$, where $N^{\text{total}}(A)(\text{monomer})$ is the total number of electrons for an atom A in a free non-interacting monomer, and $N^{\text{total}}(A)(n\text{-H}_2\text{O})$ is the total number of electrons of an atom A in the n-size water cluster. The atomic charge changes for the H3 atom are not discussed here because its atomic charge does not change in any meaningful way; the only meaningful charge changes are observed for O atoms and H2, the hydrogen directly involved in H-bonding. Note that here O serves as the average for all O atoms in the water cluster and H2 serves as the average for all H2 atoms in the cluster.

The average atomic charge for O in each water cluster size is shown in Figure 2(a). In the water dimer $Q(O)$ is $-1.171e$, which then decreases non-linearly, meaning that the O atom becomes more negatively charged as the cyclic water cluster increases in size. The trend is fitted

using Equation 1 with parameters $\alpha = 0.725$ and $\beta = 0.051$ to obtain a theoretical maximum negative charge ($Q(O)(dimer) \times 1 + \beta$) for the O atom in an infinitely large water cluster of $-1.232e$. The O atomic charge changes from the dimer to the hexamer with 57 me.
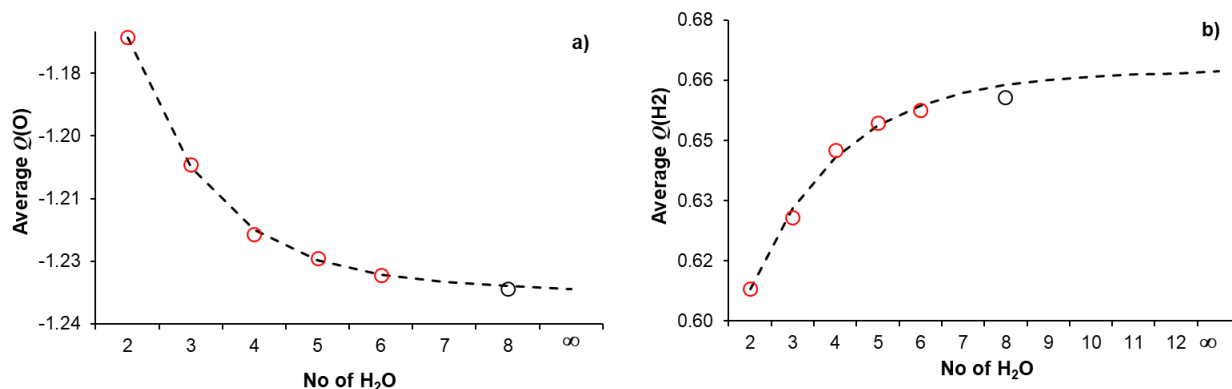
Figure 2 Part a - The trend in the average atomic charge (Q) for the oxygen atom in each cyclic water cluster. Part b - The trend in the average atomic charge (Q) for the H2 atom in each cyclic water cluster. The circles represent the computed data, and the dashed line is the fitted trend using the derived Equations 1 and 2.

$$Q(O)(n) = Q(O)(2)[1 + \beta(1 - e^{-\alpha(n-2)})] \tag{1}$$

$$Q(H2)(n) = Q(H2)(2)[1 + \beta(1 - e^{-\alpha(n-2)})] \tag{2}$$

In the previous chapter, localized and delocalized electron counts were investigated for each atom as an element of cooperativity. How changes in atomic (de)localized electron counts relate to changes in atomic net charge is shown here. The net difference between the loss of localized electrons and the gain of delocalized electrons is equal to the change of atomic charge and therefore of net charge transfer. The localized electron count of the O atom decreases by $0.603e$ from dimer to hexamer, and the delocalized electron count of the O atom increases by $0.660e$ from dimer to hexamer (Chapter 3). The difference between these two electron counts is 57me, which is the same difference as that between dimer and hexamer for the O atomic charge. This result is interesting because the charge does not originate purely from the change in the localized

electrons of the O population. The positive change in delocalization is greater than the negative change in localization for the O atom, which means that the delocalization of electrons is the primary reason for the decrease of the atomic charge. Additionally, there is a correlation with the statement at the beginning of this chapter that atomic charge is linked with the movement of electrons. There is not simply an electron exchange (i.e. conversion of localized to delocalized electrons) that takes place as would be classically expected, but rather a net movement of the electrons within the water cluster. The difference between hexamer and the maximum negative charge is 3 me, therefore the O can become even more (however slightly) negatively charged. The notion of electronegativity is expressed here in somewhat different terms – the capacity of the highly electronegative atom to become more negatively charged through increased electron delocalization is high and results in further stabilization of the molecular system as a whole.

The atomic charge for H2 in each water cluster size is shown in Figure 2(b). The trend for H2 atomic charge increases non-linearly due to the loss of electrons as the size of the water cluster increases. The trend for the H2 atomic charge is fitted using Equation 2 with parameters $\alpha = 0.460$ and $\beta = 0.089$, leading to a theoretical maximum positive charge for the H2 atom of $0.662e$. The H2 atom becomes more positively charged with its fractional electron count delocalized to the O atom and the H3 atom. The H2 atomic charge changes by 45me when going from dimer to hexamer – due to charge conservation, this is necessarily in the same range as that of the O atomic charge. The H2 atoms only have delocalized electrons within their atomic basins, and hence all charge transfer out of the H2 basin is as delocalized electrons. Interestingly, the H2 atom takes until $n = 12$ to reach a theoretical maximum plateau, which means that the hydrogen theoretically keeps losing fractional electrons until $n = 10$, which also does not exist as a cyclic structure. Notably, if the atomic charge only depended on localized electrons, then the H2 atom should not have any charge at all.

Investigating the atomic charge changes of O1 and H2 reveals an interesting cooperativity-induced effect of charge transfer. If the change in the localized and delocalized density of O1 were equal but opposite in sign, then the change in the atomic charge of O1 would be zero – i.e. the increase in cooperativity-induced delocalization would have originated entirely from the localized electrons of O1. However, since the change in delocalized electrons is greater than the change in localized electrons, a (negative) change in atomic charge is seen as a net inbound charge transfer. The origin of this charge transfer, which grows larger with increasing cluster size, is primarily the H2 atom's delocalized electrons. Therefore, the cooperative system is stabilized more by 'paying' for electron delocalization with a fraction of O1's localized electrons *as well as* H2's delocalized electrons, rather than with O1's localized electrons alone. Therefore, charge transfer can be seen as an additional mechanism to exceed the upper limit imposed by the localized electrons of O1 as discussed in the previous chapter, where H2 is an additional source of electrons to be delocalized (primarily by O atoms) in a cooperative cyclic system.

Interaction Energy

The concept of FAMSEC[2–4] is used in greater depth here than in the previous chapter to showcase the cooperativity effects. In particular, the total interaction energy of the water clusters is the focus of this section. The interaction energy incorporates all the di-atomic interactions within the system (whether intra- or intermolecular). It can be deconstructed into a classical electrostatic component and a quantum mechanical exchange-correlation component. Note that the interaction energy and its components investigated here with FAMSEC always use the *ref* → *final* chemical state difference as mentioned in the previous chapter. The *ref* state is the free non-interacting water molecules, and the *final* state is the intermolecularly bonded cyclic water cluster. The change when going from the *ref* → *final* state indicates whether the energetic component (the total interaction energy) contributes to the stability of the water cluster or if it is

110

causing instability. The intermolecular interaction energy is the most significant property of the electronic energy in terms of energetic contributions because the biggest difference between the *ref* and *final* state is that the water molecules interact. The equation for cooperativity-induced changes uses the dimer water cluster as the reference for the interaction energy section. The interaction energy ($^W E_{\text{int}}$) and its components exchange-correlation ($^W V_{\text{XC}}$) and electrostatic interaction energy ($^W V_{\text{cl}}$) are computed per water molecule in this section.

The total interaction energy and the contributions of its components are first examined from an entire water cluster perspective (see Figure 3). The total interaction energy decreases (becomes more negative) non-linearly with increasing water cluster size and therefore contributes increasingly to the stability of the cyclic water clusters. The decrease from dimer to hexamer is 45.706 kcal/mol, so there is thus a greater than 3-fold decrease in the energy values. The same non-linear decrease trend is seen for the total electrostatic interaction energy as well as being more negative (higher stability) at n = ∞ compared to the total interaction energy. The fitting parameters and energy values for n = ∞ for the total interaction energy and its components are shown in Table 1.
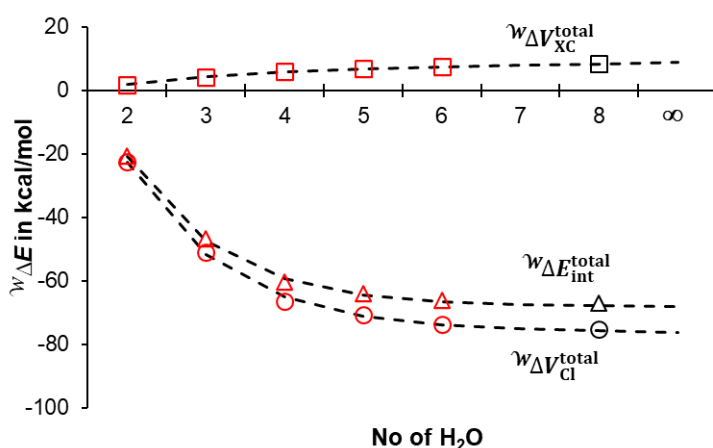
Figure 3 The total interaction energy ($^W \Delta E_{\text{int}}^{\text{total}}$) and its components' exchange-correlation ($^W \Delta V_{\text{XC}}^{\text{total}}$) and classical electrostatics ($^W \Delta V_{\text{cl}}^{\text{total}}$) for each water cluster size. The circles represent the computed data and the dashed lines are fitted trends using the derived Equations 3, 4 and 5.

$$\left({}^{W}E_{\text{int}}^{\text{total}}\right)(n) = {}^{W}E_{\text{int}}^{\text{total}}(2)\left[1 + \beta\left(1 - e^{-\alpha(n-2)}\right)\right] \tag{3}$$

$$\left({}^{W}V_{\text{XC}}^{\text{total}}\right)(n) = \left({}^{W}V_{\text{XC}}^{\text{total}}\right)(2)\left[1 + \beta\left(1 - e^{-\alpha(n-2)}\right)\right] \tag{4}$$

$$\left({}^{W}V_{\text{Cl}}^{\text{total}}\right)(n) = \left({}^{W}V_{\text{Cl}}^{\text{total}}\right)(2)\left[1 + \beta\left(1 - e^{-\alpha(n-2)}\right)\right] \tag{5}$$

The dimer to hexamer decrease is 51.269 kcal/mol, which again equates to a greater than 3-fold decrease for the total electrostatic interaction energy. The difference between dimer and hexamer shows that stabilization is taking place due to cooperativity when atoms interact with each other in an intermolecular manner.

The total exchange-correlation energy becomes more positive, also in a non-linear fashion. Exchange-correlation causes instability in the cyclic water cluster, which is unexpected when considering that the electrons that delocalize intermolecularly are the cornerstone of cooperativity. The quantum effects therefore become destabilized when water molecules start interacting with each other when viewed as a total that includes both intermolecular and intramolecular interactions. The dimer to hexamer increase is nearly 5-fold. This is a much greater degree of change compared to the interaction energy and the electrostatic interactions, which means that the exchange-correlation plays a substantial role in destabilization when the water cluster size increases. The reason for these discrepancies is investigated in this section. Another way to explain this result would be to split the exchange-correlation into its exchange and correlation components to get a better understanding of what electronic behaviour causes this instability, but this is beyond the scope of this study. Interestingly, the octamer energy values do not deviate from the trends for interaction energy and its components. One would have expected a large deviation due to the geometry not being planar.

112

When going from the *ref → final* state the water molecules start interacting intermolecularly with deformations taking place within the water molecule. These intermolecular interactions between neighbouring water molecules are examined next (see Figure 4). The intermolecular interactions take place through the intermolecular H-bond (i.e., O1–H2···O4) as well as other atoms not covalently bonded to it in the water cluster.

To recapitulate, electrons become delocalized from a water molecule to all other atoms in the water cluster as shown in the previous chapter. The intermolecular interactions are not considered as a change because only in the *final* state is it possible for water molecules to interact with each other (as opposed to the non-interacting water monomers).

Table 1 The parameters and theoretically predicted values in an infinitely large water cluster for total interaction energy ($^{W}E_{\text{int}}^{\text{total}}$) with its components' total electrostatic interaction energy ($^{W}\Delta V_{\text{cl}}^{\text{total}}$) and total exchange-correlation ($^{W}\Delta V_{\text{XC}}^{\text{total}}$).

Property	Equation	α	β	n = ∞ (kcal/mol)
$^{W}E_{\text{int}}^{\text{total}}$	3	0.835	2.276	−68.201
$^{W}V_{\text{Cl}}^{\text{total}}$	4	0.785	2.368	−76.220
$^{W}V_{\text{XC}}^{\text{total}}$	5	0.417	3.817	8.748
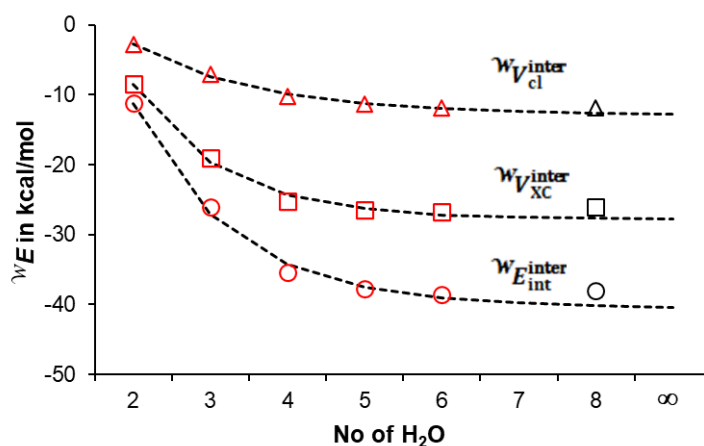
Figure 4 The intermolecular interaction energy ($^{W}E_{\text{int}}^{\text{inter}}$) and its components, exchange-correlation ($^{W}V_{\text{XC}}^{\text{inter}}$) and classical electrostatics ($^{W}V_{\text{cl}}^{\text{inter}}$) for each cyclic water cluster size. The circles represent the computed data and the dashed lines are fitted trends (starting from the top) using the derived Equations 6, 7 and 8.

$$\left(^{W}E_{\text{int}}^{\text{inter}}\right)(n) = {}^{W}E_{\text{int}}^{\text{inter}}(2)\left[1 + \beta\left(1 - e^{-\alpha(n-2)}\right)\right] \tag{6}$$

$$\left(^{W}V_{\text{XC}}^{\text{inter}}\right)(n) = \left(^{W}V_{\text{XC}}^{\text{inter}}\right)(2)\left[1 + \beta\left(1 - e^{-\alpha(n-2)}\right)\right] \tag{7}$$

$$\left(^{W}V_{\text{Cl}}^{\text{inter}}\right)(n) = \left(^{W}V_{\text{Cl}}^{\text{inter}}\right)(2)\left[1 + \beta\left(1 - e^{-\alpha(n-2)}\right)\right] \tag{8}$$

The trend for the intermolecular interaction energy ($^{W}E_{\text{int}}^{\text{inter}}$) is of a stabilizing nature for the cyclic water clusters. The greatest contribution to intermolecular interaction energy is from the exchange-correlation ($^{W}V_{\text{XC}}^{\text{inter}}$). Both intermolecular electrostatic ($^{W}V_{\text{cl}}^{\text{inter}}$) and exchange-correlation energy contribute to the stability of the water cluster here. The fitting parameters and energy value for n = ∞ are shown in Table 2.

The trend of intermolecular interaction energy decreases non-linearly, similar to the total interaction energy. There is a large jump from dimer to trimer, a 2.3-fold decrease, that is caused by the deformation occurring when another water molecule is introduced to the cyclic water cluster. Each water molecule in the trimer has two intermolecular interactions compared to only one in the dimer, pointing to why such a large decrease is seen. The trend for intermolecular interactions decreases non-linearly.

The electrostatic component of the intermolecular interaction energy has the smallest contribution in all clusters, confirming that an intermolecular H-bond is not purely an electrostatic interaction. Interestingly, the decrease from dimer to trimer is 2.6-fold for the electrostatic component, which is larger than the decrease of the intermolecular interaction energy by 0.3 orders rounded off. The greatest change when the water cluster size goes from dimer to trimer occurs for the electrostatic interactions. The atomic charge for O also showed a sharp decrease from dimer to trimer, indicating that the intermolecular electrostatic interactions of atoms are possibly caused by the deformation of electron density taking place when the dimer

goes to the trimer and thus becomes a cyclic water cluster. The exchange-correlation energy is the greatest contributor to the water cluster stability of the two components throughout all cyclic clusters.

The exchange-correlation component of the total intermolecular interaction energy corresponds to the reduction of average Coulombic electron-electron repulsion due primarily to spin-spin interactions, an effect that notably increases in magnitude with increased electron delocalization. Its dominant attractive role in the intermolecular interactions in H-bonded water clusters highlights again the importance of quantum-mechanical effects (such as covalency, dispersion and electron delocalization) in the stabilization of cyclic water clusters. Moreover, this observation aligns perfectly with $N^{\mathrm{deloc}}(\mathcal{F},\mathcal{M})$ mentioned in the previous chapter as the primary cooperativity-induced stabilization effect.

Due to water clusters remaining intact only through intermolecular interactions, it is then of paramount importance to consider these intermolecular interactions from both electronic and energetic points of view. The intermolecular interaction energy contributes –40.375 kcal/mol to the overall stability for an infinitely large water cluster, of which –27.750 kcal/mol is attributed to changes in exchange-correlation and –12.821 kcal/mol to changes in electrostatic attraction/repulsion. These results further strengthen the reason for the intermolecular delocalization of electrons serving as the cornerstone of cooperativity.

Table 2 The parameters and theoretically predicted values in an infinitely large water cluster of intermolecular interaction energy ($^{W}E_{\mathrm{int}}^{\mathrm{inter}}$) with its components' exchange-correlation ($^{W}\Delta V_{\mathrm{XC}}^{\mathrm{inter}}$) and electrostatic interaction ($^{W}\Delta V_{\mathrm{cl}}^{\mathrm{inter}}$) energy.

Property	Equation	α	β	n = ∞ (kcal/mol)
$^{W}E_{\mathrm{int}}^{\mathrm{inter}}$	6	0.781	2.608	–40.375
$^{W}V_{\mathrm{Cl}}^{\mathrm{inter}}$	7	0.617	3.637	–12.821
$^{W}V_{\mathrm{XC}}^{\mathrm{inter}}$	8	0.866	2.293	–27.750

The intramolecular interactions take place between the H and O covalent bonds and between the two H atoms within the water molecule. Only the intramolecular interaction energy is investigated next, with intermolecular and total interaction energy included for comparison (see Figure 5). The intramolecular terms have CI and NCI superscripts which denote covalent interaction (O–H) and non-covalent interactions (H···H), respectively.

The trend for non-covalent intramolecular interactions increases non-linearly in energy, causing an instability in the water cluster. From a classical electrostatic perspective, this is intuitively explained by positive charges (H) repelling each other and delocalizing an me count between them. The exchange-correlation effect is therefore also very small. The trend for intramolecular non-covalent interactions is fitted with the parameters $\alpha = 0.626$ and $\beta = 2.086$ in Equation 9 to obtain a maximum theoretically predicted energy value of 8.378 kcal/mol.
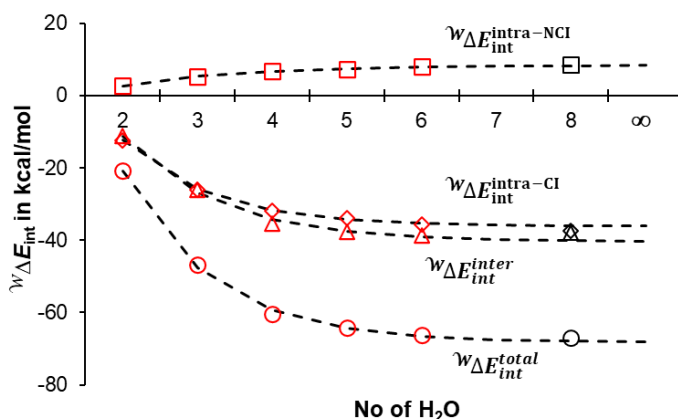
Figure 5 The intramolecular (covalent and non-covalent) and intermolecular interaction energy contributions made towards total interaction energy relative to a free water molecule and normalized to per water molecule in a cyclic water cluster. $^{W}\Delta E_{\text{int}}^{\text{intra-NCI}}$ is the non-covalent intramolecular interaction energy contribution. $^{W}\Delta E_{\text{int}}^{\text{intra-CI}}$ is the covalent intramolecular interaction energy contribution. $^{W}\Delta E_{\text{int}}^{\text{inter}}$ is the intermolecular interaction energy contribution and $^{W}\Delta E_{\text{int}}^{\text{total}}$ is the total intermolecular interaction energy. The data are fitted using Equations 9, 10, 6 and 3 starting from the top trend and moving down.

$$\left(^{W}\Delta E_{\text{int}}^{\text{intra-NCI}}(n) = \left(^{W}\Delta E_{\text{int}}^{\text{intra-NCI}}\right)(2)\left[1 + \beta\left(1 - e^{-\alpha(n-2)}\right)\right] \tag{9}$$

$$\left(^{W}\Delta E_{\text{int}}^{\text{intra-CI}}\right)(n) = \left(^{W}\Delta E_{\text{int}}^{\text{intra-CI}}\right)(2)\left[1 + \beta\left(1 - e^{-\alpha(n-2)}\right)\right] \tag{10}$$

The intramolecular covalent interaction energy and intermolecular interaction energy are close to each other, which is in some regard unexpected as these two are completely different types of interaction. One would expect the covalent bond to be of a stabilising nature as it is such a common bond in most molecules. Interestingly, the neighbouring intermolecular interactions delocalize $0.545e$ per water molecule and the covalent (H,O) delocalizes $1.445e$ per water molecule for the hexamer. Considering that the electrons delocalize intermolecularly, the count from dimer to hexamer changes by $0.978\ e$ and the exchange-correlation decreases by 18.293 kcal/mol, pointing to the stabilization effect caused by delocalization from quantum effects in the water cluster. The trend for intramolecular covalent interactions is fitted with Equation 10 and parameters $\alpha = 0.859$ and $\beta = 1.923$ to obtain a minimum theoretically predicted energy value of –36.076 kcal/mol. The intermolecular interaction energy and covalent intramolecular interaction energy are the largest contributors to the stability of the water clusters from an interaction energy perspective.

The specific intramolecular bond contributions are focused on next to show the individual di-atomic bond contributions to interaction energy and exchange-correlation plus electrostatic interaction components. The two covalent bonds within a water molecule change considerably due to the formation of intermolecular interactions.

The trend for both covalent bonds with interaction energy in the water molecule decreases non-linearly, thus contributing to the stability of the water cluster (see Figure 6). The O1–H2 bond contributes the most to the stability effect of interaction energy. The reason for this is that the O1–H2 covalent bond forms part of the intermolecular H-bond. If the water molecule were analyzed as free non-interacting, then these two covalent bonds would have the same interaction energy. The O1–H2 is fitted with parameters $\alpha = 0.916$ and $\beta = 1.876$ in Equation 12 to obtain a minimum theoretically predicted energy value of –21.972 kcal/mol. The O1–H3 is fitted with

parameters $\alpha = 0.781$ and $\beta = 2.003$ in Equation 11 to obtain a minimum theoretically predicted energy value of -14.121 kcal/mol. Despite the general inertness of H3 for all other cooperativity effects investigated (such as atomic charge and intermolecular delocalization), the cooperativity-induced changes in O1–H2 and O1–H3 are remarkably similar (especially when comparing fitting parameters). This shows that even though H3 is not a large contributor to intermolecular interactions and intermolecular delocalization, it still has a remarkably significant effect on molecular stability through its interaction with its neighbouring O atom.
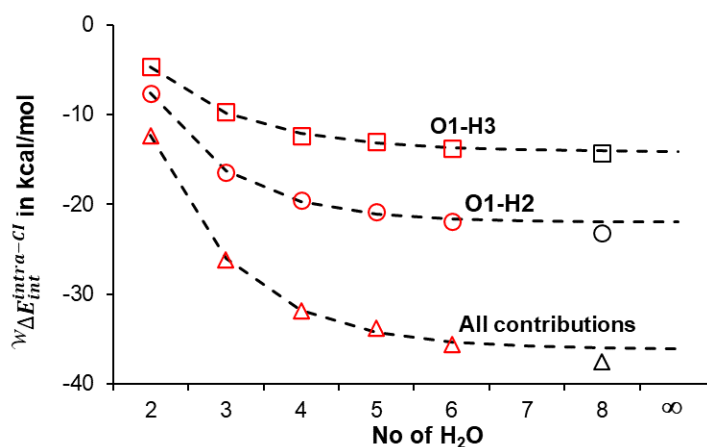
Figure 6 The largest intramolecular covalent interaction energy contributions made by diatomic interactions O1–H2 and O1–H3. The data for O1-H2 and O1–H3 are fitted using Equations 11 and 12.

$$(\,^{W}\!\Delta E_{\text{int}}^{\text{intra-CI}}(\text{O1} - \text{H3})(n) = (\,^{W}\!\Delta E_{\text{int}}^{\text{intra-NCI}})(\text{O1} - \text{H3})(2)\left[1 + \beta\left(1 - e^{-\alpha(n-2)}\right)\right] \qquad (11)$$

$$(\,^{W}\!\Delta E_{\text{int}}^{\text{intra-CI}})(\text{O1} - \text{H2})(n) = (\,^{W}\!\Delta E_{\text{int}}^{\text{intra-CI}})(\text{O1} - \text{H2})(2)\left[1 + \beta\left(1 - e^{-\alpha(n-2)}\right)\right] \qquad (12)$$

The intramolecular covalent electrostatic interaction energy follows a non-linear decrease for both covalent bonds (see Figure 7). The change from dimer to hexamer observed for the O1–H2 covalent bond is larger than that of the O1–H3 covalent bond, which means that the O1–H2 covalent bond contributes the most to the stability of the electrostatic interactions of the water cluster. The O1–H2 covalent bond has a decrease of 37.600 kcal/mol from dimer to hexamer. The computed data are fitted (see Equation 13) with parameters $\alpha = 0.789$ and $\beta = 2.279$ to

obtain a minimum theoretically predicted energy value of –56.785 kcal/mol. The difference seen here between these two covalent bonds is significant because O1–H2 forms part of the intermolecular H-bond, whereas the O1–H3 is the bond with the H pointing out of the ring. The H pointing out of the ring does thus not play a large role in terms of the stabilization of the water cluster with electrostatic interactions. The greatest change for O1–H2 is expected when one considers the change that occurs from the *ref → final* state – the O1–H2 covalent bond will change the most due to the intermolecular H-bonding. Electrostatic covalent intramolecular interactions play a noteworthy role in the stabilization of the water cluster. The O1–H3 computed data are fitted (see Equation 14) with parameters $\alpha = 0.864$ and $\beta = 1.857$ to obtain a minimum theoretically predicted energy value of –14.804 kcal/mol.
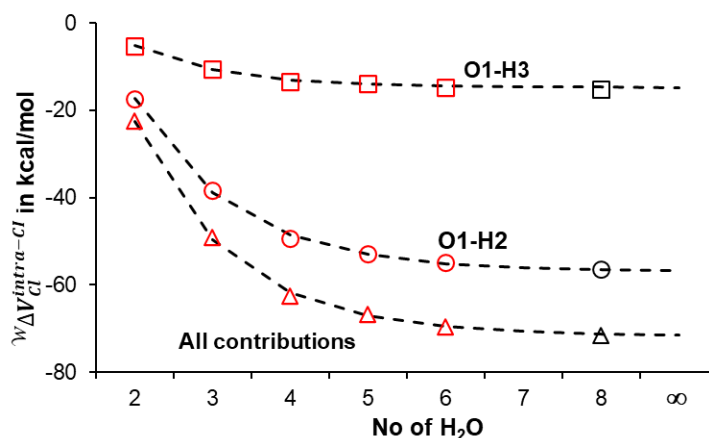
Figure 7 The largest intramolecular covalent classical electrostatic contributions made by diatomic interactions O1–H2 and O1–H3. The data for O1–H2 and O1–H3 are fitted using Equations 13 and 14.

$$({}^{W}\Delta E_{Cl}^{\text{intra-CI}}(O1 - H3)(n) = ({}^{W}\Delta E_{Cl}^{\text{intra-NCI}})(O1 - H3)(2)\left[1 + \beta\left(1 - e^{-\alpha(n-2)}\right)\right] \qquad (13)$$

$$({}^{W}\Delta E_{Cl}^{\text{intra-CI}})(O1 - H2)(n) = ({}^{W}\Delta E_{Cl}^{\text{intra-CI}})(O1 - H2)(2)\left[1 + \beta\left(1 - e^{-\alpha(n-2)}\right)\right] \qquad (14)$$

The covalent bond exchange-correlation contribution is not shown because the only meaningful contribution is from the O1–H2 covalent bond. The O1–H3 bond contributes a maximum of 5% in the dimer and decreases further as the water cluster size increases.

The large change experienced by the O1–H2 covalent bond was further investigated here, where the electron density becomes delocalized to the water cluster through this covalent bond, causing the large quantum effects that occur, leading to a more stable water cluster. The specific contributions and changes that occur with the covalent bonds within the water molecule is explored in greater detail in this section on covalent bonds.

Topological Properties

The topological properties are investigated next to reveal another set of products yielded by cooperativity within water clusters. The QTAIM-defined topological properties are obtained from AIMAll.[5] Topological properties are the spatial properties of the electronic charge distribution. The topological properties are investigated at the bond critical point (BCP) or just the critical point (CP). The fitted parameters and $n = \infty$ values are shown in Table 3.
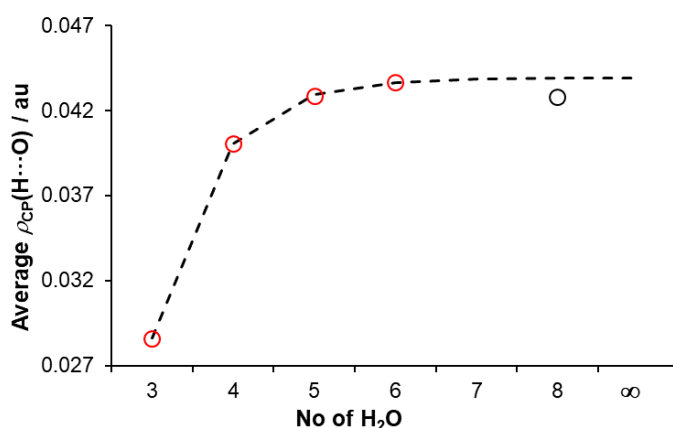
Figure 8 The trend in electron density (ρ) for each cyclic water cluster size. The circles represent computed data, and the dashed line is the predicted data using the derived Equation 15.

$$\rho(\mathrm{H} \cdots \mathrm{O})(n) = (\rho(\mathrm{H} \cdots \mathrm{O})(3)\left[1 + \beta\left(1 - e^{-\alpha(n-3)}\right)\right]$$

(15)

The most important property obtained from the topological properties is the electron density[1] (ρ). The trend for the electron density (see Figure 8) follows a non-linear increase similar to that of $N^{\text{deloc}}(\mathcal{F},\mathcal{R})$. This is expected because the electrons donated to all the atoms of a water molecule will be concentrated at the CP of an intermolecular H-bond. Notably, due to cooperativity being a molecular-wide event, the electron density is present throughout the cluster but more concentrated at the CP point. This result is linked with the large exchange-correlation contribution seen with the O1–H2 covalent bond. The trimer cyclic water cluster is the reference used here. The dimer does not fit with the equation for cooperativity-induced effects. The prime reason for this deviation is because the dimer is not a cyclic water cluster. Furthermore, the water molecules in the dimer do not delocalize electron density in both an acceptor and donor fashion. There is a 1.4-fold increase from the trimer to tetramer possibly resulting from the tetramer cyclic water cluster as the first symmetrical structure. The electron density at the CP therefore follows the same trend as for the intermolecular interaction energy (and therefore corroborates our results), with a strengthening as the cluster size increases. The hexamer water cluster has an average electron density value of 0.044 at the CP, which is the same as the limiting value. Accordingly, the hexamer electronically forms the strongest bonds when only the CP is used as an indicator.

The energetic component at the CP is focused on next. The V_{CP} term is the potential energy density, which is the average potential energy experienced by a probability-weighted electron (i.e. electron density) at the CP.[6] The G_{CP} term is the kinetic energy density, which is calculated with either the momentum or position of the electron at the critical point (which, for an arbitrary point or volume in space, is not identical; here the calculation of momentum kinetic energy density is used). The two types of energy density are summed with the total energy density $H_{\text{CP}} = V_{\text{CP}} + G_{\text{CP}}$. Lastly, the ratio of absolute potential energy density and kinetic energy density

$|V_{CP}|/G_{CP}$ is a somewhat useful descriptor of the nature of the interaction; this was used in previous years as an estimate of covalency.[7] Additionally the H_{CP} can also be used to determine if stability or instability is taking place at the CP.

The potential energy density (see Figure 9(a)) follows a non-linear decrease such as seen for $N^{deloc}(\mathcal{F},\mathcal{F})$ and $N^{self}(\mathcal{F})$. The field then experienced by the individual electrons at the CP becomes more negative and ultimately leads to an increase in stability.

The reason for the decrease is due to stabilisation taking place with higher electron delocalization, resulting in more exchange-driven electron-electron repulsion reductions, which are the quantum effects stabilizing the water cluster.
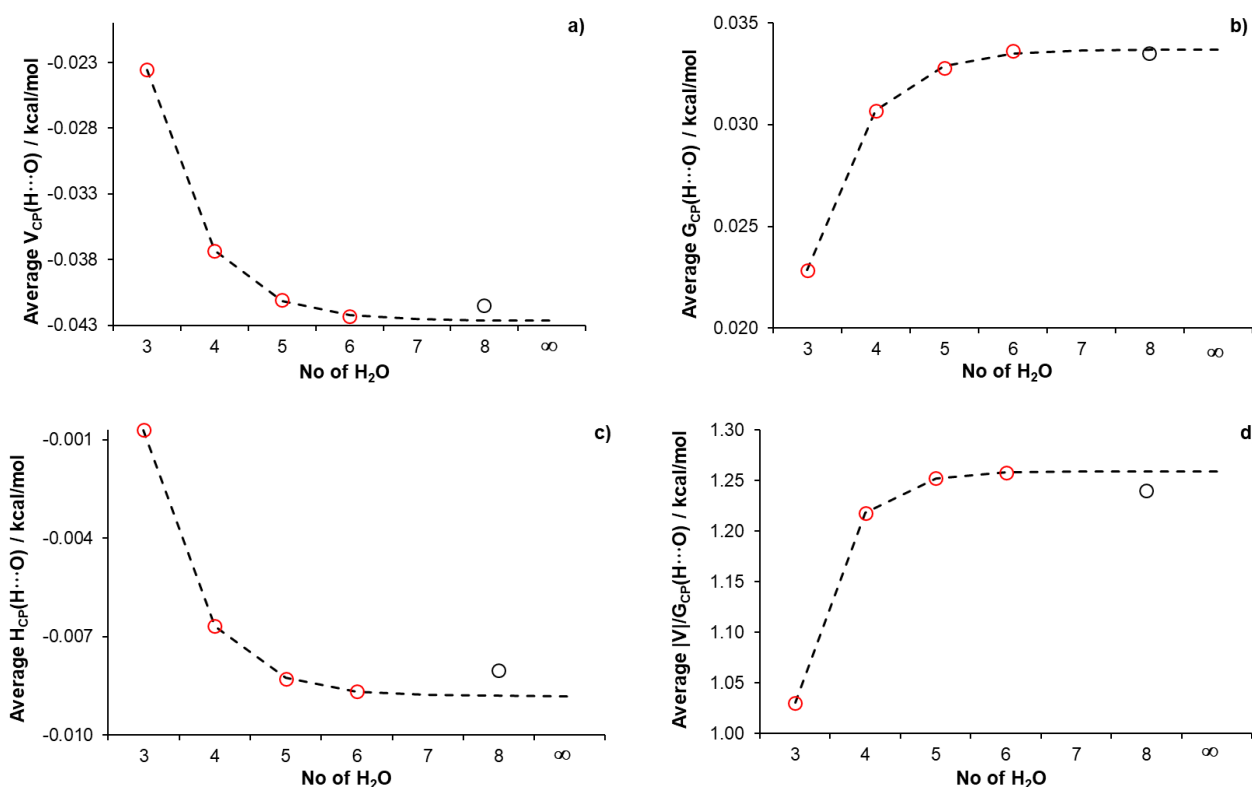
Figure 9 The topological properties for each cyclic water cluster – (a) potential energy density (V_{CP}), (b) kinetic energy density (G_{CP}), (c) the sum of potential energy and kinetic energy density (H_{CP}), and (d) the absolute potential energy and kinetic energy density ratio ($|V_{CP}|/G_{CP}$). Each property is fitted using a derived cooperativity effects equation (Equations 16, 17, 18 and 19).

$$V_{CP}(\text{H} \cdots \text{O})(n) = (V_{CP}(\text{H} \cdots \text{O})(3)\left[1 + \beta\left(1 - e^{-\alpha(n-3)}\right)\right] \tag{16}$$

$$G_{CP}(\text{H} \cdots \text{O})(n) = (G_{CP}(\text{H} \cdots \text{O})(3)\left[1 + \beta\left(1 - e^{-\alpha(n-3)}\right)\right] \tag{17}$$

$$H_{CP}(\text{H} \cdots \text{O})(n) = (H_{CP}(\text{H} \cdots \text{O})(3)\left[1 + \beta\left(1 - e^{-\alpha(n-3)}\right)\right] \tag{18}$$

$$|V|/G(\text{H} \cdots \text{O})(n) = (|V|/G(\text{H} \cdots \text{O})(3)\left[1 + \beta\left(1 - e^{-\alpha(n-3)}\right)\right] \tag{19}$$

The kinetic energy density (G_{CP}) (see Figure 9(b)) follows a non-linear increase and therefore contributes a destabilizing component to the topological description of the interactions. This is expected simply due to the increase in electron density and concentration of electron density observed earlier.

The sum of potential energy density and kinetic energy density H_{CP} (see Figure 9 (c)) follows a non-linear decrease due to the potential energy density being larger in absolute value than the kinetic energy density. In other words, from a topological point of view, stabilizing effects (negative elements potential energy density) outweigh destabilizing effects (positive elements of the potential energy density and kinetic energy), and in an increasing manner with increasing cluster size. This shows that the electron density concentrating at the CP is of a stabilizing nature.[7] Moreover, this correlates with the electronic counts discussed in the previous chapter and the findings from the FAMSEC section in this chapter.

The covalency or absolute potential energy density and kinetic energy density ratio $|V_{CP}|/G_{CP}$ (see Figure 9(d)) increase non-linearly due to the increase in stability as the water cluster increases in stability and the increase in electrons delocalized throughout the molecule. The covalency increases due to the symmetry and increase in number of electrons delocalized. The plateau is essentially reached at the hexamer because this is the largest cyclic planar and most

stable cyclic structure that exists. Again, this observation lines up with the observations made regarding intermolecular electron delocalization in the previous chapter.

Table 3 The parameters and theoretically predicted values for an infinitely large water cluster size for the topological properties of potential energy density (V_{CP}), kinetic energy density (G_{CP}), total energy density (H_{CP}) and absolute potential energy density kinetic energy density ratio ($|V_{CP}|/G_{CP}$).

Property	Equation	α	β	n = ∞ (au)
ρ	15	1.375	0.535	0.044
V_{CP}	16	1.277	0.810	–0.043
G_{CP}	17	1.291	0.475	0.034
H_{CP}	18	1.339	11.453	–0.009
$|V_{CP}|/G_{CP}$	19	1.716	0.222	1.259

Geometrical Properties

The next section deals with the intermolecular H-bond distance and how it correlates with the different properties considered in this and the previous chapter. The intermolecular H-bond distance results from the various attractions and repulsions between particles of the water molecules in each water cluster.
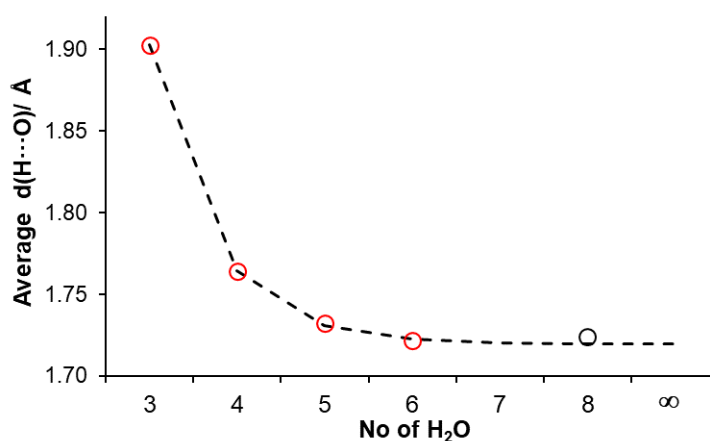
Figure 10 The average intermolecular interaction distance for each cyclic water cluster size. The circles represent the computed data and fit using derived Equation 15.

$$d(\text{H} \cdots \text{O})(n) = (d(\text{H} \cdots \text{O})(3)\left[1 + \beta\left(1 - e^{-\alpha(n-3)}\right)\right] \tag{20}$$

124

The average intermolecular distance for each cyclic water cluster is focused on first. Note that only the cyclic water clusters are considered here (i.e. the dimer is excluded) due to the cooperativity-induced effects equation not fitting when the dimer is included. This suggests that the geometry of the dimer does not follow the trend otherwise established by the cyclic water clusters. The average intermolecular distance (see Figure 10) decreases non-linearly due to the water molecules moving closer to each other and the electrons delocalized between neighbours increasing in number as well as in strength.

The decrease from trimer to hexamer is 0.181 Å, showing that the water molecules move closer to ensure that the stability is optimal and electron delocalization is at its maximum. Interestingly, as shown in the previous chapter, it is easier to break the hexamer apart than the dimer, yet the hexamer has water molecules in closer proximity.

The trend for average intermolecular distance is fitted with parameters $\alpha = 1.405$ and $\beta = -0.096$ (see Equation 20) to obtain a minimum theoretically predicted intermolecular interaction distance of 1.720 Å. The average intermolecular distance for the hexamer is 1.722 Å, whereas the dimer O1–H2 covalent bond has a distance of 0.966 Å. There is then a 0.758 Å difference, meaning that almost two covalent bonds can fit within a hexamer intermolecular H-bond and yet the intermolecular bond strength is close to that of the covalent bond. The O1–H2 intramolecular covalent bond elongates as the cluster size increases, which is what other authors found.[8–10]

The intermolecular interaction distance against various properties considered in this and the previous chapter is investigated in this section. The data in this section are not fitted with the equation for cooperativity-induced effects because our model at this stage is only designed for single-variate regression (i.e. $N^{\text{deloc}}(\mathcal{F},\mathcal{R})$, d(H···O) etc.). The circles (computed data) are therefore connected with a dotted line to show the approximate trend followed to investigate the correlation.

125

According to our findings, the trend for electronic energy is the main confirmation of cooperativity (see previous chapter). It is then of interest to investigate the electronic energy with intermolecular distances for each water cluster (see Figure 11). The possible trend for electronic energy vs. intermolecular interaction distance follows the distinctive non-linear decrease as seen for equation trends of cooperativity-induced effects.
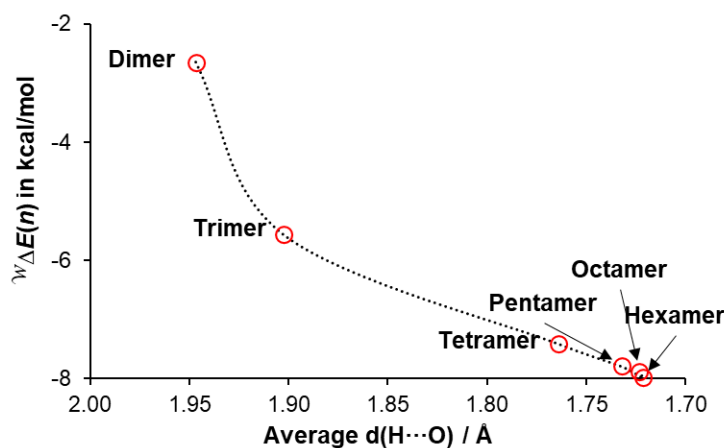
Figure 11 The electronic energy per water molecule against the average H⋯O interaction distance. Circles represent the computed data. The x-axis is inverted here.

The biggest difference seen here is the increasing steepness of the trend when plotted against intermolecular interaction distance. The possible plateau would be reached here much further than the hexamer compared to the original graph in the previous chapter where the plateau was close to the hexamer. The relationship between intermolecular distance and electronic energy is similar here to the relationship when only the water cluster size was used as the x-axis. The biggest difference is the spacing of the water cluster size.

The different electron counts considered in the previous chapter were correlated with the intermolecular interaction distance to investigate the relationships between them (see Figure 12). First considering the number of electrons delocalized to all atoms in the water cluster ($N^{\mathrm{deloc}}(\mathcal{F},\mathcal{R})$), the possible trend is similar to that seen when the water cluster size is used as the x-axis. The pentamer, hexamer and octamer are almost one data point showing the point where a

possible plateau is reached. There is an increase in the number of electrons delocalized as the intermolecular distance becomes shorter.
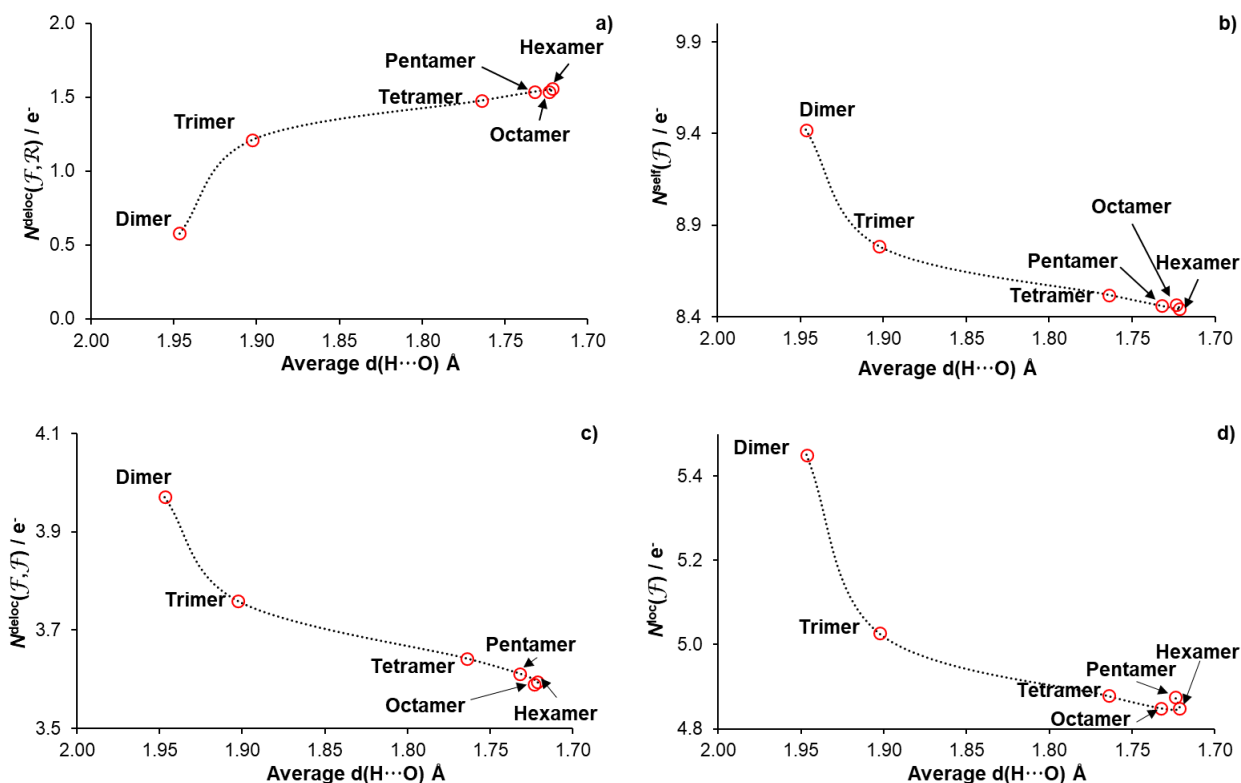
Figure 12 The number of electrons (a) delocalized from $\mathcal{F}$ to the remaining atoms in the water cluster, (b) associated with a water molecule, (c) delocalized within a water molecule and (d) localized within a water molecule, per water molecule, against the average H···O interaction distance. The circles represent the computed data. The x-axis is inverted here.

Similarly, the remaining three electron counts decrease as expected due to the loss of electrons. All the trends follow the possible trends that are like those fitted with the cooperativity-induced equation, which means that this is another product because of the cooperativity within the water cluster. Everything occurs in the water cluster and changes to yield the lowest energy and therefore the greatest stability. All the electron counts with the respective intermolecular distance reach a possible plateau – a strong correlation between electron count and intermolecular interaction distance is observed here.

The last property considered regarding the intermolecular interaction distance is the total interaction energy (see Figure 13). The jumps in intermolecular distances can be seen in the

graphs in this section where there are in essence two groups: dimer, trimer and tetramer, and pentamer, hexamer and octamer.
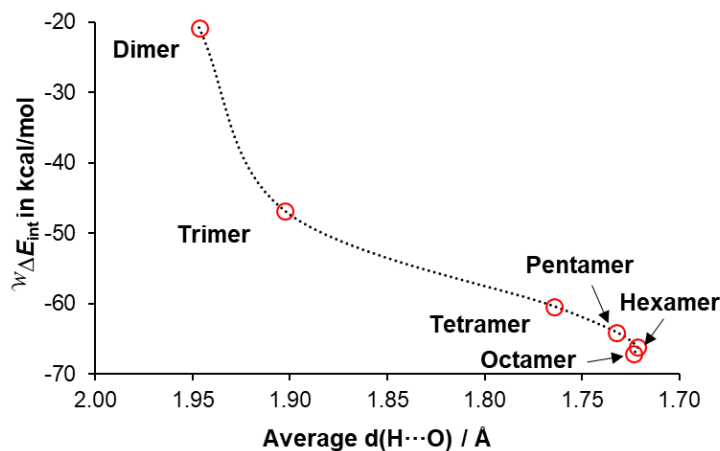
Figure 13 The intermolecular interaction energy, per water molecule, against the average H⋯O interaction distance. The circles represent the computed data. The x-axis is inverted here.

The second group is much more symmetrical than the first, which is possibly the reason why this occurs. The addition of the intermolecular interaction distance is a secondary component of the effect of cooperativity within water clusters which strengthens the same conclusions and adds more information to the overall picture.

Conclusions

The changes that occurred due to cooperativity are linked with every single property of the water cluster. The water cluster undergoes energetic and electronic changes that ensure its highest possible stability. According to our investigations, the most important changes that occurred were the atomic charges, the topological properties of the interaction energy and the geometrical changes described by the intermolecular interaction distance. The atomic charge of the O atom became more negative in a non-additive fashion. The H atom became more positive in a non-additive manner. The increase in the negative charge of the O atom was caused by the increase in the number of delocalized electrons because the number of localized electrons decreased. The H atom only has delocalized electrons, which are donated to the O atom, causing

128

the atomic charge to become more positive. The change in total interaction energy was dominated by the contribution of the electrostatic interaction energy with destabilization caused by the change in exchange correlation. The intermolecular interaction energy was of a stabilizing nature for both the electrostatic interaction energy and the exchange correlation. The intermolecular interaction energy was dominated by the contribution of the exchange correlation. The intramolecular interaction energy and classical electrostatic interaction had the greatest stabilization contribution from the O1–H2 covalent bond. The H⋯H intramolecular non-covalent interaction caused destabilization within the water molecule. The potential energy density contributed the most to the total energy density. This is due to the quantum effects between water molecules. The topological properties were considered at the CP(H2,O4). When the degree of covalency was used as an indicator, the hexamer had the strongest intermolecular H-bonds. Similar conclusions were drawn from the various electron and energetic properties against the intermolecular interaction distance as when the property was only considered against the number of water molecules.

References

1   R. F. W. Bader, *Atoms in molecules: A quantum theory*, Clarendon Press, 1990, 169–180.

2   I. Cukrowski, F. Sagan and M. P. Mitoraj, *J. Comput. Chem.*, 2016, **37**, 2783–2798.

3   I. Cukrowski, G. Dhimba and D. L. Riley, *Phys. Chem. Chem. Phys.*, 2019, **21**, 16694–16705.

4   I. Cukrowski, D. M. E. Van Niekerk and J. H. De Lange, *Struct Chem*, 2017, **28**, 1429–1444.

5   Todd A. Keith, AIMAll (version 19.10.12) Gristmil Softare, USA 2019.

6   E. Espinosa, E. Molins and C. Lecomte, *Chem. Phys. Letts.*, 1998, **285**, 170–173.

7   D. Cremer and E. Kraka, *Croa. Chemi. Act.*, 1984, **6**, 1259–1281.

8   S. Iwata, *Phys. Chem. Chem. Phys.*, 2014, **16**, 11310–11317.

9   E. Miliordos, E. Aprà and S. S. Xantheas, *J. Chem. Phys.*, 2013, **139**, 114302–114314.

10 K. Liu, J. D. Cruzan and R. J. Saykally, *Science*, 1996, **271**, 929–933.

Chapter 5

3D Hexamer Structures

Introduction

3D hexamer water clusters (($H_2O)_n$, $n = 6$) are a popular water cluster type investigated[1–23] by researchers due to the fact that in theoretical studies more stable molecular structures start to appear than in cyclic water clusters. 3D hexamer water clusters are the first type of water clusters in which water molecules involved in double-donor or double-acceptor type H-bonds are found. 3D hexamer water clusters have the following types of H-bonds within the water cluster: 1) single-donor single-acceptor (da), 2) double-donor single-acceptor (dda), and 3) single-donor double-acceptor (daa). The first difference is that cyclic water clusters only consist of da H-bonds in contrast to the 3D structures. The second difference is that every intermolecular H-bond is in a unique environment within the 3D hexamer water clusters compared with the same intermolecular H-bonds found in cyclic water clusters, where all H-bonds are in identical environments. The 3D nature of the water molecules is an important factor here, which is investigated in this chapter. As there are various stable molecular structures for the hexamer water cluster,[7,11,19] it was decided to use the **book**, **bag**, **cage** and **prism** conformers for this study.

The focus of this chapter is on the cooperativity effect within 3D hexamer water clusters from a molecular-wide perspective – MOWED. The first section deals with the validity of the electronic energy data computed at our level of theory. The second section starts with the electronic energy and continues with the number of intermolecular delocalized electron count. The focus is then on these intermolecular delocalization patterns visualized with isosurfaces. The chapter concludes with a contrasting view of anti-cooperativity and a summary of the new knowledge gained.

Results

Overview of 3D clusters

The different 3D hexamer water clusters and cyclic hexamer water cluster investigated are shown in Figure 1. The bag water cluster consists of one dda and one daa water molecule.
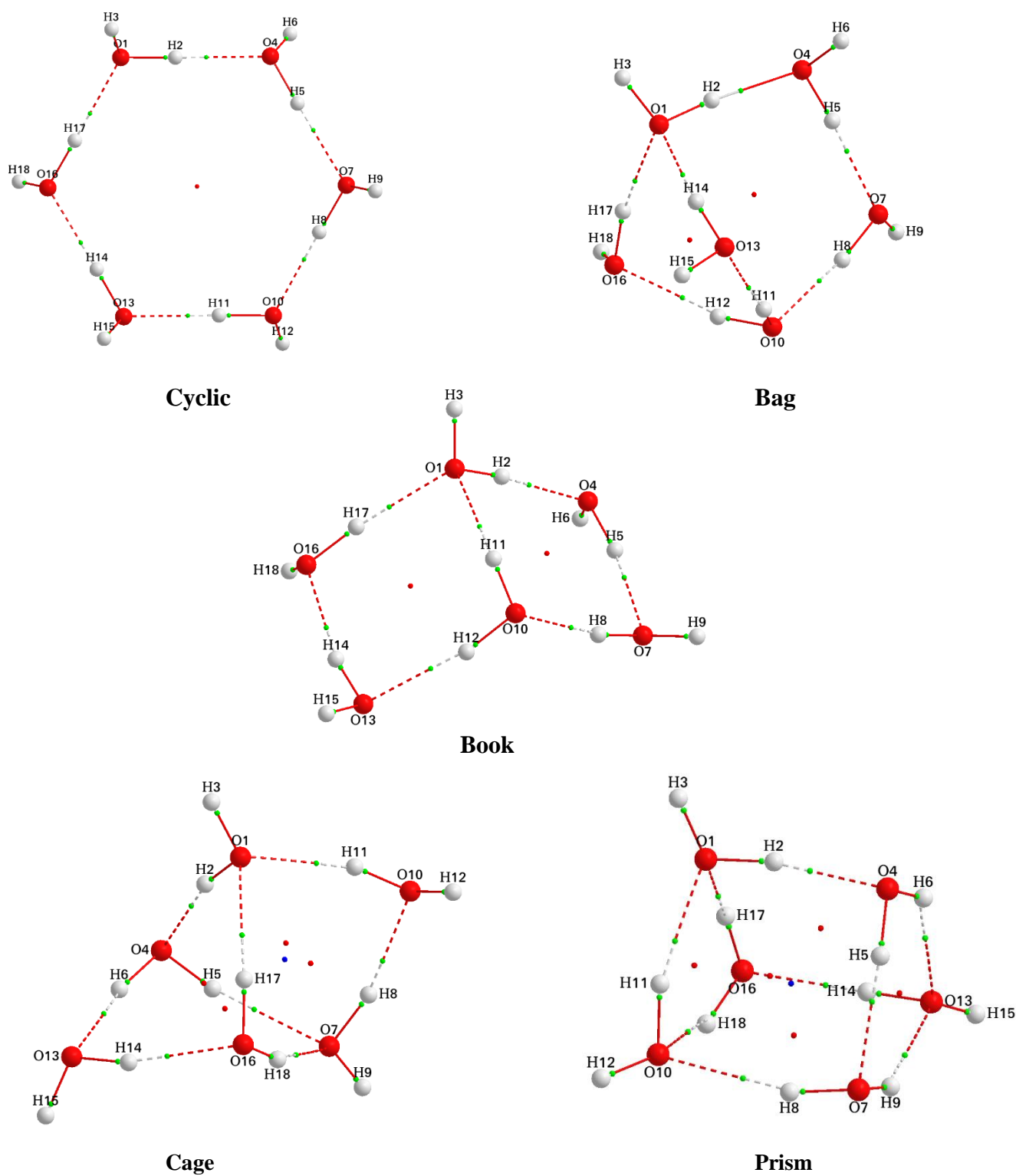
Figure 1 The cyclic, bag, book, cage and prism water hexamer conformers.

The book water cluster also has one of each H-bond. The cage water cluster has two dda H-bonds and one daa H-bond. The prism water cluster has four dda and two daa H-bonds. The remaining H-bonds in each of these 3D hexamer water clusters mentioned are type da as seen for the cyclic hexamer. The three different types of H-bonds discussed in this investigation are shown in Figure 2.

da   **dda**   **daa**
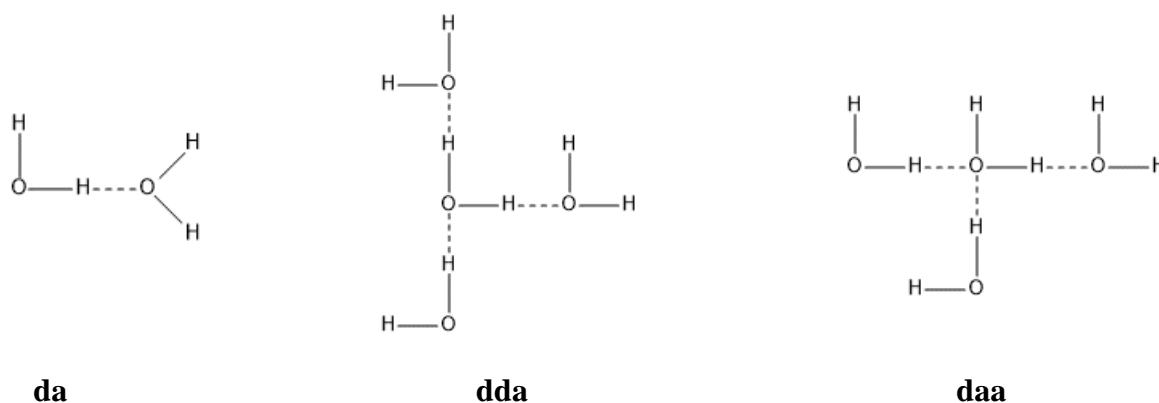
Figure 2 The donor-acceptor (da), double-donor single-acceptor (dda) and single-donor double-acceptor (daa) type H-bonds, the different H-bonds found in the investigated water clusters.

As in previous chapters, the 3D hexamer clusters were optimized at B3LYP/aug-cc-pVTZ.

Validation of electronic structure model chemistry

The relative energy data computed by Bates and Tschumper[1] is at a CCSD(T)/CBS level of theory, which is the gold standard and compares excellently with our level of theory. The relative energy values of Dahlke *et al*[3] and Hincapié *et al*[7], both at MP2/aug-cc-pVTZ level of theory, are much closer to each other. The biggest difference in relative energy values between our computed data and theirs is that of the cyclic water cluster. The relative energy values of Miliordos *et al*[13] at CCSD(T)/aug-cc-pVTZ level of theory differ somewhat from those obtained with our level of theory. The same closely spaced data was found by Tsai and Jordan[19] and Xantheas[22] at MP2 level of theory with aug-cc-pVDZ and uag-cc-pV5Z basis sets respectively. It is therefore reasonable to use our level of theory due to its good comparison with the CCSD(T)/CBS and CCSD(T)/aug-cc-

pVTZ levels of theory by Olson.[15] The same sequence of 3D hexamer conformers was obtained

by all the referred authors, matching our sequence.

Table 1 The relative energy values for the **cyclic, bag, book, cage** and **prism** 3D hexamer water clusters compared at various levels of theory by various authors.

Molecular energies of 3D hexamer water clusters relative to prism / kcal/mol						
Authors	**Level of theory**	**Cyclic**	**Bag**	**Book**	**Cage**	**Prism**
Our data	B3LYP/aug-cc-pVTZ	2.15	1.34	0.8	0.25	0
Bates and Tschumper[1]	CCSD(T)/CBS	2.48	1.62	0.87	0.25	0
Dahlke *et al*[3]	MP2/aug-cc-pVTZ	1.25	1.18	0.31	0.01	0
Hincapie *et al*[7]	MP2/aug-cc-pvdz	1.6	1.2	0.8	1.1	0
Kim and Kim[10]	MP2/DZP	2.1	1.1	2	0.67	0
Kryachko[11]	MP2(full)/aug-cc-pVDZ	2.06	N/A	1.16	0.25	0
Miliordos[13]	CCSD(T)/aug-cc-pVDZ	2.65	N/A	1.68	0.44	0
Olson *et al*[15]	CCSD(T)/aug-cc-pVTZ	2.1	N/A	1.2	0.3	0
Tsai and Jordan[19]	MP2/aug-cc-pVDZ	0.93	N/A	0.31	0.21	0
Xantheas[22]	MP2/aug-cc-pV5Z	1.17	N/A	0.31	0.08	0

MOWED-based cooperativity in 3D hexamers

Relative molecular energies for the different 3D hexamer conformers are plotted in Figure 3. Notably, while the total number of water molecules remains constant, a large stabilization is observed in the 3D conformers relative to the cyclic structure, and varies quite significantly for the different conformers. The obvious difference between the 3D water clusters is the cumulative number of dda and daa H-bonds. The cyclic hexamer only consists of water molecules involved in two H-bonds (da configuration), whereas the prism conformer has water molecules each involved in three H-bonds (dda or daa configurations) The prism shows the classical electronic energy limit reached for the hexamer water cluster – a single water molecule cannot formally be involved in

more than three H-bonds. The relative energies of the series of 3D conformers therefore seem to be indicative of the number and nature of H-bonds that each water molecule is involved in. Whether this observed energy stabilization is cooperative will be a focal point of this chapter.
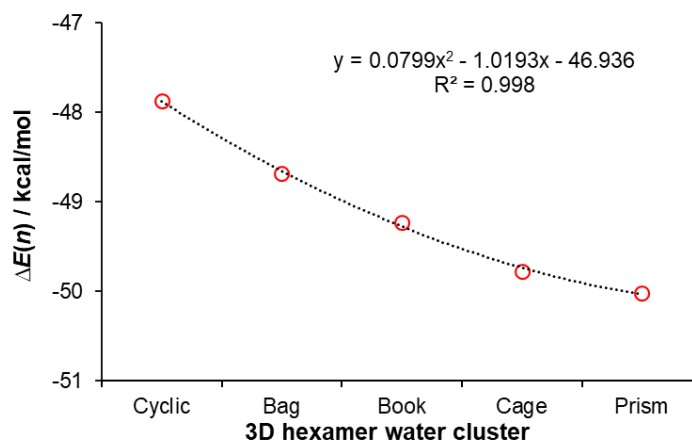
Figure 3 The $\Delta E(n)$ computed for the indicated hexamer water clusters. The circles represent computed data and the dotted line is the fitted second order polynomial with the fit of goodness given as well.

The electronic energy data are fitted with a second order polynomial and not the cooperativity equation due to the same number of water molecules for each 3D hexamer water cluster. The electronic energy difference between cyclic and prism conformers is 2.152 kcal/mol. If the stabilization in the prism relative to the cyclic structure is cooperative in nature, then it follows that a statistical water molecule in the cluster is energetically more stable in the prism than in the cyclic hexamer. ~~We expect that~~ Water molecules in the 3D clusters are stabilized in the same manner through which a statistical water molecule in the cyclic hexamer is stabilized relative to the water dimer or cyclic trimer as a result of cooperativity. In the cyclic structures (see Chapter 3), all water molecules are in a da configuration and the observed non-linear energy stabilization with increasing cluster size is therefore a function of the increasing number of da H-bonds. Here the concentration is on increase in the number of daa and dda H-bonds to investigate whether the same non-linear stabilization will be observed.

135

For comparison to the cyclic structures in Chapter 3, trends of $^W\Delta E(n)$ and total $\Delta E(n)$ for the 3D structures are plotted in Figure 4.
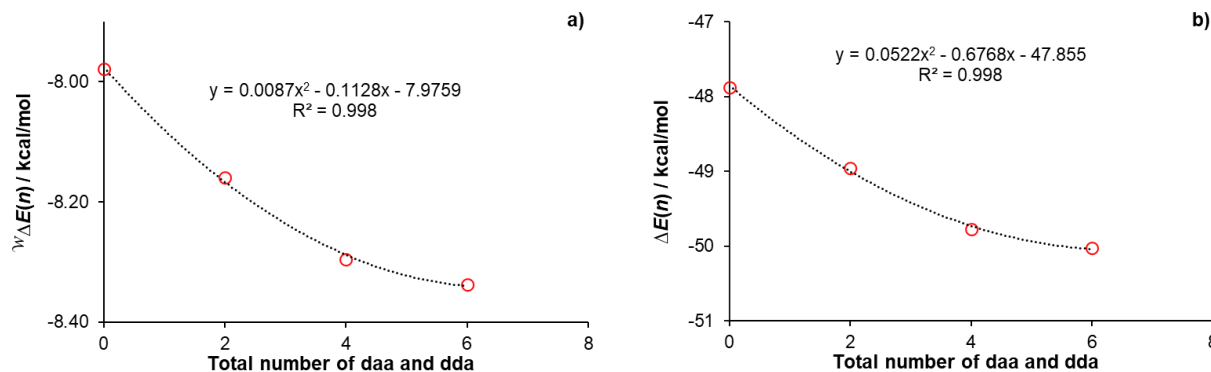
Figure 4 (a) Relative to a free water molecule, decrease of $^W\Delta E(\text{H}_2\text{O})$ obtained for the different 3D hexamer water clusters against the number of dda and daa. (b) Total $E(\text{H}_2\text{O})$ for the different 3D hexamer water clusters against the number of dda and daa. The circles represent computed data and the dotted line is the fitted second order polynomial with the fit of goodness given as well.

The prism structure, containing a total of 6 daa and dda H-bonds, is the maximum obtainable number of daa and dda H-bonds in a hexamer water cluster. On the other hand, the cyclic hexamer structure contains zero daa and dda H-bonds, and therefore represents a lower limit to the 3D conformational effects of energetic stabilization. From Figure 4 it is observed that – between the minimum cyclic and maximum prism structures – a clear, non-linear trend of energetic stabilization with increasing daa and dda H-bonds emerges. This trend is very similar to trends with increasing water molecules in cyclic structures, and it is clear that increasing dda and daa H-bonds are also a cause of cooperative energetic stabilization.

In Chapter 3 it was concluded that intermolecular (and molecular-wide) electron delocalization is the primary cause of cooperativity. Therefore, having established that the number of dda and daa H-bonds in 3D hexamer structures also display a cooperative trend, the intermolecular electron delocalization count is investigated next to determine whether it forms the same basis of cooperativity as for the cyclic structures.

Intermolecular electron delocalization

If the intermolecular electron delocalization can explain the stability decrease observed in Figure 4, then the intermolecular electron delocalization itself would be expected to increase non-linearly with an increasing number of daa and dda H-bonds. This is exactly what is observed – Figure 5 shows the increase of $N^{\text{deloc}}(\mathcal{F},\mathcal{M})$ (the total number of electrons delocalized by a fragment $\mathcal{F}$ with the remainder of the cluster) with increasing daa and dda H-bonds (as determined by FALDI[24–28] and the LDO algorithm). The number of delocalized intermolecular electrons increases until the maximum is reached at the prism water cluster. When considering the total number of electrons delocalized, the cyclic hexamer water cluster delocalizes a total of $9.341e$ compared to the $11.335e$ for the prism, which equates to a difference of $1.994e$. This is almost an electron pair or a Lewis-defined[29] chemical bond. It is conceivable that a covalent bond quantity of electrons could be extracted from water molecules by repositioning them to establish three hydrogen bonds for each individual water molecule.
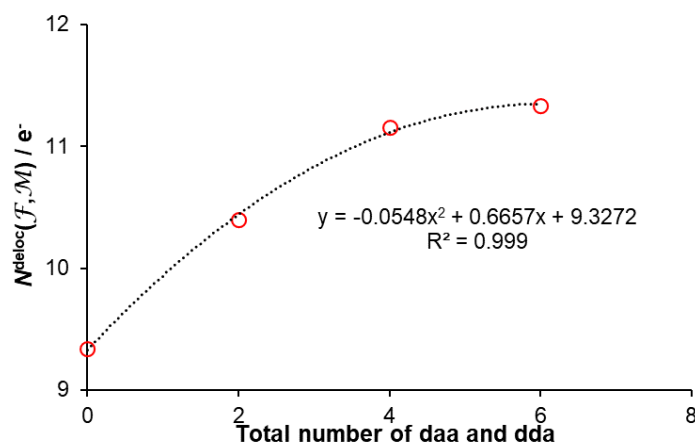
Figure 5 The total number of electrons delocalized by a single water molecule to all the atoms of the remaining water molecules in a cluster, $N^{\text{deloc}}(\mathcal{F},\mathcal{M})$ for the total number of dda and daa. The circles represent computed data and the dotted line is the fitted second order polynomial with the fit of goodness given as well.

The $\mathcal{F}1$ fragment was used as a case study to compare: 1) the cyclic hexamer $\mathcal{F}1$, which is a da type of water molecule compared to the daa water molecule type in the prism, 2) the $\mathcal{F}1$ cyclic

hexamer water molecule delocalizes a total of $1.556e$ and $\mathcal{F}1$ prism water molecules; in contrast, $2.112e$ in total are delocalized. The increased number of delocalized electrons can be correlated to the increased number of intermolecular H-bonds. Interestingly, and what is not seen on the molecule graph in both hexamer conformers, the $\mathcal{F}1$ water molecule delocalizes to all five of the other water molecules in the water cluster. Both the stability and delocalized electrons are at a maximum for the prism water cluster. Notably, the prism serves as an absolute limit (as determined by the number of dda and daa H-bonds) to the maximum electrons delocalized and the stability of the hexamer at the prism water cluster. It was hypothesized in Chapter 3 that the self-electron count of a fragment $N^{\text{self}}(\mathcal{F})$, and more importantly, the atom-localized electron count ($N^{\text{loc}}(\mathcal{F})$) of oxygen atoms serve as a limit to the number of electrons that can be delocalized by a fragment to the rest of the cluster. As the number of interfragment delocalized electrons increased, so the self-electron count decreased. Since electrons are finite, it is expected that there will be an increasing energy cost of delocalizing atom-localized electrons. ~~We now investigate~~ How the self- and localized electron counts act in the 3D structures is investigated next.

Figure 6 shows the average $N^{\text{self}}(\mathcal{F})$, $N^{\text{loc}}(\mathcal{F})$ and $N^{\text{deloc}}(\mathcal{F},\mathcal{F})$ electron counts for a water molecule $\mathcal{F}$ in the 3D structures. As expected, all of these fragment-localized electron counts decrease as the number of dda and daa H-bonds increase, showing that – as for the cyclic clusters – fragment-localized electrons are being utilized for molecular-wide electron delocalization. However, a significant difference is observed with respect to the composition of $N^{\text{self}}(\mathcal{F})$ relative to the cyclic clusters: atom-localized electrons ($N^{\text{loc}}(\mathcal{F})$), which correspond solely to electrons localized to O atoms, display a local minima when dda+daa is equal to 4. In addition, extremely small changes in $N^{\text{loc}}(\mathcal{F})$ are observed over the different 3D conformers. Therefore, as hypothesized in Chapter 3, $N^{\text{loc}}(\mathcal{F})$ does indeed serve as a limit to the number of electrons that can be delocalized. However, the prism structure is able to delocalize even more electrons by further

weakening the O-H covalent bonds (as evidenced by the continuous decrease of $N^{\text{deloc}}(\mathcal{F},\mathcal{F})$ in Figure 6).
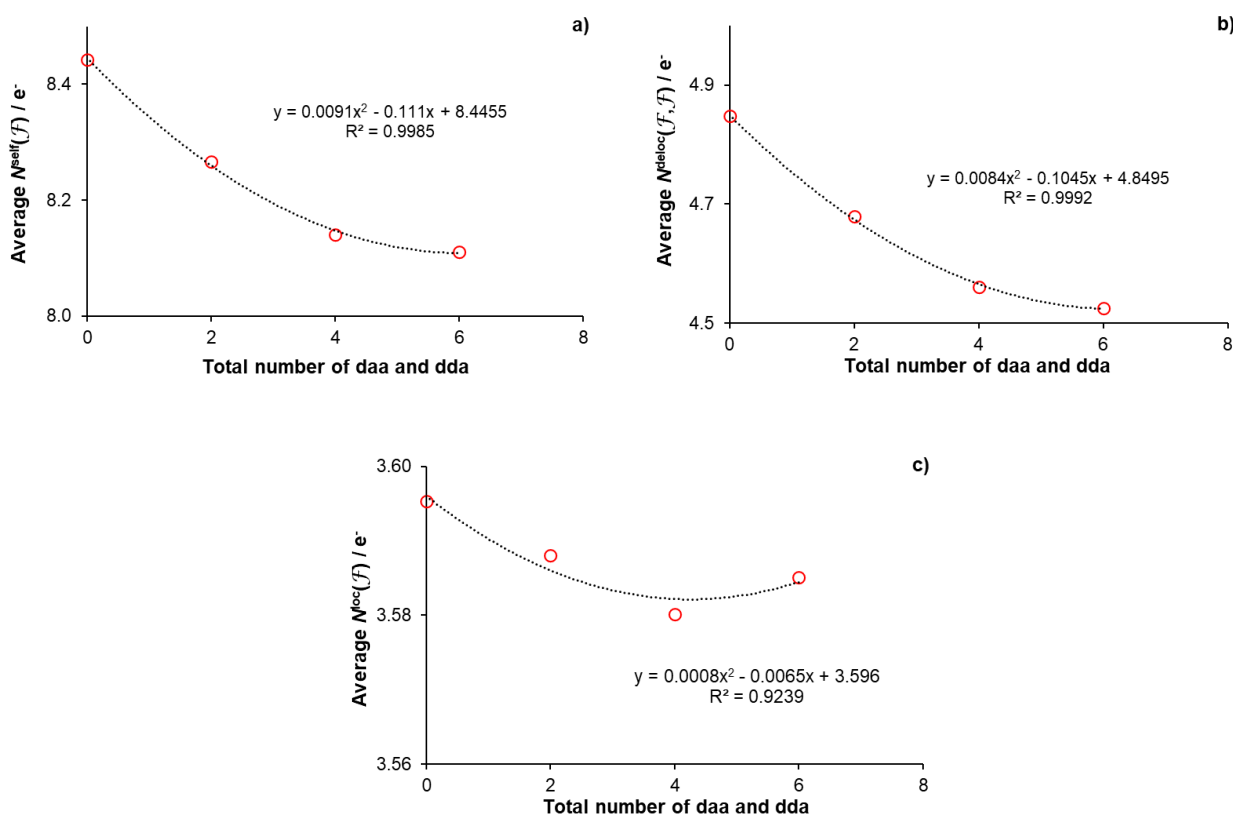
Figure 6 a) The total number of electrons localized to a single water molecule, $N^{\text{self}}(\mathcal{F})$, b) the total number of electrons delocalized between the atoms of a single water molecule, $N^{\text{deloc}}(\mathcal{F},\mathcal{F})$, and c) the total number of electrons localized to the atoms of a single water molecule, $N^{\text{loc}}(\mathcal{F})$. All trends are calculated for the total number of dda and daa. The circles represent computed data and the dotted line is the fitted second order polynomial with the fit of goodness given as well.

An interesting mechanism of cooperativity through electron delocalization arises naturally from the results in Figures 5 and 6. As the number of dda and daa H-bonds increase, so does the the intermolecular electron delocalization. The origin of these energy-stabilizing delocalized electrons is predominantly from electrons localized to O atoms (i.e. lone-pairs). As the number of atom-localized electrons decrease, an energetic limit is neared where the stabilization gained from delocalization is less than the potential energy of electrons localized to an atom. To gain further intermolecular delocalization, intramolecular delocalized electrons (such as from O-H covalent bonds) are utilized, as evidenced in the prism.

The way in which electron density is delocalized starts to become much more complex than the simpler way in which cyclic water clusters became delocalized. The need to describe and define formally what a chemical bond is becomes apparent from these results. Larger water clusters that consist of more dda and daa will need to be studied to determine whether the cooperativity equation works for these types of systems.

Delocalization patterns within the 3D water hexamer clusters

The 3D water clusters showed electron delocalization from each water molecule to all the others in the water cluster. The possible intermolecular density paths not on the molecular graph were investigated. The two fragment pairs that delocalize significant electron density after all the intermolecular interactions on the molecular graph were chosen for visualization using VMD[30] to obtain isosurfaces. The order of the isosurfaces is from the highest to the lowest energy as seen from the electronic energy (Figure 3) – the cyclic hexamer is omitted because it has already been shown in Chapter 3. The isovalue is shown below the isosurface which is in atomic units. Various electron channels form within the water cluster which is coined electron 'highways'.

The intermolecular delocalization patterns are shown below in Figures 7 – 10. The sequence is Bag, Book, Cage, Prism. The explanation of the highway network is discussed first followed by the intermolecular delocalization patterns.

Bag

Two 'highways' are formed for the delocalized electrons to travel on $\mathcal{F}5$, $\mathcal{F}1$ and $\mathcal{F}6$ and $\mathcal{F}5$, $\mathcal{F}4$ and $\mathcal{F}6$. The electrons then delocalize through the central path. The 'highway' is first formed between $\mathcal{F}3$, $\mathcal{F}4$ and $\mathcal{F}6$, and then the intermolecular interaction not on the molecular graph is formed between $\mathcal{F}3$ and $\mathcal{F}6$.

Book

A 'highway' is formed between $\mathcal{F}4$, $\mathcal{F}6$ and $\mathcal{F}5$ with electron density increasing somewhat at $\mathcal{F}1$. The central delocalization then forms, with $\mathcal{F}1$ and $\mathcal{F}6$ forming another 'highway'. Two different 'highways' are formed between $\mathcal{F}1$, $\mathcal{F}2$ and $\mathcal{F}3$, $\mathcal{F}4$, after which $\mathcal{F}3$ and $\mathcal{F}2$ connect and then the central 'highway' is formed.

Cage

The sequence of 'highway' formation is different between $\mathcal{F}2$ and F6 here – the central highway forms first. Some electron density is also present at $\mathcal{F}3$ and $\mathcal{F}5$. The first 'highway' is formed between $\mathcal{F}4$ and $\mathcal{F}3$ after which the central highway forms and then lastly the $\mathcal{F}1$ fragment become part of the 'highway' network.

Prism

A single 'highway' is formed between $\mathcal{F}5$ and $\mathcal{F}6$, after which the central 'highway' between $\mathcal{F}3$ and $\mathcal{F}6$ is formed. Lastly, the 'highway' connects with $\mathcal{F}4$. Two distinct 'highways' are formed between $\mathcal{F}1$, $\mathcal{F}2$ and $\mathcal{F}5$, $\mathcal{F}6$, respectively. The central 'highway' is then formed between $\mathcal{F}2$ and $\mathcal{F}6$.

Bag $\mathcal{F}5\cdots\mathcal{F}6$

Total e delocalized
between $\mathcal{F}4$ and $\mathcal{F}6$: $0.211e$

Isovalue 0.0005 au
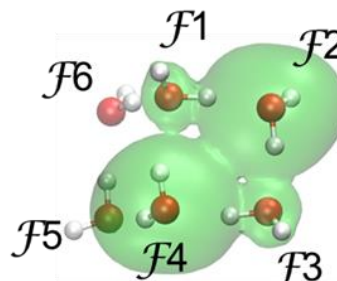

Isovalue 0.00005 au

Isovalue 0.00003 au
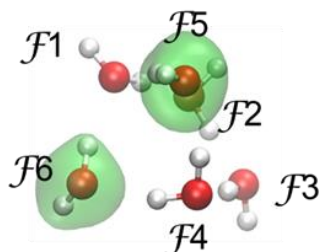
Isovalue 0.000015 au

Bag $\mathcal{F}3\cdots\mathcal{F}6$

Total e delocalized
between $\mathcal{F}4$ and $\mathcal{F}6$: $0.144e$
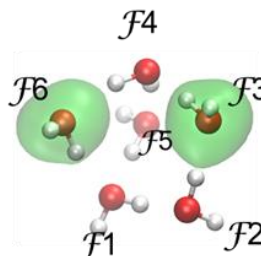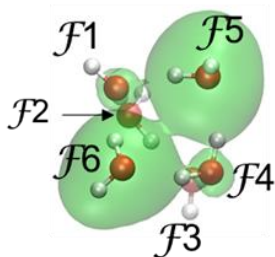
Isovalue 0.0002 au
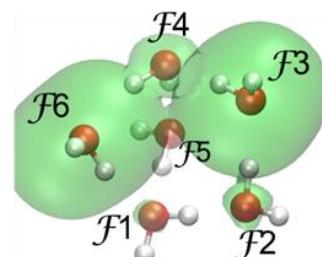
Isovalue 0.00003 au
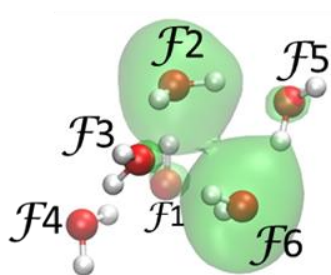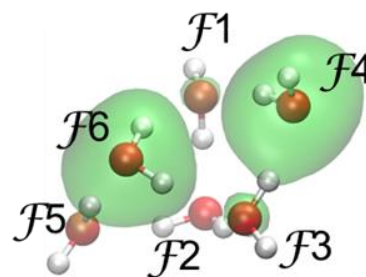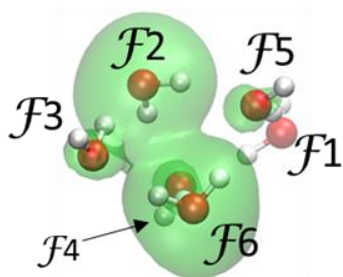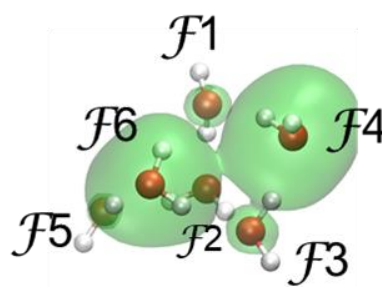

Isovalue 0.000012 au
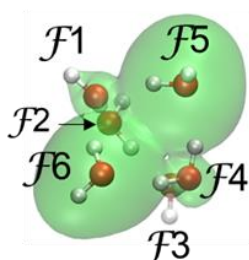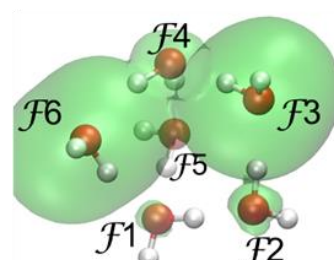
Isovalue 0.00001 au

Figure 7 The isosurfaces for the intermolecular electron delocalization between $\mathcal{F}5$, $\mathcal{F}6$ and $\mathcal{F}3$, $\mathcal{F}6$ for the bag water cluster.

142

Book $\mathcal{F}4\cdots\mathcal{F}6$

Total e delocalized
between $\mathcal{F}4$ and $\mathcal{F}6$: 0.212e

Isovalue 0.0003 au

Isovalue 0.00009 au

Isovalue 0.00003 au
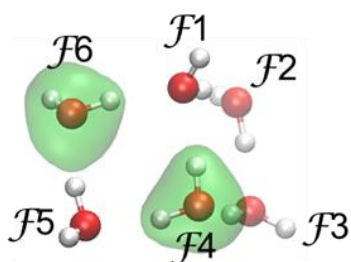
Isovalue 0.00001 au

Book $\mathcal{F}2\cdots\mathcal{F}4$

Total e delocalized
between $\mathcal{F}2$ and $\mathcal{F}4$: 0.168e
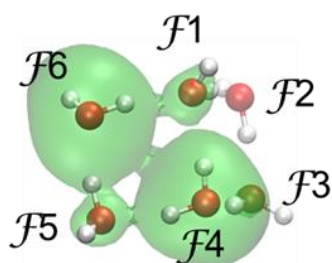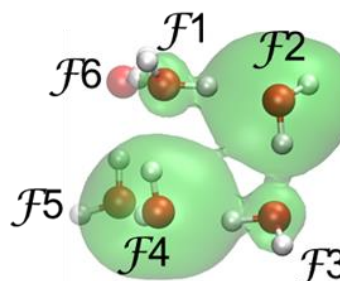
Isovalue 0.0003 au
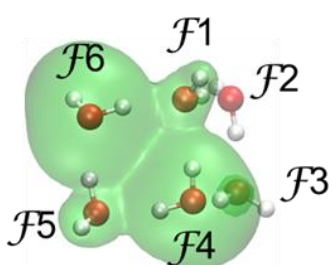
Isovalue 0.00004 au

Isovalue 0.00003 au

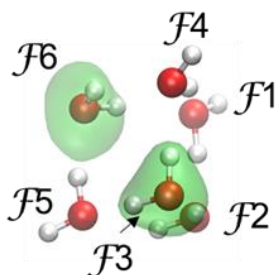*Isovalue 0.000017 au*

Figure 8 The isosurfaces for the intermolecular electron delocalization between $\mathcal{F}4$, $\mathcal{F}6$ and $\mathcal{F}2$, $\mathcal{F}4$ for the book water cluster
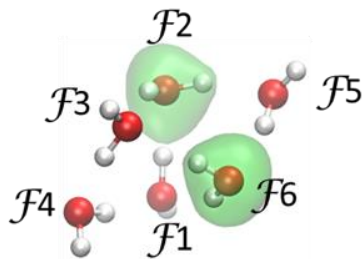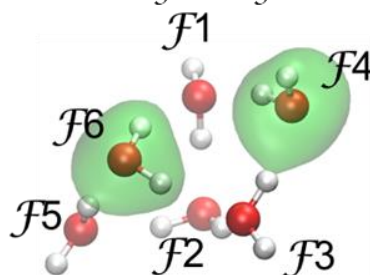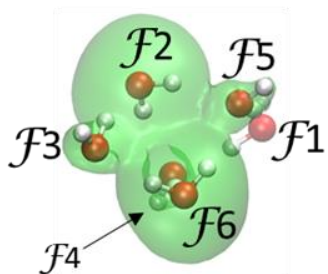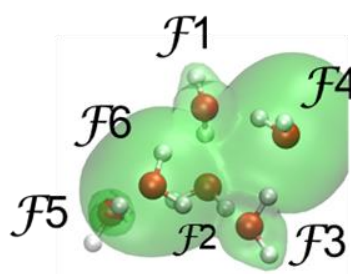
Figure 9 The isosurfaces for the intermolecular electron delocalization between $\mathcal{F}2$, $\mathcal{F}6$ and $\mathcal{F}4$, $\mathcal{F}6$ for the cage water cluster
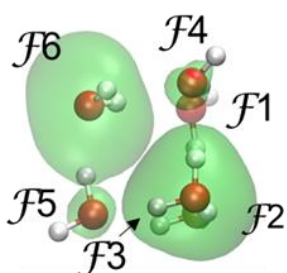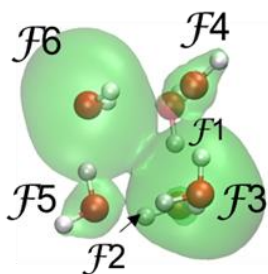
144

Prism $\mathcal{F}3\cdots\mathcal{F}6$

Total e delocalized
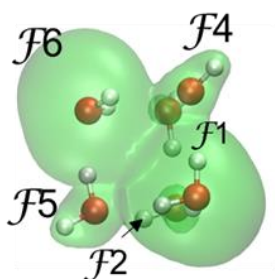between $\mathcal{F}3$ and $\mathcal{F}6$: 0.193e
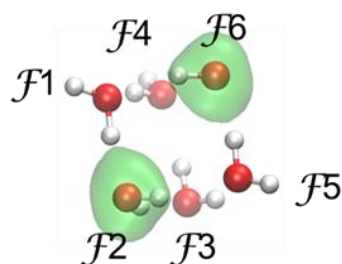

Isovalue 0.0005 au

Isovalue 0.0004 au

Isovalue 0.00002 au

Isovalue 0.00001 au
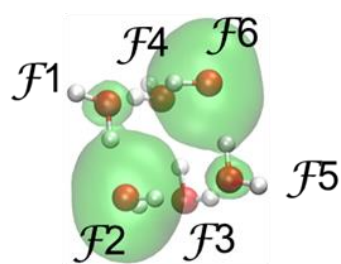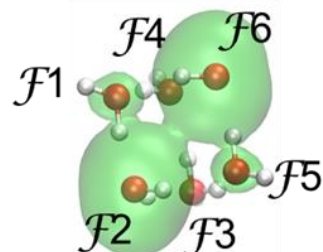
Prism $\mathcal{F}2\cdots\mathcal{F}6$

Total e delocalized
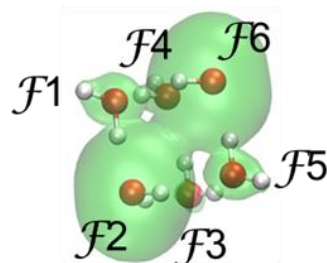between $\mathcal{F}2$ and $\mathcal{F}6$: 0.167e

Isovalue 0.0005 au

Isovalue 0.00004 au

Isovalue 0.00003 au

Isovalue 0.00001 au

Figure 10 The isosurfaces for the intermolecular electron delocalization between $\mathcal{F}3$, $\mathcal{F}6$ and $\mathcal{F}2$, $\mathcal{F}6$ for the prism water cluster.

145

The biggest trend seen with the isosurfaces of the 3D hexamer water clusters is that one or two 'highways' between neighbours form first, then afterwards the central 'highway' is formed. Firstly, it should be stressed that these intermolecular interactions are not seen on the molecular graph (i.e. the density does not form a *privileged* exchange channel resulting in a density bridge), yet they play an important role in the delocalization pattern of the water cluster. These 'highways' – which themselves can be seen as unprivileged exchange channels – are a novel finding in terms of water clusters. The intermolecular electron delocalization leads to the overall stability. This intermolecular delocalization taking place between non-neighbouring water molecules is not formally defined as a chemical bond.

The term anti-cooperativity is often used in reports with regard to water clusters due to the different ways in which water molecules can be orientated relative to each other, such as homodromic and anti-homodromic.[6] The results from this study show that there is an increase in stability when the numbers of dda and daa increase. The effect of instability or anti-cooperativity is rather a local event taking place within the water cluster – a sacrifice made to yield a lower electronic energy.

Conclusions

The 3D hexamer water clusters (cyclic, bag, book, cage, prism) were investigated using FALDI and FAMSEC protocols. The electronic energy trend showed cyclic > bag > book > cage > prism conformers, which all have the same number of water molecules. The same sequence was found in the literature at higher levels of theory. The energy difference is significant but still results in the same trend. Our aim in this chapter therefore was to show that the same mechanism – that of

increasing intermolecular electron delocalization – is responsible for the cooperative energetic stabilization observed in both cyclic clusters and 3D hexamer clusters.

The prism structure represents a hard chemical limit for hexamer structures with respect to the type and number of H-bonds that can be present. ~~We observed that~~ The intermolecular electron delocalization is higher for the prism than the cyclic water cluster by $0.332e$ and it was concluded that this originated from the hexamer cyclic water cluster consisting of only donor-acceptor (da) type water molecules, and that the prism in contrast only has double-donor single-acceptor (dda) or single-acceptor double-donor (daa) type water molecules. A similar non-linear increase in intermolecular delocalization was observed with respect to the number of dda and daa water molecules in the 3D structures as was observed in cyclic clusters with respect to the increasing number of water molecules. Therefore, concluding that the same mechanism – that of molecular-wide electron delocalization – can explain cooperativity in both series studied.

The origin of intermolecular electron delocalization is the 'self'-electron density of a water fragment, which consists of atom-localized electrons (predominantly O's lone-pair electrons) and intra-molecular delocalized electrons (predominantly electrons shared along O–H covalent bonds). While the atom-localized electron counts were observed to decrease greatly in the cyclic structures and therefore formed most of the origin of the observed increase in intermolecular delocalization, the same was not observed for the 3D structures. Rather, the intermolecular delocalization originated predominantly from a decrease in intramolecular delocalization. This observation supports our hypothesis that localized electrons form a hard limit to the amount of intermolecular delocalization, but that a further weakening of intramolecular O–H bonds can further enhance intermolecular delocalization and thus cooperativity.

The 'highways' of electron density are a completely new and different way of looking at how electrons move within water clusters. The molecular-wide (MOWED) behaviour of electrons

shows its fullest potential with these 'highways'. Cyclic and 3D hexamer water molecules undergo

a molecular change to ensure that stability is highest with the most efficient electron delocalization.

References:

1   D. M. Bates and G. S. Tschumper, *J. Phys. Chem. A*, 2009, **113**, 3555–3559.

2   Y. Chen and H. Li, *J. Phys. Chem. A*, 2010, **114**, 11719–11724.

3   E. E. Dahlke, R. M. Olson, H. R. Leverentz and D. G. Truhlar, *J. Phys. Chem. A*, 2008, **112**, 3976–3984.

4   J. L. Galvez Vallejo, J. D. Heredia and M. S. Gordon, *Phys. Chem. Chem. Phys.*, 2021, **23**, 18734–18743.

5   M. J. Gillan, F. R. Manby, M. D. Towler and D. Alfè, *J. Chem. Phys.*, 2012, **136**, 244105–244118.

6   J. M. Guevara-Vela, E. Romero-Montalvo, V. A. Mora Gómez, R. Chávez-Calvillo, M. García-Revilla, E. Francisco, Á. M. Pendás and T. Rocha-Rinza, *Phys. Chem. Chem. Phys.*, 2016, **18**, 19557–19566.

7   G. Hincapié, N. Acelas, M. Castaño, J. David and A. Restrepo, *J. Phys. Chem. A*, 2010, **114**, 7809–7814.

8   J. C. Howard, J. D. Enyard and G. S. Tschumper, *J. Chem. Phys.*, 2015, **143**, 214103–214108.

9   A. K. Kelkkanen, B. I. Lundqvist and J. K. Nørskov, *J. Chem. Phys.*, 2009, **131**, 046102–046103.

10   J. Kim and K. S. Kim, *J. Chem. Phys.*, 1998, **109**, 5886–5895.

11   E. S. Kryachko, *Chem. Phys. Lett.*, 1999, **314**, 353–363.

12   B. J. Mhin, J. Kim, S. Lee, J. Y. Lee and K. S. Kim, *J. Chem. Phys.*, 1994, **100**, 4484–4486.

13   E. Miliordos, E. Aprà and S. S. Xantheas, *J. Chem. Phys.*, 2013, **139**, 114302–114314.

14   A. Nandi, C. Qu, P. L. Houston, R. Conte, Q. Yu and J. M. Bowman, *J. Phys. Chem. Lett.*, 2021, **12**, 10318–10324.

15   R. M. Olson, J. L. Bentz, R. A. Kendall, M. W. Schmidt and M. S. Gordon, *J. Chem. Theory Comput.*, 2007, **3**, 1312–1328.

16   J. M. Pedulla, K. Kim and K. D. Jordan, *Chem. Phys. Lett*, 1998, **291**, 78–84.

17   B. Santra, A. Michaelides, M. Fuchs, A. Tkatchenko, C. Filippi and M. Scheffler, *J. Chem. Phys.*, 2008, **129**, 194111–194124.

18   P. L. Silvestrelli, *Chem. Phys. Lett.*, 2009, **475**, 285–288.

19   C. J. Tsai and K. D. Jordan, *Chem. Phys. Lett*, 1993, **213**, 181–188.

20   A. Ünal and U. Bozkaya, *Int. J. Quantum Chem.*, 2020, **120**, e26100-1–e26100-15.

21   S. S. Xantheas, *Chem. Phys.*, 2000, **258**, 225–231.

22   S. S. Xantheas, C. J. Burnham and R. J. Harrison, *J. Chem. Phys.*, 2002, **116**, 1493–1499.

23   M. B. Ahirwar, S. R. Gadre and M. M. Deshmukh, *J. Phys. Chem. A*, 2020, **124**, 6699–6706.

24   J. H. De Lange and I. Cukrowski, *J. Comput. Chem.*, 2017, **38**, 981–997.

25   J. H. De Lange and I. Cukrowski, *J. Comput. Chem.*, 2018, **39**, 1517–1530.

26   J. H. De Lange, D. M. E. Van Niekerk and I. Cukrowski, *Phys. Chem. Chem. Phys.*, 2019, **21**, 20988–20998.

27   J. H. De Lange, D. M. E. Van Niekerk and I. Cukrowski, *J. Comput. Chem.*, 2018, **39**, 973–985.

28   J. H. De Lange, D. M. E. Van Niekerk and I. Cukrowski, *J. Comput. Chem.*, 2018, **39**, 2283–2299.

29   G. N. Lewis, *J. Am. Chem. Soc.*, 1916, **38**, 762–785.

30   W. Humphrey, A. Dalke and K. Schulten, *J. Molec. Graphics,* 1996, **14**, 33–38.

Chapter 6

Conclusions

Overview of work done

The phenomenon of cooperativity in water clusters was investigated in this work. The water clusters are connected only through intermolecular H-bonds. The intermolecular H-bonds are often referred to in this work to show the effect of cooperativity. Cooperativity was considered from a molecular perspective – the **MO**lecular **W**ide **E**lectron **D**ensity approach (MOWED) – for cyclic water clusters and 3D hexamer water clusters in this work.

The main aim of this work was to quantify cooperativity in a manner that considers the whole molecule. Cooperativity is not described as a new finding in this work, rather the focus is on using a different perspective to consider cooperativity compared to the localised view used in the literature. All the trends considered in this work follow a non-additive trend as this is associated with cooperativity in our view. Cooperativity is discussed for cyclic water clusters in Chapter 3. The effects resulting from cooperativity in cyclic water clusters are explored in Chapter 4. These results build on the main contributions to cooperativity shown in Chapter 3. 3D hexamer water clusters are considered in a broad way rather than in detail as in Chapters 3 and 4.

Cooperativity in cyclic water clusters of sizes $(H_2O)_n$ where $n = 2–6, 8$ were investigated in Chapter 3. Cooperativity is primarily defined by electronic energy. The trend for the electronic energy is fitted with a newly developed exponential equation. The electronic energy is directly correlated with the number of intermolecular delocalized electrons ($N^{\mathrm{deloc}}(\mathcal{F},\mathcal{M})$), which travel through the water cluster on 'highways' of H-bonds. The H-bond acceptor delocalizes more electron density than the H-bond donor. It was shown that the {O1–H2···O4} H-bond shares $2.65e$ with all the other fragments in the water cluster. The stability of water clusters was aided by intermolecular H-bonds, but a higher stability contribution was seen from the O 3-atom fragment as shown with *mol*-FAMSEC. The delocalization patterns showed the highways that electrons travel on. The 1D cross-section of CP(H2,O4) showed that only 63.7% of the *deloc*-ED came from the three atoms involved, O1–H2···O4, meaning that 36.3% of the total *deloc*-ED is from the other

151

atoms in the water cluster. The intramolecular electron count showed that fewer electrons are associated with increasing water cluster size due to the delocalization of electrons.

The cooperativity-induced effects in cyclic water clusters were the focus of Chapter 4. The equation developed in Chapter 3 was fitted to the cooperativity-induced effects in this chapter. The first cooperativity-induced effect is the atomic charge. The trend for the atomic charge of O followed a decrease, which means that greater electron density is associated with each O atom, and that the H2 atom followed an increase, indicating that it lost electron density. The interaction energy was a fundamental property considered as a cooperativity-induced effect. The total interaction energy followed a decreasing trend, with its components' total exchange-correlation increasing and total electrostatic interactions decreasing. The intermolecular interaction energy of both its components decreased. The intermolecular interaction energy and intramolecular covalent interaction energy were similar in magnitude. The topological properties showed that the electron density at the CP followed the same trend as seen for $N^{\text{deloc}}(\mathcal{F},\mathcal{M})$. The potential energy density decreased while the kinetic energy density increased. The potential energy density showed that there is an increase in stability at the CP and that the kinetic energy showed instability. The net effect was a stabilising one due to potential energy density dominating over kinetic energy density, which was shown by the sum of the two energy densities. The last property investigated for cooperativity-induced effects was the geometrical descriptors – the correlation between intermolecular interaction distance and the properties considered previously. Similar trends were observed with intermolecular distance against the properties investigated.

The electronic energy decreases for the 3D hexamer water clusters in a non-additive way but is fitted with a second order polynomial. The $N^{\text{deloc}}(\mathcal{F},\mathcal{M})$ increased in an opposite non-additive manner as electronic energy. The direct correlation between electronic energy and $N^{\text{deloc}}(\mathcal{F},\mathcal{M})$ was found for the 3D hexamer water clusters, therefore proving that they are correlated regardless of the geometry and type of H-bonds present. The 3D electron delocalization patterns showed the

'highways' along which electrons travel. New 'highways' are seen here which are not seen in cyclic water clusters.

Cyclic Water Clusters

Firstly, the correlation between electronic energy and $N^{\text{deloc}}(\mathcal{F},\mathcal{M})$ is an important finding. Cooperativity is then linked with the increase in $N^{\text{deloc}}(\mathcal{F},\mathcal{M})$ due to this correlation.

The newly developed equation makes it easy to quickly see if cooperativity is present within a set of water clusters. The equation showed the maximum or minimum of the property fitted. The equation needs to be extended to other molecular systems to investigate the universal applications. The electronic energy decreases with an increase in water molecules until $n = 6$. The significance is that there is a limit to planar cyclic water clusters. This limit is –8.316 kcal/mol, 0.34 kcal/mol lower than the hexamer. The hexamer water cluster delocalizes $1.557e$ per water molecule, which means that $9e$ are delocalized throughout the hexamer cyclic water cluster. This is a large number of electrons that serve to create a privileged channel leading to lower electronic energy.

The intermolecular electron delocalization patterns showed new ways in which electrons travel and ensure the highest stability of the water cluster. The hexamer and tetramer showed arterial paths through the centre of the water molecule. The water cluster therefore goes beyond the classical bonds to delocalize electron density to stabilize the water cluster.

Molecular-wide events are seen with a significant number of electrons delocalized to the H-bonds; this was shown with fragments $\mathcal{G}$ and $\mathcal{H}$. The electron density is thus delocalized far beyond just the covalent bond or the intermolecular H-bond. The wider effect of electron delocalization should not be neglected as proved by these results.

Another proof of molecular-wide effects within the water cluster was found with the 1D cross-section of CP(H2,O4). The remaining 36.3% is mostly made up of O4,H5, O4,O6 and O1,H3. The

153

large significance of this is that the intermolecular H-bond (H2,O4) is electronically affected by other bonds that delocalize electron density to it.

The intramolecular electron counts for a water molecule delocalize its electron density to other water molecules in the water cluster to increase stability, leading to a decreased count but still ensuring the integrity of the water molecule.

The final conclusion is that electron density is distributed throughout the water molecule and not isolated to the H-bonds within the water cluster. The molecular-wide distribution of the electron density causes the increased stability. The water molecule changes its electronic character to ensure that stability is maximised by delocalizing electron density to the whole water cluster. This view of a water cluster is most probably not isolated to water molecules alone. One should thus extend this type of approach to electron-rich molecular systems.

Cooperativity Effects

The stability of the atomic charge of O increases, but the localized water molecule ($N^{loc}(\mathcal{F})$) electron count decreases. The decrease in charge is therefore a result of an increased number of electrons delocalized to the O atomic basin. The charge of an atom is linked with both the localized and delocalized electron counts. This clearly links with the previous chapter in the sense that a molecular-wide event is taking place. The electrons delocalize to all the atoms in the water cluster, making these atoms more negative and more positive. The H2 atom becomes more positive due to losing a fraction of its electron. The known concept of atomic charge depending on localized electron count alone would lead to the wrong atomic charge values.

The total interaction energy stabilizes, which is expected because the water clusters remain intact. The destabilising nature of the total exchange correlation is due to the destabilising effect of the exchange-correlation in covalent bonds, which is larger than the stabilising effect of intermolecular interaction exchange-correlation. This means that the electron channel between

covalently bonded O and H is working against the stability of the water cluster whereas the intermolecular interactions are more beneficial to the water cluster. More intermolecular interactions therefore equate to large stability even for the same number of water molecules (see result of Chapter 5). The classical interactions are of a stabilising nature in both covalent bonds and intermolecular interactions, which is expected due to the difference in atomic charge, and is the reason why the H-bond is theorized as a pure electrostatic interaction. The important factor here is that both components contribute to stability, which means that one should consider both when looking at a molecular system.

The topological properties supported the findings already found. The electron density at the CP followed the same trend as $N^{\text{deloc}}(\mathcal{F},\mathcal{M})$, which means the same as what was already stated, namely that electronic energy and $N^{\text{deloc}}(\mathcal{F},\mathcal{M})$ are directly correlated. The potential energy density at the intermolecular CP decreased due to the increase in electron density at the CP, contributing to the stability of the water cluster. The kinetic energy density at the intermolecular CP contributed to the instability of the water cluster. The net effect was of a stabilising nature as shown by the sum of potential and kinetic energy density. The measure of covalence also increases in line with the findings of $N^{\text{deloc}}(\mathcal{F},\mathcal{M})$. The last property – geometrical descriptors – showed that with decreased intermolecular distance the same is found for water clusters. The electronic energy and $N^{\text{deloc}}(\mathcal{F},\mathcal{M})$ have a similar correlation because the size of the water cluster and the intermolecular interaction distance are linked.

The cooperativity-induced effects showed primarily the change that a cyclic water cluster undergoes when cooperativity is present for the electronic energy to be at its lowest. Notably, molecular systems should be judged by both electronic and energetic effects. Furthermore, both of these effects are molecular-wide, meaning that a large error occurs when the isolated atoms or isolated bonds approach is taken.

Cyclic water clusters are complex when one considers the whole molecule as an entity with electronic and energetic character. One needs to fully quantify both these factors for a complete picture. Cyclic water clusters need to be considered in a new light, because when a MOWED approach is not considered the full explanation is not found.

3D Hexamer Structures

The electronic energy sequence and relative values for 3D hexamer water clusters were validated by comparing them to higher levels of theory,[1–9] and they were found to closely match them.

The electronic energy and $N^{\text{deloc}}(\mathcal{F},\mathcal{M})$ correlated, which means that this is a universal correlation for water clusters. Moreover, the same will possibly be seen for other cooperativity molecular systems. This set of water clusters has the same number of water molecules, which means that the additional intermolecular H-bonds for the 3D hexamer water clusters increase the stability. The prism water hexamer conformer, which only has dda and daa type H-bonds, is the limit in terms of stability and electrons delocalized for hexamers because it is not possible for a water molecule to have more H-bonds per water molecule. The prism conformer then has the lowest energy with the highest $N^{\text{deloc}}(\mathcal{F},\mathcal{M})$ and the highest cooperativity for a hexamer water cluster.

The most important result from this chapter is the electron delocalization patterns, which showed that electrons travel on 'highways' using the intermolecular H-bonds but that there are channels that pass through the 3D space within the water cluster. Therefore, an entirely new way of electron delocalization is shown here which has not yet been seen or discussed. This result is of the greatest value here because the MOWED approach is shown in its fullest form. The way in which molecular systems delocalize electron density and 'bond' should be viewed in an entirely new light based on the results obtained in this work.

Future Work

The cyclic water clusters were investigated almost fully with very little left to look at. Linear water chains need to be considered with the MOWED perspective of cooperativity. The cooperativity equation needs to be fitted to the electronic energy and the intermolecular electron delocalization trend to see if the equation holds for these types of water clusters. Only 3D hexamer water clusters were investigated for 3D-type water clusters. Therefore, larger 3D water clusters need to be investigated and plotted to see what trend is followed. The cooperativity-induced changes should be looked at for 3D hexamer and larger water clusters. The equation will possibly require an additional 3D parameter to improve the fitting. Unconventional 3D water clusters have been optimised, such as a dimer or trimer inside an octamer to investigate different environments for water molecules and cooperativity. This has unfortunately not been done due to time constraints. Lastly, a full uniform explanation and equation are needed for cooperativity that fits all scenarios.

References:

1   D. M. Bates and G. S. Tschumper, *J. Phys. Chem. A*, 2009, **113**, 3555–3559.

2   E. E. Dahlke, R. M. Olson, H. R. Leverentz and D. G. Truhlar, *J. Phys. Chem. A*, 2008, **112**, 3976–3984.

3   G. Hincapié, N. Acelas, M. Castaño, J. David and A. Restrepo, *J. Phys. Chem. A*, 2010, **114**, 7809–7814.

4   J. Kim and K. S. Kim, *J. Chem. Phys.*, 1998, **109**, 5886–5895.

5   E. S. Kryachko, *Chem. Phys. Lett.*, 1999, **314**, 353–363.

6   E. Miliordos, E. Aprà and S. S. Xantheas, *J. Chem. Phys.*, 2013, **139**, 114302.

7   R. M. Olson, J. L. Bentz, R. A. Kendall, M. W. Schmidt and M. S. Gordon, *J. Chem. Theory Comput.*, 2007, **3**, 1312–1328.

8   C. J. Tsai and K. D. Jordan, *Chem. Phys. Lett.* 1993, **213**, 181–188.

9   S. S. Xantheas, C. J. Burnham and R. J. Harrison, *J. Chem. Phys.*, 2002, **116**, 1493–1499.

Appendix I

Molecular-wide and electron density (MOWED)-based definition and quantification of cooperativity in cyclic water clusters

Prepared for submission to:

Physical Chemistry Chemical Physics journal 2023

Supplementary Information

Molecular-wide and electron density (MOWED)-based definition and quantification of cooperativity in cyclic water clusters

Ignacy Cukrowski,[*a] Stéfan Zaaiman,[a] Shahnawaz Hussain[a,b] Jurgens H. de Lange[*a]

[a] *Department of Chemistry, Faculty of Natural and Agricultural Sciences, University of Pretoria, Lynnwood Road, Hatfield, Pretoria 0002, South Africa*
[b] *Elective student at the University of Pretoria. Permanent position: a student in the Department of Computer Science and Engineering at the Indian Institute of Technology, Kharagpur, India*

Electronic Supporting Information

Table S1. Coordinates for a water monomer (Part a), water dimer (Part b), and cyclic water trimer (Part c), tetramer (Part d), pentamer (Part e), hexamer (Part f), and octamer (Part g) of optimised structures at the B3LYP/aug-cc-pVTZ/GD3 level of theory in the gas phase.

Part a – H_2O monomer.

Atom	X	Y	Z
O1	-0.446654	0.606380	0.000000
H2	0.514497	0.643373	0.000000
H3	-0.732643	1.524747	0.000000

Part b – H_2O dimer.

Atom	X	Y	Z
O1	0.959520	-0.052738	-0.142356
H2	1.918076	-0.129607	-0.018542
H3	0.738689	0.842577	0.127278
O4	3.812213	-0.552236	0.133385
H5	3.929181	-1.313447	0.710764
H6	4.152322	-0.825449	-0.724628

Part c – cyclic H_2O trimer.

Atom	X	Y	Z
O1	-0.099353	0.031363	0.215384
H2	0.727519	0.543930	0.296234
H3	0.034932	-0.583716	-0.510249
O4	1.666397	2.186424	0.417868
H5	0.808495	2.651138	0.389307
H6	2.089795	2.457824	1.236800
O7	-1.082371	2.653121	0.270501
H8	-1.069958	1.684096	0.159701
H9	-1.570957	3.005219	-0.478047

Part d – cyclic H_2O tetramer.

Atom	X	Y	Z
O1	-0.122531	3.262718	0.264670
H2	0.034435	2.292007	0.301757
H3	0.199194	3.617931	1.097465
O4	-0.060303	0.530838	0.323057
H5	-1.013540	0.369372	0.139712
H6	0.428202	0.028405	-0.334306
O7	-2.737897	0.456501	-0.222797
H8	-2.889242	1.426776	-0.285868
H9	-3.363145	0.130183	0.429753
O10	-2.798157	3.188557	-0.290733
H11	-1.849237	3.350321	-0.086495
H12	-2.981379	3.662491	-1.106216

Part e – cyclic H_2O pentamer.

Atom	X	Y	Z
O1	-0.092653	3.414821	-0.435109
H2	0.276768	2.512258	-0.289084
H3	0.493678	4.020164	0.025443
O4	0.839791	0.900700	-0.005030
H5	0.098462	0.304694	0.254649
H6	1.275052	0.469334	-0.745180
O7	-1.280039	-0.669964	0.630230
H8	-2.119104	-0.178730	0.465748
H9	-1.355198	-1.038299	1.514271
O10	-3.525553	0.782107	0.173968
H11	-3.295934	1.735684	0.074235
H12	-4.059985	0.556926	-0.592063
O13	-2.797767	3.381885	-0.111221
H14	-1.821183	3.460562	-0.213519
H15	-3.045535	3.990057	0.589760

Part f – cyclic H_2O hexamer.

Atom	X	Y	Z
O1	-0.493641	3.425248	0.159911
H2	-0.005066	2.577190	0.041013
H3	-0.142220	3.822490	0.960820
O4	0.873158	1.107431	-0.140230
H5	0.381391	0.260669	-0.024990
H6	1.395350	1.002291	-0.939612
O7	-0.448354	-1.237658	0.146435
H8	-1.426501	-1.241067	0.022535
H9	-0.282400	-1.741970	0.946994
O10	-3.137960	-1.276047	-0.159910
H11	-3.626535	-0.427990	-0.041013
H12	-3.489382	-1.673291	-0.960818
O13	-4.504758	1.041769	0.140231
H14	-4.012991	1.888530	0.024989
H15	-5.026947	1.146909	0.939615
O16	-3.183247	3.386859	-0.146438
H17	-2.205100	3.390267	-0.022536
H18	-3.349199	3.891169	-0.946997

Part g – cyclic H_2O octamer.

Atom	X	Y	Z
O1	-0.095848	4.566979	0.549298
H2	0.314063	3.707841	0.298299
H3	0.295129	4.809579	1.392162
O4	1.172498	2.269886	-0.110364
H5	0.836099	1.353845	0.019706
H6	1.676336	2.252631	-0.927660
O7	0.397617	-0.299646	0.228895
H8	-0.475782	-0.689555	-0.004028
H9	0.679031	-0.744525	1.032045
O10	-1.939352	-1.513573	-0.390600
H11	-2.844994	-1.195159	-0.172600
H12	-2.011798	-1.957215	-1.239119
O13	-4.480987	-0.788108	0.184675
H14	-4.890492	0.097211	0.051508
H15	-4.870981	-1.140384	0.988397
O16	-5.749770	1.576927	-0.155580
H17	-5.412511	2.467539	0.093814
H18	-6.259122	1.703384	-0.959757
O19	-4.972943	4.080630	0.512149
H20	-4.098866	4.496846	0.333501
H21	-5.262650	4.429318	1.358687
O22	-2.634528	5.364421	0.060032
H23	-1.730483	5.019885	0.241790
H24	-2.557741	5.903010	-0.731237

163
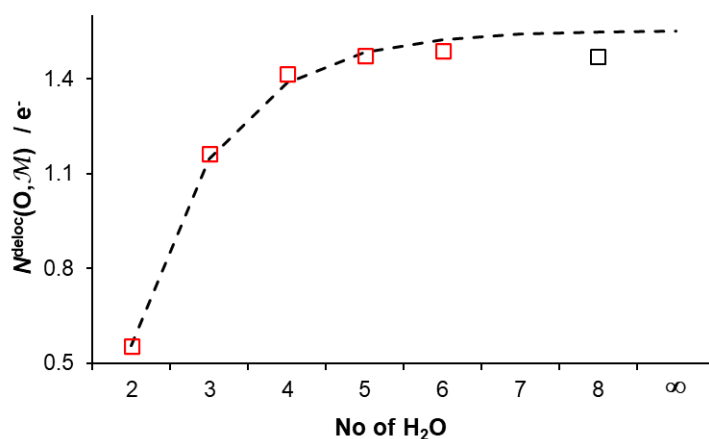
Figure S1 The count of computed (squares) electrons delocalized by a statistical O-atom to the remaining water molecules in water clusters. The dashed line represents a fitted trend using Eq. 17 (in the main body) and dimer as a reference state.
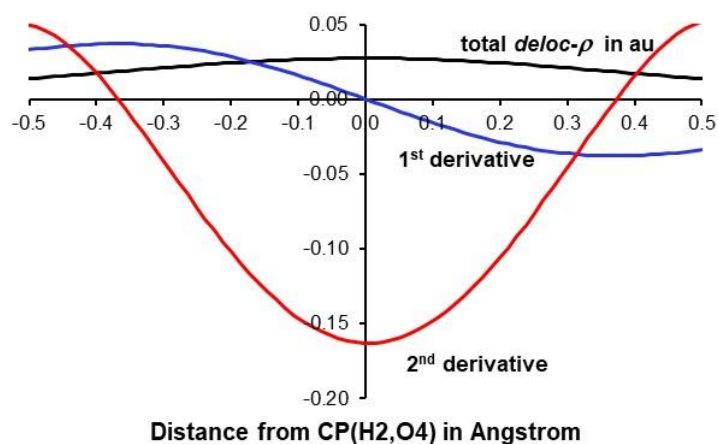
Figure S2. Data obtained for the total delocalized electron density, *deloc-ρ*, from the 1D cross-section originating at the CP(H2,O4) in the cyclic tetramer. The 1st and 2nd derivatives stand for the 1st and 2nd partial derivatives computed on the total delocalised ED along the λ_2-eigenvector crossing the CP(H2,O4).

164
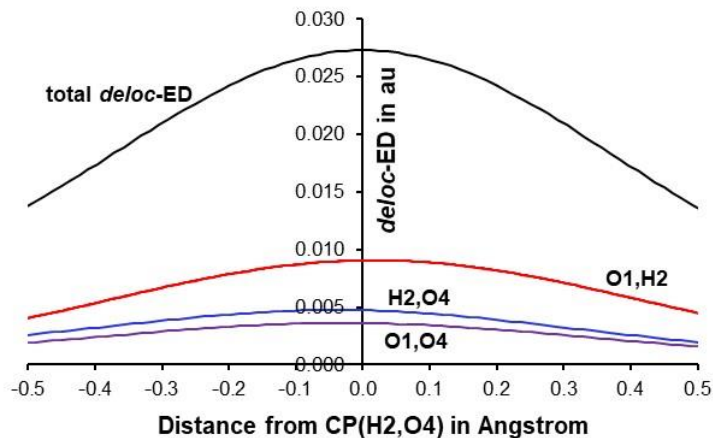
Figure S3. Comparative analysis of the total *deloc*-ED = *total-ρ* and major contributions made by atom-pairs constituting the classical intermolecular O1–H2···O4 H-bond in the cyclic water tetramer.
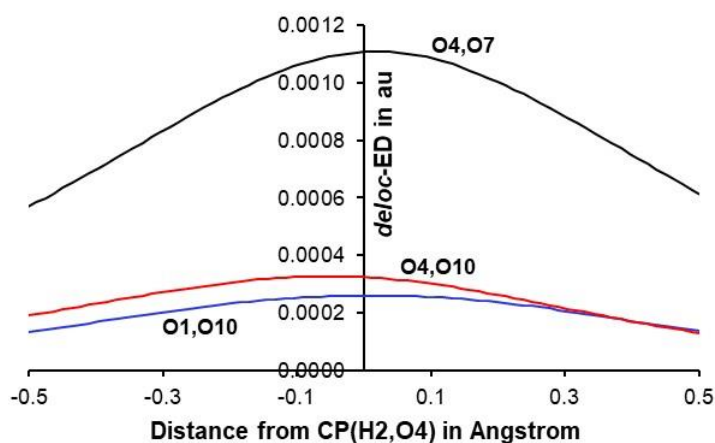
Figure S4. Contributions made by the indicated distant oxygen atom-pairs in the cyclic water tetramer to the total delocalised ED at the CP(H2,O4).
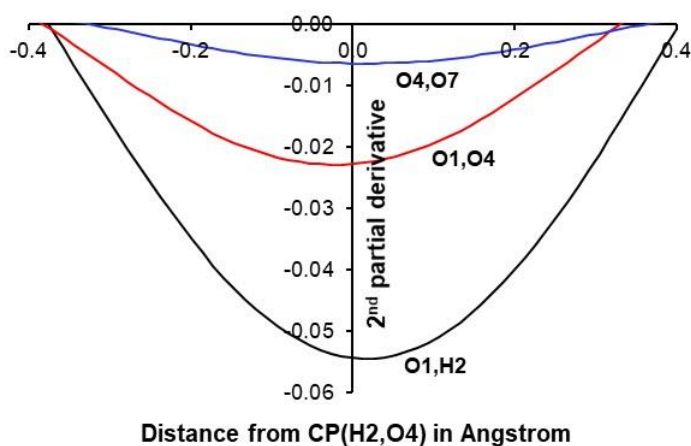
Figure S5. Second partial derivative computed on contributions made by the indicated atom-pairs in the cyclic water tetramer to the total delocalised ED at the CP(H2,O4).

165

Table S2. Relative to a free, non-interacting water molecule, a change in the self-energy of a statistical water molecule, O-atom and H-atoms in water dimer and cyclic water clusters. The values for the *loc*-FAMSEC energy term are also provided. Values are in kcal/mol

Energy term	2-H_2O	3-H_2O	4-H_2O	5-H_2O	6-H_2O	8-H_2O
$\Delta E_{\text{self}}(\mathcal{F})$	18.6	42.1	53.9	57.3	59.2	60.1
$\Delta E_{\text{self}}(O1)$	11.0	25.4	32.3	34.1	34.9	34.8
$\Delta E_{\text{self}}(H2)$	7.2	15.9	20.8	22.7	23.6	24.4
$\Delta E_{\text{self}}(H3)$	0.5	0.8	0.8	0.5	0.7	0.9
loc-FAMSEC	51.1	78.7	84.5	86.6	87.2	87.8

Table S3. Specified (de)localization indices computed for water clusters. $N^{\text{deloc}}(\mathcal{F},\mathcal{F})$ = a count of electrons delocalized within a water molecule. $N^{\text{deloc}}(O1,\mathcal{R})$ = a count of electrons delocalized by O1 to the remaining atoms of a molecular system. $N^{\text{deloc}}(\mathcal{F}1,\mathcal{M})$ = a count of electrons delocalised by a water molecule to remaining water molecules in a cluster. $N^{\text{deloc}}(O1,\mathcal{M})$ = a count of electrons delocalised by O1-atom to remaining water molecules in a cluster.

	2-H_2O	3-H_2O	4-H_2O	5-H_2O	6-H_2O	8-H_2O
Intramolecular contributions						
$N^{\text{loc}}(O1)$	5.451	5.027	4.879	4.849	4.848	4.874
e-shared(O1,H2)	1.899	1.702	1.589	1.554	1.541	1.536
e-shared(O1,H3)	2.063	2.050	2.047	2.050	2.048	2.047
$N^{\text{deloc}}(\mathcal{F},\mathcal{F})$	3.971	3.759	3.642	3.611	3.595	3.590
$N^{\text{deloc}}(O1,H2)$	1.523	1.378	1.295	1.270	1.260	1.256
$N^{\text{deloc}}(H2,O1)$	0.376	0.324	0.294	0.285	0.281	0.280
$N^{\text{deloc}}(O1,H3)$	1.643	1.633	1.623	1.633	1.631	1.631
$N^{\text{deloc}}(H3,O1)$	0.420	0.417	0.417	0.418	0.417	0.417
Counts of the total delocalized electrons						
$N^{\text{deloc}}(O1,\mathcal{R})$	3.721	4.175	4.340	4.375	4.380	4.357
$N^{\text{deloc}}(H2,\mathcal{R})$	0.403	0.374	0.357	0.351	0.347	0.344
$N^{\text{deloc}}(H3,\mathcal{R})$	0.426	0.424	0.424	0.425	0.424	0.424
Intermolecular contributions						
e-shared(O1,O4)	0.635	0.679	0.778	0.800	0.807	0.801
$N^{\text{deloc}}(O1,O4)$	0.362	0.362	0.413	0.424	0.428	0.426
$N^{\text{deloc}}(O4,O1)$	0.274	0.317	0.365	0.376	0.379	0.375
$N^{\text{deloc}}(\mathcal{F},\mathcal{M})$	0.578	1.214	1.479	1.539	1.557	1.535
$N^{\text{deloc}}(O1,\mathcal{M})$	0.555	1.164	1.415	1.473	1.490	1.470
$N^{\text{deloc}}(H2,\mathcal{M})$	0.022	0.047	0.604	0.063	0.063	0.061
$N^{\text{deloc}}(H3,\mathcal{M})$	0.001	0.003	0.004	0.004	0.004	0.004

166

Appendix II

3D Hexamer water clusters

Table S1. Coordinates for a cyclic hexamer (Part a), 3D bag hexamer (Part b), 3D book hexamer (Part c), 3D cage hexamer (Part d), 3D prism hexamer (Part e) of optimised structures at the B3LYP/aug-cc-pVTZ/GD3 level of theory in the gas phase.

Part a – cyclic hexamer.

Atom	X	Y	Z
O1	-0.493641	3.425248	0.159911
H2	-0.005066	2.577190	0.041013
H3	-0.142220	3.822490	0.960820
O4	0.873158	1.107431	-0.140230
H5	0.381391	0.260669	-0.024990
H6	1.395350	1.002291	-0.939612
O7	-0.448354	-1.237658	0.146435
H8	-1.426501	-1.241067	0.022535
H9	-0.282400	-1.741970	0.946994
O10	-3.137960	-1.276047	-0.159910
H11	-3.626535	-0.427990	-0.041013
H12	-3.489382	-1.673291	-0.960818
O13	-4.504758	1.041769	0.140231
H14	-4.012991	1.888530	0.024989
H15	-5.026947	1.146909	0.939615
O16	-3.183247	3.386859	-0.146438
H17	-2.205100	3.390267	-0.022536
H18	-3.349199	3.891169	-0.946997

Part b – Bag hexamer.

Symbol	X	Y	Z
O1	-0.94668	2.398653	-1.63367
H2	-0.07142	2.113247	-2.0123
H3	-1.3755	2.939249	-2.3022
O4	1.403848	1.513875	-2.51895
H5	1.714486	0.8551	-1.84657
H6	2.11615	2.154593	-2.59731
O7	2.152934	-0.1186	-0.53974
H8	1.470874	-0.01355	0.175108
H9	2.347404	-1.05656	-0.60383
O10	0.214191	0.313167	1.254613
H11	0.16788	1.280495	1.365239
H12	-0.62309	0.096176	0.805933
O13	-0.2083	3.113187	1.004603
H14	-0.54142	3.023106	0.092988
H15	-0.93397	3.479524	1.517385
O16	-2.11074	0.183763	-0.37103
H17	-1.80263	0.920521	-0.93236
H18	-2.31232	-0.54164	-0.96783

Part c – Book hexamer.

Symbol	X	Y	Z
O1	-0.32977	3.565719	0.499029
H2	0.532944	3.628064	0.014979
H3	-0.29488	4.20785	1.2129
O4	2.035411	3.480853	-0.75744
H5	2.229693	2.510308	-0.74213
H6	2.134632	3.759553	-1.67152
O7	2.240415	0.806028	-0.62295
H8	1.385127	0.622915	-0.15746
H9	2.923408	0.353005	-0.12189
O10	-0.10001	0.654917	0.689887
H11	-0.25156	1.59898	0.850731
H12	-0.88985	0.362202	0.192297
O13	-2.43468	0.246002	-0.78885
H14	-2.62416	1.200964	-0.89959
H15	-3.20619	-0.12887	-0.35578
O16	-2.65282	3.001693	-0.9015
H17	-1.84137	3.303071	-0.44446
H18	-2.67345	3.460949	-1.74506

Part d – Cage hexamer.

Symbol	X	Y	Z
O1	-1.94631	3.400566	-0.13021
H2	-1.36106	2.656298	0.18339
H3	-2.20313	3.904851	0.6459
O4	-0.31777	1.343904	0.324705
H5	-0.46415	0.917141	-0.53487
H6	0.574849	1.736918	0.254909
O7	-1.03063	0.889848	-2.44581
H8	-1.96973	1.183708	-2.40484
H9	-0.99469	0.138862	-3.04346
O10	-3.44244	2.052384	-1.98997
H11	-3.08293	2.621024	-1.2756
H12	-3.8108	2.649824	-2.64665
O13	1.914777	2.884791	-0.28268
H14	1.429065	3.21633	-1.06895
H15	2.804892	2.673433	-0.5743
O16	0.09531	3.562716	-2.24463
H17	-0.60099	3.831265	-1.62574
H18	-0.18007	2.676437	-2.53071

171

Part e – Prism hexamer.

Symbol	X	Y	Z
O1	-2.09251	3.004348	0.156102
H2	-1.10751	3.165797	0.128323
H3	-2.52624	3.857496	0.077993
O4	0.555728	3.10479	0.138653
H5	0.722106	2.504224	0.895744
H6	0.812577	2.548991	-0.61212
O7	0.724316	0.848383	1.764207
H8	-0.21977	0.703349	1.940106
H9	0.888584	0.409887	0.915724
O10	-2.1716	0.820874	1.84617
H11	-2.29402	1.704739	1.445791
H12	-2.72345	0.788153	2.631862
O13	0.74588	0.497476	-1.148
H14	-0.22845	0.388227	-1.23503
H15	1.147275	-0.03937	-1.83591
O16	-1.99035	0.430346	-1.08054
H17	-2.18923	1.371346	-0.94055
H18	-2.20855	0.035642	-0.22563

Delocalization patterns

Bag $\mathcal{F}5 \cdots \mathcal{F}6$
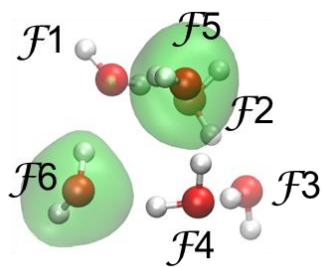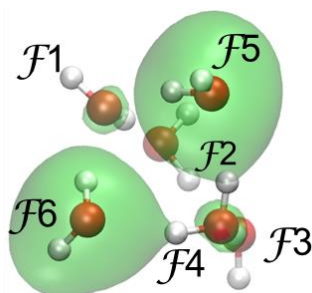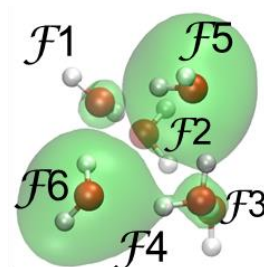
0.0002	0.00006	0.00004
0.000035	0.000025	0.00002
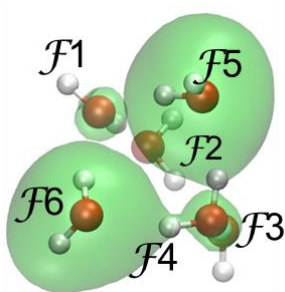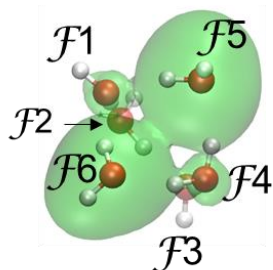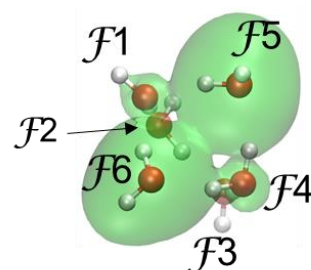
Figure S1 The isosurfaces for the intermolecular electron delocalization between $\mathcal{F}5$ and $\mathcal{F}6$ for the bag water cluster.

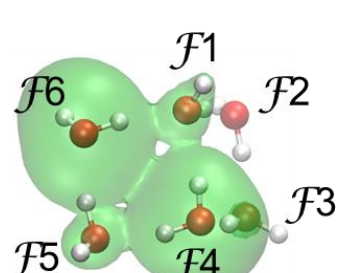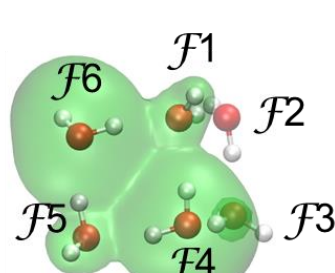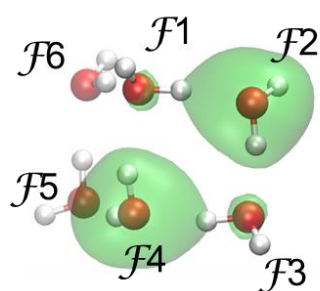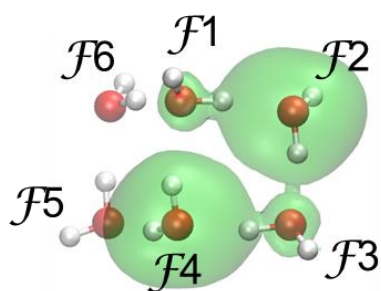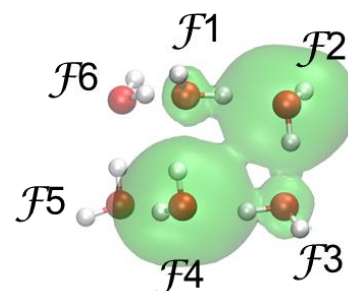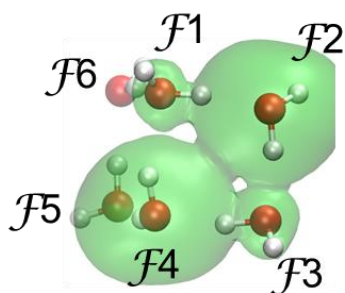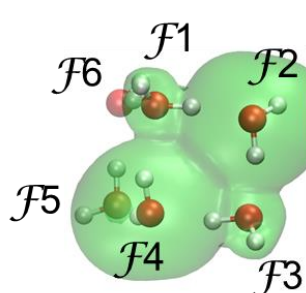**Bag $\mathcal{F}3 \cdots \mathcal{F}6$**
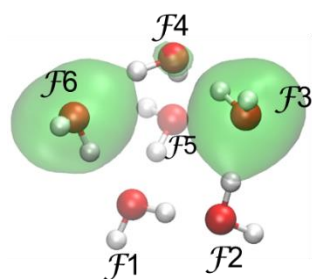
0.00009
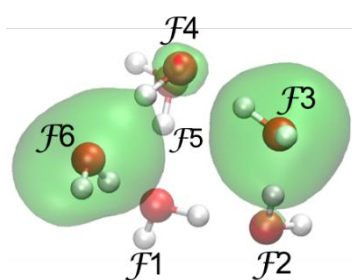
0.00005
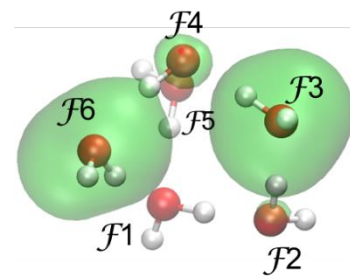
0.00004
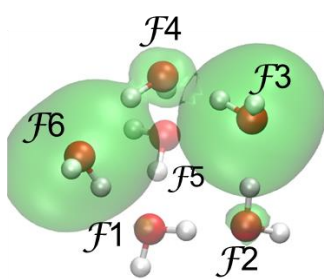
0.00002
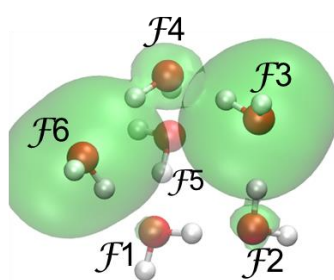
0.000015

Figure S2 The isosurfaces for the intermolecular electron delocalization between $\mathcal{F}3$ and $\mathcal{F}6$ for the bag water cluster.

Book $\mathcal{F}4 \cdots \mathcal{F}6$
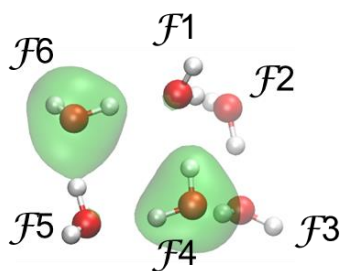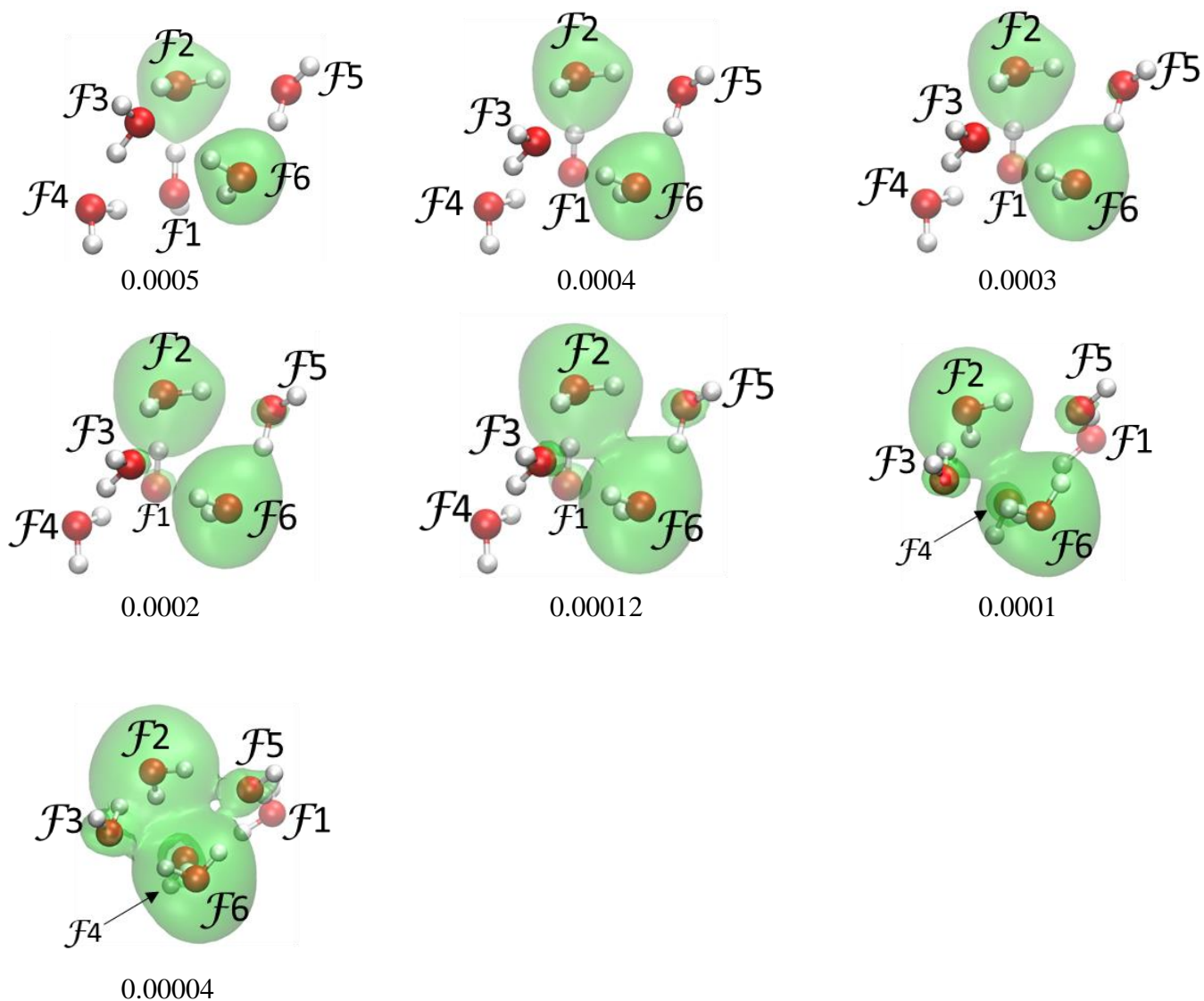

0.0002
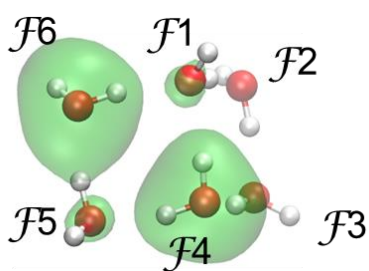
0.00007
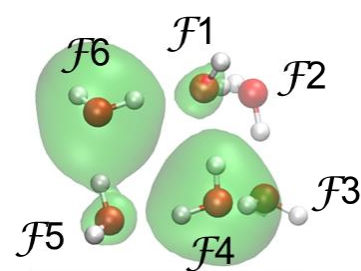
0.00005
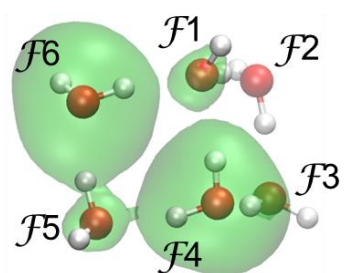
0.000035

0.00002

0.000009

Figure S3 The isosurfaces for the intermolecular electron delocalization between $\mathcal{F}4$ and $\mathcal{F}6$ for the book water cluster.

Book $\mathcal{F}2 \cdots \mathcal{F}4$

0.0001

0.000035

0.000025

0.00002

0.00001

Figure S4 The isosurfaces for the intermolecular electron delocalization between $\mathcal{F}2$ and $\mathcal{F}4$ for the book water cluster.
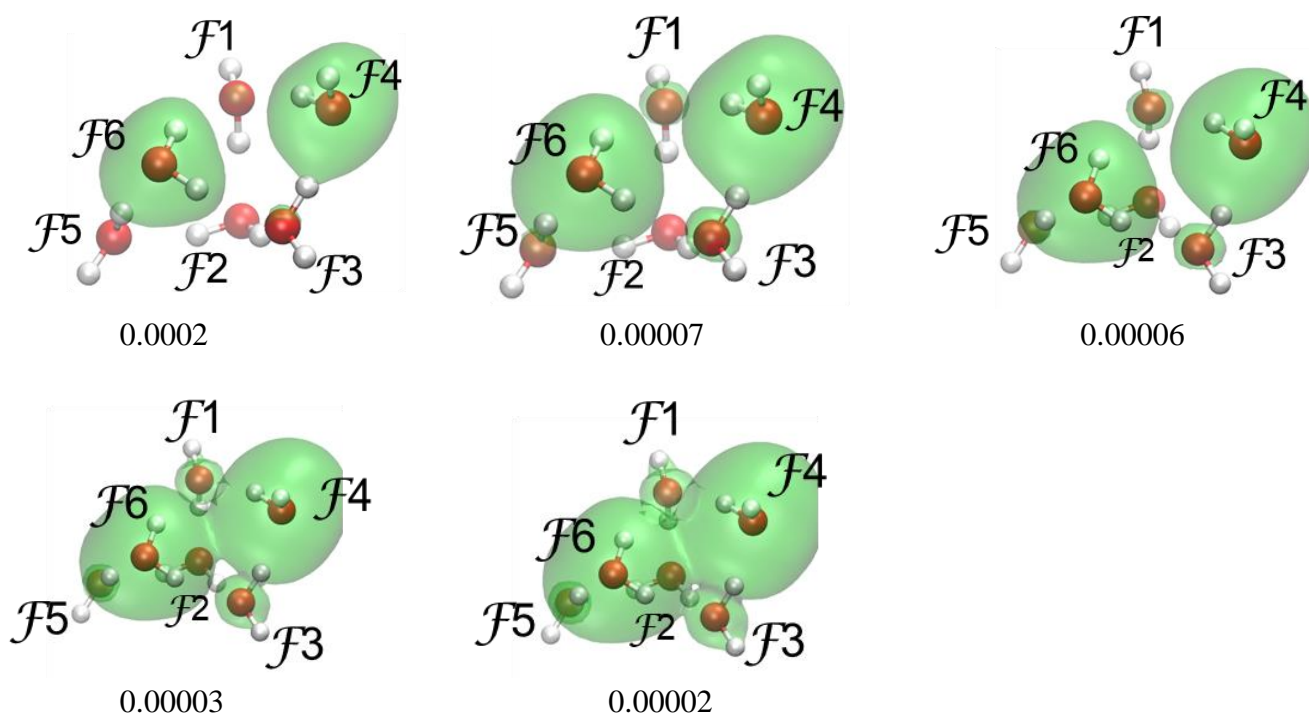
Cage $\mathcal{F}2 \cdots \mathcal{F}6$

0.0005

0.0004

0.0003

0.0002
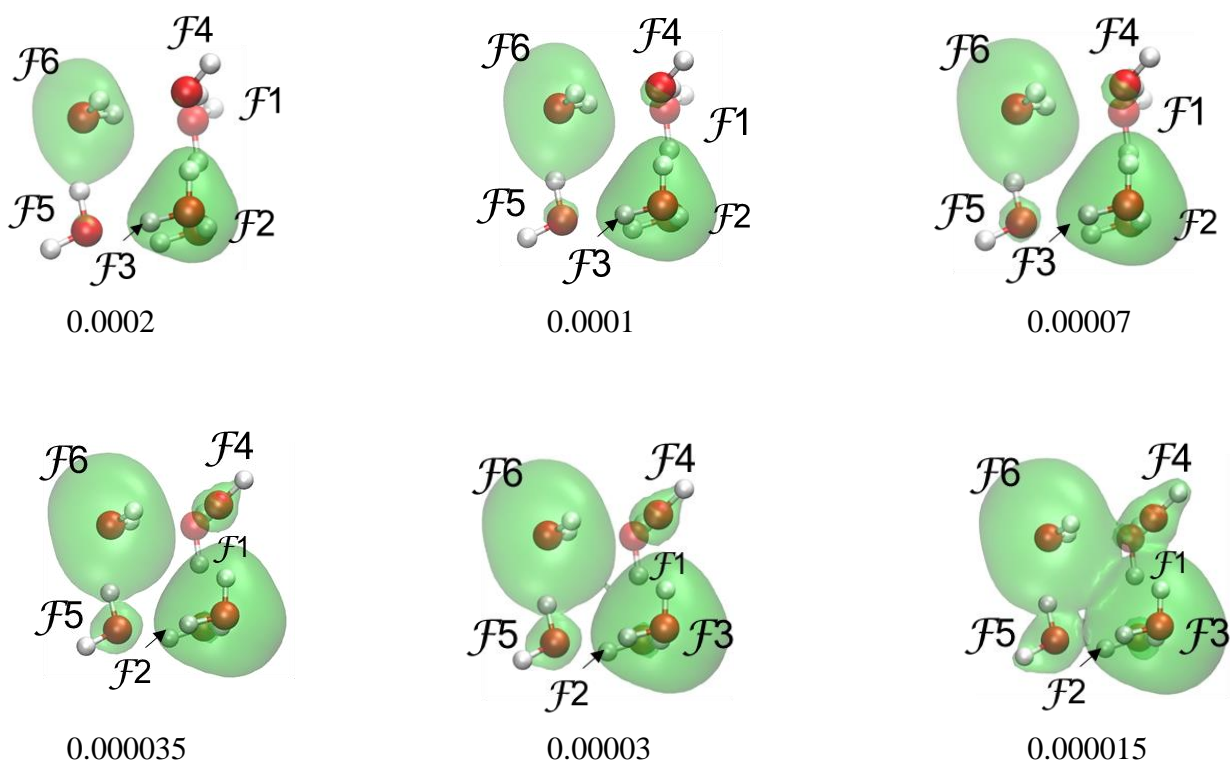

0.00012

0.0001

0.00004

Figure S5 The isosurfaces for the intermolecular electron delocalization between $\mathcal{F}2$ and $\mathcal{F}6$ for the cage water cluster.

Cage $\mathcal{F}4 \cdots \mathcal{F}6$

0.0002   0.00007   0.00006

0.00003   0.00002

Figure S6 The isosurfaces for the intermolecular electron delocalization between $\mathcal{F}4$ and $\mathcal{F}6$ for the cage water cluster.

Prism $\mathcal{F}3 \cdots \mathcal{F}6$

0.0002   0.0001   0.00007

0.000035   0.00003   0.000015

Figure S7 The isosurfaces for the intermolecular electron delocalization between $\mathcal{F}3$ and $\mathcal{F}6$ for the prism water cluster.
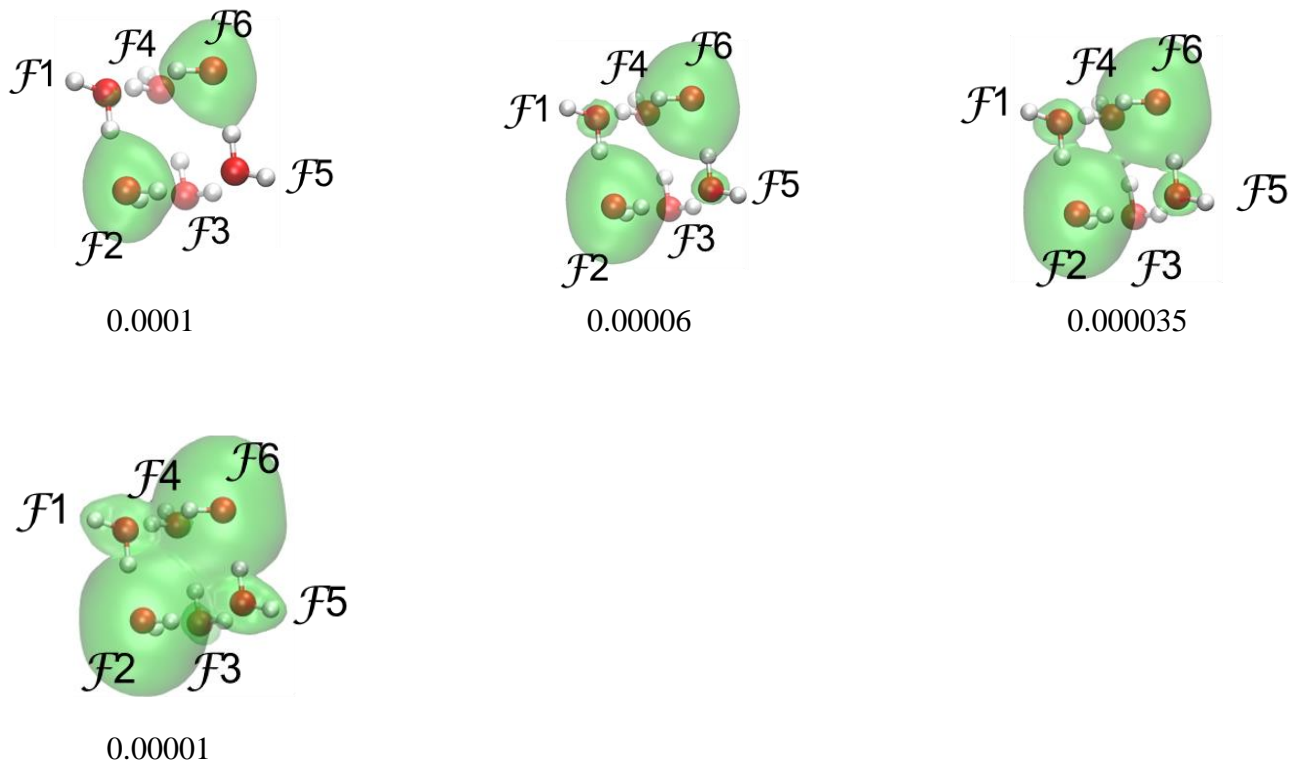
Prism $\mathcal{F}2 \cdots \mathcal{F}6$

Total electron delocalization between $\mathcal{F}2$ and $\mathcal{F}6$: $0.167e$

0.0001

0.00006

0.000035

0.00001

Figure S8 The isosurfaces for the intermolecular electron delocalization between $\mathcal{F}2$ and $\mathcal{F}6$ for the prism water cluster.